5-2017

Targeting the glucose metabolism of myeloid-derived suppressor cells (MDSCs) to stimulate cancer immunity.

Jaspreet Grewal
University of Louisville

TARGETING THE GLUCOSE METABOLISM OF MYELOID-DERIVED SUPPRESSOR CELLS (MDSCs) TO STIMULATE CANCER IMMUNITY

By

Jaspreet Grewal, M.D., M.P.H.
University of Louisville

A Dissertation
Submitted to the Faculty of the
School of Medicine
in Partial Fulfillment of the Requirements
for the Degree of

Doctor of Philosophy in Pharmacology and Toxicology

Department of Pharmacology and Toxicology
University of Louisville
Louisville, Kentucky

May 2017

TARGETING THE GLUCOSE METABOLISM OF MYELOID-DERIVED SUPPRESSOR CELLS (MDSCs) TO STIMULATE CANCER IMMUNITY

By

Jaspreet Grewal, M.D., M.P.H.
University of Louisville

A Dissertation Approved On

April 20, 2017

by the following Dissertation Committee:

_____

Jason Chesney, M.D., Ph.D.
Dissertation Director

_____

Kavitha Yaddanapudi, Ph.D.
Co-mentor

_____

Brian Clem, Ph.D.

_____

Leah Siskind, PhD.

_____

Russell Salter, Ph.D.

DEDICATION

To my wife Rimy for her unconditional love and support

To my father Albel and grandfather Iqbal for teaching me the virtues of hard work, honesty and commitment

To all the exceptional doctors and scientists who have committed their lives to the discovery of new treatments for cancer patients

To my mentor Jason Chesney who believed in me and gave me the opportunity to pursue my dream to become a physician scientist

To all the brave cancer patients who never gave up and taught us the meaning of life

ACKNOWLEDGEMENTS

This day would not have been possible in my life without the support of my loving wife, Preetkanwal (Rimy) Kaur Grewal, MD. Rimy, through happiness or despair, you have always been there for me. You always encouraged me to pursue my dreams. You taught me to face failures bravely and learn from my mistakes. In the times of distress, you told me to look at the bigger picture and not lose focus. Our son, Zoravar who arrived in our lives in the summer of 2015, brought with him a whole bunch of happiness. He is my stress reliever especially when he calls me “Dadda” and comes running at me with the cutest smile on his face. This is a special moment to thank my father Albel Singh Grewal and my mother Harkanwaljit Kaur Grewal. My parents always taught me the value of education and they worked incredibly hard to make sure that I had all the available resources to succeed in any career I chose. I would also like to thank my younger brother, Jugraj for the good times we spent with each other, played basketball and hung-out to help relieve work stress.

I would also like to acknowledge my mentor, Dr. Jason Chesney. He is an exceptional person who has always helped others to succeed including myself. Dr. Chesney believed in me and saw the passion I had for the pursuit of a scientific career. He encouraged me to not give up and helped me turn my failures in to success.

Next, I would like to thank Dr. Kavitha Yaddanapudi. She is an amazing woman with limitless energy. If Dr. Chesney showed me the dream of becoming a physician scientist, Dr. Yadddanapudi helped me make it come true. Throughout my project she was exceptionally patient and taught me everything that I needed to know to prove my hypothesis.

A special thanks to the members of Yaddanapudi lab – Dr. Numan Al-Rayyan, Jamaal Ritchie and Paxton Schowe. Thank you, Dr. Al-Rayyan for helping and teaching me mouse tumor injections and *in vivo* experiments.

I would also like to take this opportunity to thank Brooke DeGroote, Dr. Sucheta Telang, Dr. Nadiia Lypova, Dr. Yoannis Fernandez, Shelia Thomas, Dr. Tariq Malik, Lillibeth Lanceta, Ashley Wise, Dr. Lee Schmidt, Dr. Robert Mitchell, Dr. Howard Donninger and Dr. Cameron Falkner. Thank you, Brooke for placing all the lab orders for me and for all the wonderful get-togethers that you arranged for everyone. I am very thankful to Dr. Cameron Falkner for teaching me how to use the SeaHorse® analyzer.

Thank you Melissa Hall and Amy Clem for collecting late-stage melanoma patient blood samples for my experiments.

Sincere thanks to Dr. Brian Clem, Dr. Leah Siskind and Dr. Russell Salter for their valuable feedback and suggestions as my committee members.

Thank you Dr. Donald Miller, Dr. Goetz Kloecker and the medical oncology and hematology fellowship program at the University of Louisville for giving me the opportunity to train in this subspecialty and continue with my PhD studies.

Last but not the least; I would also like to thank all our friends and the City of Louisville for the wonderful past five years full of love and happiness.

ABSTRACT

TARGETING THE GLUCOSE METABOLISM OF MYELOID-DERVIED SUPPRESSOR CELLS (MDSCs) TO STIMULATE CANCER IMMUNITY

Jaspreet Grewal

April 20, 2017

Myeloid derived suppressor cells (MDSCs) are a heterogeneous group of immature myeloid cells that are significantly increased in cancer patients and correlate with higher stage and poor prognosis (1-4). MDSCs negatively modulate anti-tumor immunity, suppress T cell activity, promote angiogenesis and increase the risk of metastasis (1). In this study, we report that monocytic-MDSCs (M-MDSCs) but polymorphonuclear-MDSCs (PMN-MDSCs) over-express 6-phosphofructo-2-kinase/fructose-2, 6-bisphosphatases 3 (PFKFB3), an important regulator of glycolysis. Furthermore in the melanoma model, M-MDSCs but not PMN-MDSCs suppressed T cell function which correlated with PFKFB3 over-expression and increased rate of glycolysis. PFKFB3 inhibition with the first-in-class small molecule inhibitor, PFK-158 reversed M-MDSC mediated T cell suppression and decreased the expression of arginase 1 and inducible nitric oxide synthase (iNOS) both *in vitro* and *in vivo*. In addition, both in

B16-F10 tumor-bearing mice and patients enrolled in Phase 1 clinical trial, PFKFB3 inhibition resulted in decrease in M-MDSC frequency and increase in effector T cell populations. In this first-of-a-kind study, we present strong evidence for targeting metabolic profile of M-MDSCs to modulate their immune suppressive phenotype. This study provides the basis to study PFK-158 as an immunomodulatory agent in combination with immune checkpoint blockade therapies to improve T cell activity and anti-tumor responses.

TABLE OF CONTENTS

Page

LIST OF FIGURES

LIST OF TABLES

1. INTRODUCTION

1.1 Historical background

About 35 years ago, Strober *et al* identified a population of myeloid cells with T-cell suppressive functions affecting alloreactive immune responses in allogeneic bone marrow chimera experiments (1, 5). Because of the lack of common phenotypic markers, these cells were originally called the “natural suppressor (NS)” cells (5). Initially, these cells were thought to appear only transiently during certain phases of life such as in the placenta during pregnancy, fetus and during maturation of lymphoid tissues in neonates (5). However, later these cells were also identified following immune system manipulation such as following total body irradiation (TBI) or chemotherapy, in chronic inflammatory states, graft-versus-host disease (GVHD) and cancer (5). Due to technical difficulties associated with the isolation and disagreements in the scientific community regarding phenotypic characterization, these cells were defined on the basis of their suppressive function.

First evidence for the involvement of NS cells in lowering immune surveillance and in promoting cancers came in 1995. It was noticed that following the administration of an antibody directed against the glutathione reductase 1 (GR1 or GSR) antigen, which recognizes cross-reacting molecules of lymphocyte antigen 6 complex locus C and G or Ly6C and Ly6G, to immunocompetent mice reduced the growth of UV light-induced tumor (5). It was initially thought that the GR1 antibody resulted in the elimination of granulocytes; however, subsequent studies showed that the $GR1^{pos}$ cells were mainly $CD11b^{pos}$ (integrin-αM) polymorphonuclear and mononuclear cells at different stages of maturation along the myelomonocytic differentiation lineage (5, 6).

Subsequently, observations were made during therapeutic anticancer vaccine research with powerful immunogens which revealed dysfunction of $CD8^{pos}$ cytotoxic T-lymphocytes (CTLs) in immunocompetent hosts (7). This observation was attributed to accumulation of splenic $CD11b^{pos}GR1^{pos}$ cells (7). Following elimination of this cell population, CTL function was restored both *in vitro* and *in vivo* (7). In 2001, it was reported that the decrease in the dendritic cells (DCs) in the peripheral blood of cancer patients correlated with the appearance of immature cells lacking markers of mature lymphoid and myeloid cells (7). These immature cells capable of suppressing T-cell responses were called “immature myeloid cells” (ImCs) and were characterized by the absence of lineage markers such as CD3, CD19 and CD57 (7). They were positive for CD13, CD33 and lacked the expression for HLA-DR and CD15. After few years, the term “ImCs” was dropped and it was proposed that these cells be called “Myeloid

Suppressor Cells" (MSC) (1). A myeloid cell suppressive population characterized as $CD14^{pos}HLA\text{-}DR^{low/neg}$ was identified for the first time in melanoma patients treated with an anti-cancer vaccine containing GM-CSF as an adjuvant (7). Finally in 2007, the term MDSC was formally introduced to characterize these immature myeloid cells in both mice and humans (1, 8).

1.2 Phenotype of myeloid derived suppressor cells (MDSCs)

MDSCs are a heterogeneous group of bone marrow derived immature myeloid cells at different stages of differentiation which are greatly expanded in cancers, inflammation, trauma and infection, and suppress both innate and adaptive immune responses (**Fig. 1**) (1, 2, 4, 7-35). This population of cells includes immature monocytes, granulocytes and other myeloid progenitors (9, 11-13, 17, 25, 26, 28, 36). MDSCs are characterized by morphological, phenotypic and functional heterogeneity which essentially demonstrates the plasticity of this immune suppressive cell population (35). This further outlines how different tumors, infectious agents or inflammatory states can result in similar biological effects on myeloid progenitors despite the differences in the factors that they produce (8). This heterogeneity over the years created tremendous amount of ambiguity and confusion in developing a standard definition and other biological characteristics of MDSCs. To overcome this limitation, standard definitions characterizing the phenotypical and functional characteristics of these cells were published recently (35).

Cells with typical MDSC phenotype are present in the bone marrow and in the spleens of healthy individuals as well as naïve mice (13, 17, 24, 37). Under normal conditions, these cells make up about 20-40% of the bone marrow and about 2-4% of all splenocytes (9, 11, 13, 17, 24, 36, 37). However, these cells are not suppressive and largely represent ImCs (7, 13, 15, 22, 37). Under normal conditions, these ImCs migrate to the peripheral lymphoid organs and differentiate into macrophages, DCs, and granulocytes/neutrophils (1, 17, 35, 37). In cancer, hematopoietic differentiation pathway is altered and maturation of these cells into normal myeloid cells is blocked. These cells under the influence of tumor-derived soluble factors (TDSFs) become activated, expand exponentially (>20% of all splenocytes in some tumor models) and accumulate in peripheral blood, lymph nodes, spleen, tumors, and immune-activated tissues and develop in to immune suppressive MDSCs (1, 11, 12, 22, 35, 38). Interestingly, acute bacterial infection or stress does not necessarily result in the generation of MDSCs. They accumulate only during chronic infection, inflammation, or cancer (24).

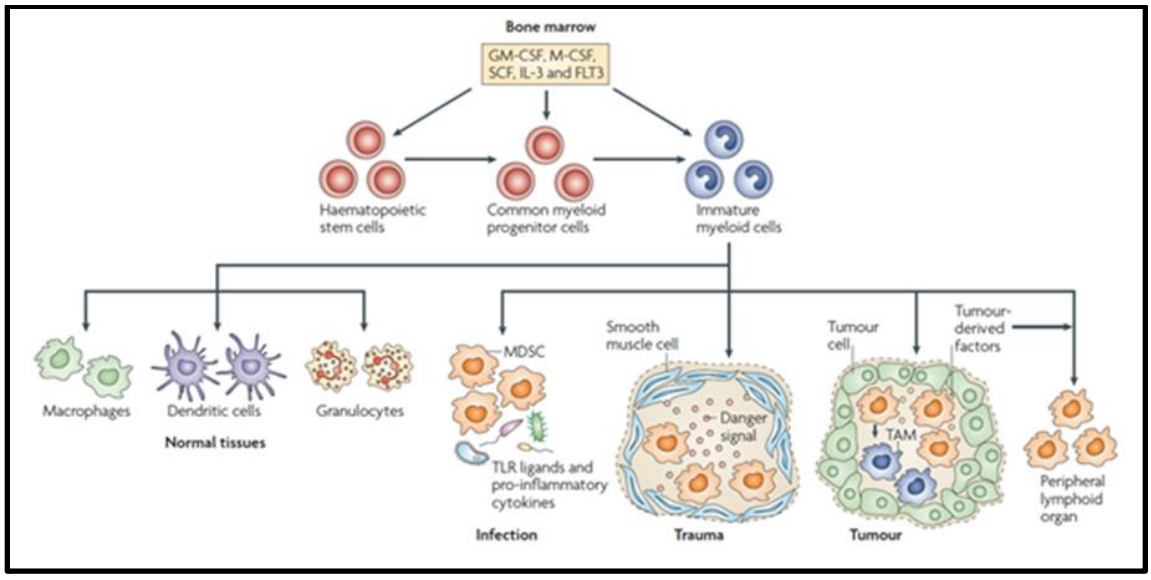

Figure 1. Normal vs. abnormal differentiation of immature myeloid cells to terminally differentiated cells and MDSCs (25).

In mice, MDSCs are generally defined as CD11b and GR1 positive (6, 8-16, 19-22, 24, 25, 27, 28, 30, 35-37, 39-41). Further classification of murine MDSCs to monocytic (M-) and granulocytic or polymorphonuclear (PMN- or G-) MDSCs is based on graded measurements of GR1 expression or by using two different GR1 epitopes (8, 12, 20, 35). To differentiate MDSCs from steady state granulocytes, it is now proposed to use the term PMN-MDSCs as opposed to G-MDSCs (35). Murine M-MDSCs are $SSC^{low}CD11b^{pos}Ly6C^{high}Ly6G^{neg}$ $CD49d^{pos}$ (or $GR1^{low}$) and G- or PMN-MDSCs are $SSC^{high}CD11b^{pos}Ly6C^{low}Ly6G^{pos}$ $CD49d^{neg}$ (or $GR1^{high}$) (1, 5-22, 24-26, 30, 33-38, 41-46). Both subsets express IL-4Rα (CD124); however, expression is higher in $GR1^{low}$ compared to $GR1^{high}$ subset (7, 42, 47, 48). Murine M-MDSCs also express chemokine receptor 2 (CCR2) and low levels of F4/80, and PMN-MDSCs express CD244 (7, 42). Macrophage – colony stimulating factor receptor (M-CSFR or CD115) is

expressed by both subsets (7). On May-Grünwald-Giemsa staining, PMN-MDSCs are morphologically similar to neutrophils and M-MDSCs are similar to monocytes (5, 7, 47, 49).

Human M-MDSCs are generally defined as $CD11b^{pos}CD14^{pos}CD15^{neg}CD33^{pos}HLA\text{-}DR^{low/neg}$ and PMN-MDSCs as $CD11b^{pos}CD14^{neg}CD15^{pos}CD33^{dim}CD66b^{pos}$ (1, 4-12, 15-19, 22, 24-26, 28, 30, 34, 35, 37, 44, 45, 49, 50). Another population of more immature progenitors lacking lineage specific antigens (Lin^{neg}) such as CD3, CD14, CD15, CD19, CD20, CD40, CD56, CD57, CD80 and CD83 but positive for CD33 has been recently classified as "early-stage MDSC (eMDSC)" (1, 7, 17, 19, 35). Both mature monocytes and granulocytes express HLA-DR. Interleukin – receptor alpha (IL-4Rα or CD124), IL-13, vascular endothelial growth factor receptor (VEGFR) and macrophage – colony stimulating factor receptor (M-CSFR or CD115) are other markers that define immune suppressive MDSCs in humans (1, 6, 13, 15, 19-21, 37).

1.3 Functional characteristics of MDSCs

Tumors and TDSFs not only sustain the accumulation of MDSCs but also determine their functional differentiation leading to their heterogeneity in different cancers and tumor models. This makes it important to not only determine the presence of all MDSC subsets in each cancer patient, but also which MDSC subsets have clinical relevance in a particular tumor environment/model (21).

Both MDSC subsets undergo substantial expansion in the peripheral blood, lymphoid organs and spleens of tumor bearing animals and cancer patients. PMN-MDSCs expand in much greater numbers accounting for 70–80% of the MDSC population in a tumor bearing host, whereas M-MDSCs account for 20–30% of MDSCs (Fig. 2) (5, 7, 8, 13, 21, 24, 25). M-MDSC, however, is the dominant subset at the tumor site (21, 51). This may be secondary to the chemokines produced by the tumor cells that support preferential migration of M-MDSCs to the tumor site or alternatively, the TME may not support PMN-MDSC survival because of hypoxia, low pH, and accumulation of metabolic products (**Fig. 2**) (21, 51). Regardless, M-MDSCs are more suppressive on a per cell basis compared with PMN-MDSCs in most tumor models and cancer patients (5, 8, 36, 42, 47). Interestingly, MDSC frequencies start to increase early during tumor development, but only MDSCs from mice with established tumors demonstrate a strong immune suppressive phenotype (48).

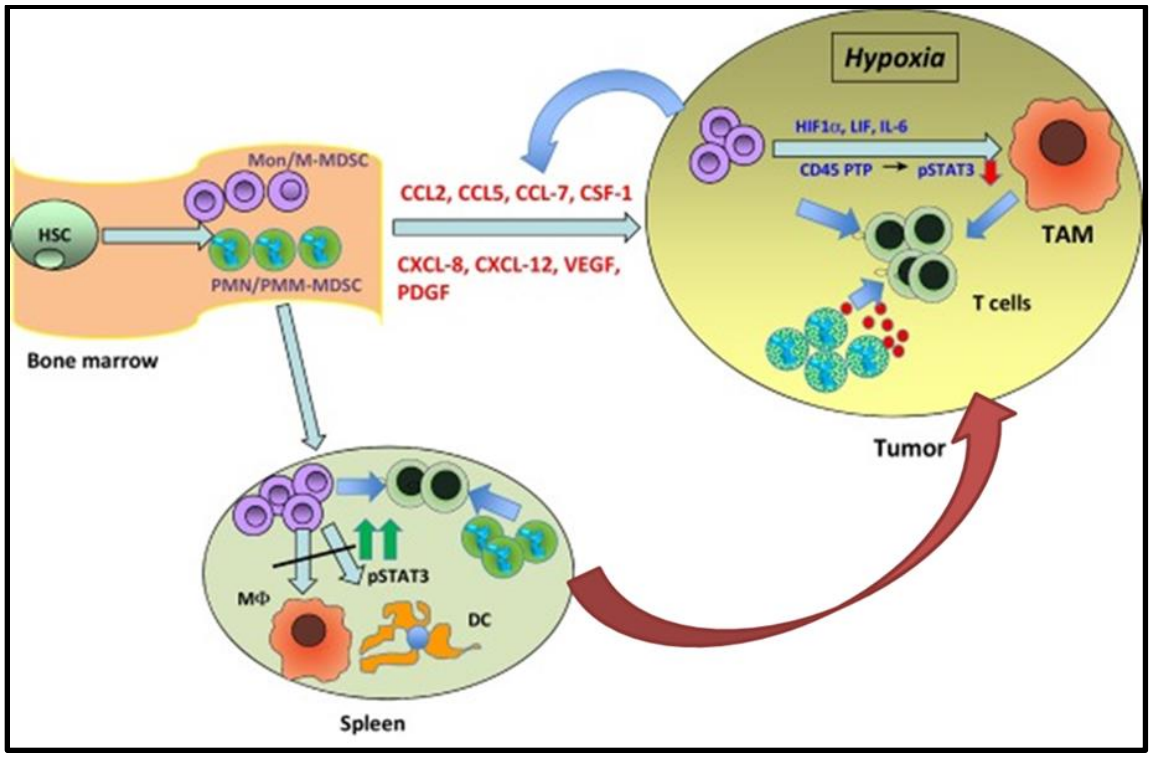

Figure 2. Expansion and migration of MDSCs from the bone marrow to peripheral lymphoid organs and tumor (51).

MDSCs potently suppress both innate and adaptive immunity through inhibition of T cell activation, disruption of naive T-cell homing to lymph nodes, suppression of NK cell cytotoxicity, expansion of Tregs cells and arrest of DC maturation (1, 15-18, 20, 32, 45, 52). In addition, MDSCs protect tumors from the effects of chemotherapy and radiotherapy, drive tumor growth by promoting cancer stemness, promote angiogenesis through upregulation of vascular endothelial growth factor (VEGF), beta – fibroblast growth factor (bFGF), VEGF analogue Bv8, stroma deposition and epithelial-to-mesenchymal transition (EMT), and facilitate tumor cell motility and metastasis through expression of matrix metalloprotease (MMP9) (6, 8, 11, 12, 17, 25, 33, 53).

MDSC employ several mechanisms to inhibit T cell activity which includes arginine depletion through expression of the enzyme arginase 1 (Arg1), production of reactive oxygen species (ROS) and reactive nitrogen species (RNS), expression of inducible nitric oxide synthase (iNOS) and nitric oxide (NO) production, up-regulation of cyclooxigenase-2 (COX-2) and prostaglandin E2 (PGE2) production, induction of Tregs, expression of transforming growth factor – β (TGF-β) and interleukin – 10 (IL-10), sequestration of other amino acids such as cysteine, cystine and phenylalanine, depletion of tryptophan through expression of indolamine 2, 3-dioxygenase (IDO) and down-regulation of L-selectin expression on T cells (1, 9, 10, 13, 15-17, 24-26, 31, 36, 39, 45, 46, 51).

Functional differences between MDSC subsets pertain to their mechanism of T cell suppression. PMN-MDSCs mainly suppress T cell function through production of high levels of ROS, expression of Arg1 and myeloperoxidase (MPO) whereas M-MDSCs suppress T cell function by depleting arginine through expression of Arg1, and production of NO and RNS through expression of iNOS (**Fig. 3**) (5, 6, 12, 13, 15, 21, 24, 25, 37).

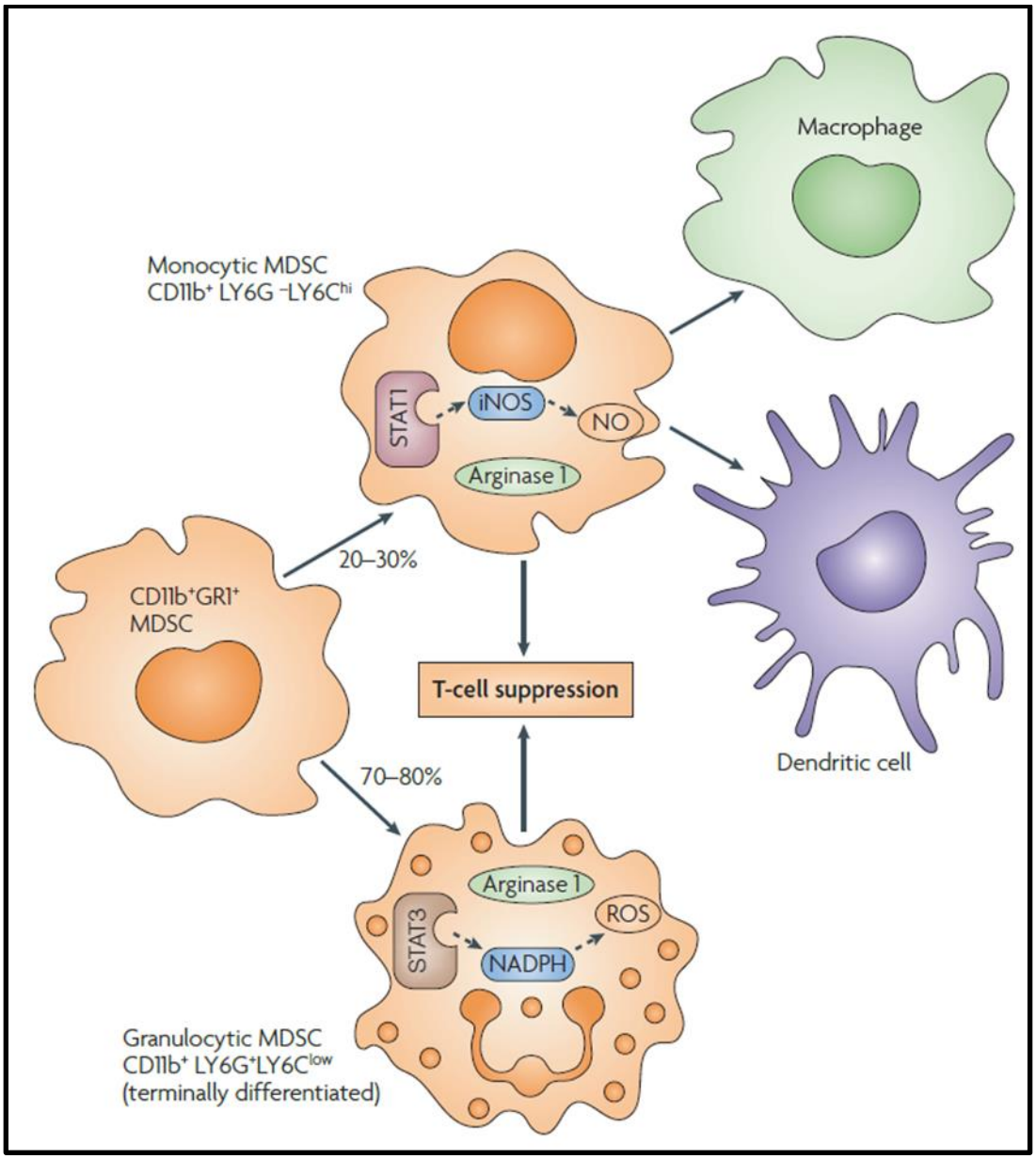

Figure 3. Markers of suppression of polymorphonuclear- and monocytic-MDSCs (25).

Similarly, MDSCs isolated from peripheral lymphoid organs and tumors have profound functional differences despite similar phenotype and morphology. Tumor MDSCs suppress both antigen-specific and nonspecific T cell activity (8, 11, 25). However, MDSCs isolated from peripheral lymphoid organs fail to

suppress antigen-nonspecific T cell function but mediate antigen-specific T-cell tolerance by processing and presenting tumor associated antigens (TAAs) to T cells in the context of major histocompatibility complex class – I (MHC-1) (8, 9, 11, 25). This observation is supported by the fact that despite the presence of a large number of MDSCs in the spleens and lymph nodes of tumor-bearing mice and in the peripheral blood of cancer patients with advanced disease, T cells mostly retain the ability to respond to different tumor-nonspecific stimuli including viruses, lectins, costimulatory molecules, IL-2, and stimulation with CD3- and CD28-specific antibodies (11).

Molecular mechanisms behind MDSC recruitment, expansion, and activation are still not clear. However, a “two-signal” model has been proposed (8, 18, 34, 51). First step is promoted by chronic inflammation resulting in accumulation of immature cells and involves factors such as granulocyte colony stimulating factor (G-CSF), macrophage-colony stimulating factor (M-CSF), GM-CSF, C-X-C motif chemokine ligand 5 (CXCL5), CXCL12, C-C motif chemokine ligand 2 (CCL2), cyclooxygenase-2 (COX-2) and PGE2, VEGF, IL-1β, IL-4, IL-6, IL-8, IL-10, IL-12, IL-13, IL-17, FMS like tyrosine kinase 3 ligand (FLT3L), fibroblast growth factor – 2 (FGF-2), S100A8/A9, stem cell factor (SCF or KIT ligand), TGF-β and tumor necrosis factor α (TNFα) (Fig. 4) (1, 5, 6, 12, 13, 15, 18, 21, 25, 26, 28, 30, 32-34, 38, 39, 42, 47, 51). These signals converge on one common pathway – Janus kinase/signal transducers and activators of transcription 3 (JAK/STAT3) pathway involved in cell survival, proliferation and differentiation (Fig. 4) (9, 12, 20, 21, 46). MDSCs isolated from tumor bearing

mice and patients with malignant melanoma have dramatically increased levels of phosphorylated STAT3 (pSTAT3) compared to ImCs from naive mice or healthy donors (Fig. 4) (8, 9, 15, 21, 25, 30). STAT3 is important for MDSC recruitment and suppressive activity through increased levels of Arg1, NADPH-oxidase 2 (NOX2), iNOS or Nos2, IDO, VEGF, GM-CSF, S100A8/A9, cyclooxygenase (COX)-2, IL-1β, IL-6 and IL-10 (Fig. 4) (9, 12, 15, 21, 26, 30, 34, 39, 46). In addition, STAT3 is responsible for maintaining MDSCs in immature state and preventing their differentiation through upregulation of B-cell lymphoma XL (BCL-XL), cyclin D1, MYC and survivin (8, 12, 15, 21, 25, 30, 34).

The second signal is needed for the pathological activation of these cells. The factors involved in the second signal are produced mainly by activated T cells, tumor stromal cells or are induced by different bacterial and viral products, or result from tumor-cell death, and include molecules such as IFN-γ, IL-1β, IL-4, IL-13, TGFβ and TLR ligands (51). These factors activate several signaling pathways in MDSCs that involve STAT1, STAT6 and nuclear factor-κB (**Fig. 4**) (15, 25, 30, 46, 51).

Bronte *et al* have reported that CCAAT/enhancer-binding protein beta (C/EBPb) family of transcription factors along with STAT proteins regulate shift from normal to aberrant hematopoiesis, allowing differentiation into MDSCs, recruitment and activation (Fig. 4) (46). In a separate study, Ostrand-Rosenberg *et al* proposed that MDSC levels in developing tumors are maintained by resistance to apoptosis by FasL+ expressing activated T cells which is mediated by inflammation and secretion of TGFβ by the tumors (8, 18, 34).

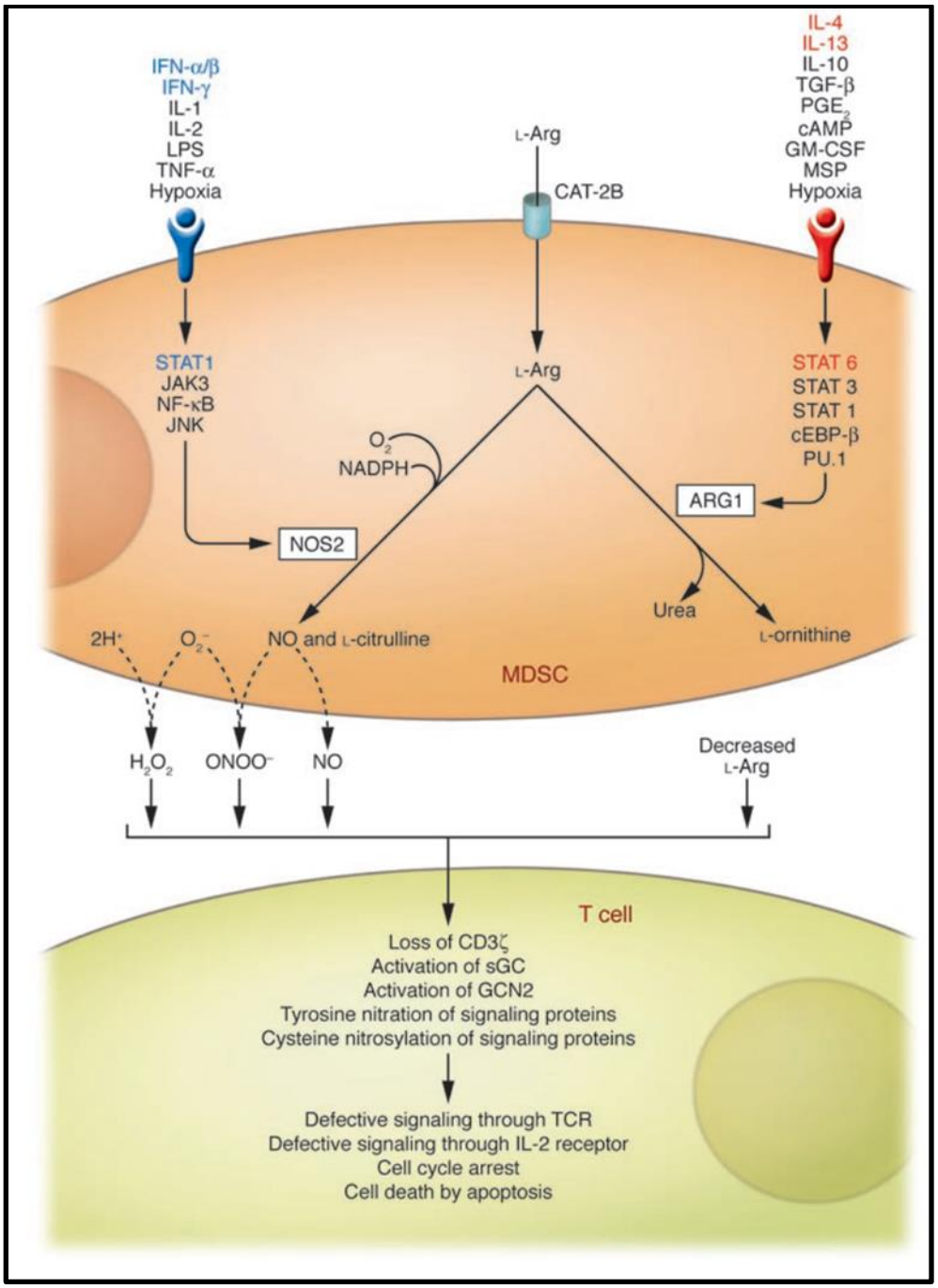

Figure 4. External and internal signals involved in MDSC accumulation, expression of markers and mechanisms of suppression (46).

1.3.1 Arginine depletion

Both MDSC subsets – PMN- and M-MDSCs use L-arginine depletion as mechanism for their T cell inhibitory activity. M-MDSCs from tumor-bearing mice express high levels of Arg1 and this is accompanied by high iNOS activity likely through the combined autocrine action of IL-13 and IFN-γ (4, 12, 19, 34, 36). Arg1 hydrolyzes the amino acid L-arginine to ornithine and urea, and iNOS/NOS2 oxidizes L-arginine to generate NO and citrulline (**Fig. 4**) (1, 17, 21, 36, 42, 46). In mice, Arg1 remains cytoplasmic while in humans it is secreted from the cell (12, 36).

L-arginine is essential for T cell replication and proliferation (1). Increased Arg1 activity leads to enhanced L-arginine catabolism resulting in depletion of this non-essential amino acid from the TME. This depletion results in translational blockade of the CD3ζ (CD247) chain and prevents T cells from responding to various stimuli (10, 26, 38). Further, lack of L-arginine blocks protein translation through the accumulation of empty aminoacyl-t-RNAs. This in turn results in activation of general control nonderepressible 2 (GCN2) kinase and phosphorylation of the translation initiation factor eukaryotic initiation factor 2 α (eIF2α). Phosphorylation of eIF2α increases its affinity for eIF2β which blocks the exchange of GDP with GTP, thus interfering with protein synthesis. Finally, L-arginine depletion results in G_0–G_1 cell cycle arrest through upregulation of cyclin D3 and cyclin dependent kinase 4 (cdk4) but not cyclin D1, cyclin D2, and cdk6 (1, 6, 12, 19, 21, 25, 34, 36). Tumor-infiltrating M-MDSCs further upregulate expression of Arg1 which is accompanied by antigen-nonspecific T cell

suppression (42). Inhibition of Arg1 restores T-cell function *in vitro* and induces an antitumor response *in vivo*. Arg1 acts as a tumor-landscaping gene by supporting tumor growth and suppressing antitumor immune responses (54).

In melanoma patients, ARG1 expression has been shown to be a dominant mechanism of T cell suppression (19). A recent study had demonstrated that the increased numbers of MDSCs in the peripheral blood of esophageal, gastric and renal cancer patients correlated with low L-arginine and high ornithine levels in plasma, and a profound T-cell dysfunction (4, 12, 36).

1.3.2 Nitric Oxide (NO)

Monocytic subset of MDSCs is the predominant producer of NO through increased expression of iNOS/NOS2 (42). iNOS is another L-arginine catabolizing enzyme which results in the production of NO as a byproduct following the conversion of L-arginine to citrulline (**Fig. 4**).

High levels of NO produced by M-MDSCs inhibit T cell activity through different mechanisms. Similar to Arg1 activity, iNOS expression results in the depletion of L-arginine causing down regulation of CD3ζ chain, thus rendering the T cells unresponsive (36, 52). NO can result in the nitration of proteins involved in interferon receptor signal transduction which reduces responsiveness of immune cells to cytokine stimulation (31). In human T cells, NO affects the stability of IL-2 mRNA and the release of IL-2. High concentrations of NO can inhibit T-cell signaling cascade downstream of the IL-2 receptor in an antigen independent manner by blocking the phosphorylation of JAK1, JAK3, STAT5,

extracellular signal-regulated kinase (ERK) and protein kinase B (PKB/AKT) which are important downstream signaling molecules (6, 34). High levels of NO prevent downregulation of L-selectin (CD62L) but cause downregulation of homing cell adhesion molecule (CD44) and selectin P ligand (CD162) (34). NO negatively regulates intracellular signaling proteins either directly, by S-nitrosylation of crucial cysteine residues, or indirectly, by activation of soluble guanylate cyclase and cyclic-GMP-dependent protein kinase (34). Increased production of NO inhibits the expression of MHC class II and induces T-cell apoptosis likely mediated by the accumulation of the tumor suppressor protein p53, signaling by CD95 (Fas) and TNF receptor family members, or signaling through caspase-independent pathways (6, 25, 36).

1.3.3 Peroxynitrite (PNT)

Both subsets of MDSC produce increased levels of PNT (ONOO−). PNT is a product of interaction between NO and superoxide (O2•–), therefore, increased level of either ROS or NO would result in increased PNT (12, 13, 34, 36, 55). PNT can also be produced by the combined activity of Arg1 and iNOS. L-arginine depletion by Arg1 switches on the reductase domain on iNOS leading to the production of superoxide anion and subsequently PNT (6, 34). It is one of the most powerful oxidants and is present at sites characterized by accumulation of MDSC, inflammatory cells, or ongoing immune reactions (36).

Increased PNT activity is associated with nitration and nitrosylation of the amino acids cysteine, methionine, tryptophan, and importantly tyrosine in

different proteins and enzymes, thus changing their biological functions (6, 12, 25, 34). PNT also causes oxidation of lipids and nucleic acids, and thus affecting their normal functions (6, 34). PNT directly inhibits T cell activity through nitration of TCRs, thereby reducing their responsiveness to cognate antigen-MHC complexes (8, 12, 21, 36). Nitration of the TCR also reduces binding of antigenic peptides to MHC molecules on tumor cells. Moreover, PNT can act on α and β chains of the lymphocyte TCR, preventing signaling and promoting dissociation of the CD3ζ chain from the complex (6). High levels of PNT block T cell migration by nitrating T cell–specific chemokines and promote homing of immune-suppressive subsets other than T cells (6, 8, 12).

High levels of PNT are directly implicated in tumor progression, via modification and inactivation of different proteins (25). Association of high PNT levels with tumor progression has been documented in breast, colon, head and neck, lung and pancreatic cancers, malignant gliomas, melanoma and mesothelioma (36, 55). In breast cancer patients, high tumor PNT levels correlated with reduced disease-free survival (DFS) and OS (55).

1.3.4 Reactive oxygen species (ROS)

PMN-MDSCs induce T cell suppression mainly through production of high levels of ROS. PMN-MDSCs significantly increase the expression of NOX2, primarily p47phox and gp91phox catalytic subunits, an enzyme that reduces oxygen to superoxide anions using electrons supplied by NADPH (9, 10, 21, 36). Another mechanism involved in the generation of ROS involves the combined

activity of Arg1 and iNOS. During L-arginine deprivation caused by increased Arg1 activity, iNOS utilizes molecular oxygen as the principal substrate to produce superoxide anions (21, 36).

Expression of NOX2 subunits is finely tuned at transcriptional and posttranslational level. Cytokines such as IL-3, IL-6, IL-10, TGFβ, TNF-α and IFN-γ, growth factors such as platelet derived growth factor (PDGF), GM-CSF and VEGF, and transcription factors mainly STAT3 upregulate NOX2 levels, whereas specific phosphorylation patterns and subunit availability modulate its activity (6, 25).

Increased levels of ROS are responsible for maintaining the immature phenotype of MDSCs and inhibit their differentiation to mature myeloid cells (9). ROS results in the loss of T cell receptor (TCR) ζ-chain which is very important for transduction of activating signals required for T cell proliferation and cytokine secretion (1, 12, 17, 42). Similar to the PNT activity, ROS can cause protein oxidation, frequently affecting tyrosine side chains. This impairs the ability of TCR to interact with peptide-MHC complexes and prevent appropriate T cell response (12). It also causes oxidation of lipids, nucleic acids and proteins which modifies their tertiary and quaternary structures and subsequently results in modification of signaling cascades and modulation of biological processes, including immune responses (6).

1.3.5 Regulatory T cells (Tregs) and Th17 cells

Tregs represent another immune suppressive population that potently inhibits T cell and NK cell function in cancer patients and tumor-bearing mice. $CD4^{pos}CD25^{pos}$ Tregs expressing the transcription factor, forkhead box P3 (Foxp3) inhibit autoimmune responses and promote tumor growth. Depletion of Tregs, thus results in improved antitumor immune responses and delays tumor growth (42). MDSCs specifically M-MDSCs promote the induction and proliferation of these Tregs, thereby downregulating anti-tumor immune responses (12, 25, 52).

M-MDSCs produce increased levels of CCR5 ligands CCL3, CCL4, and CCL5. Because CCR5 is preferentially expressed on Tregs, tumor-infiltrating M-MDSCs directly attract high numbers of Tregs via CCR5 *in vitro*. Further *in vivo* studies showed that the intratumoral injection of CCL4 or CCL5 increased tumor-infiltrating Tregs, and deficiency of CCR5 led to their significant decrease. Studies done in CCR5-deficient mice, showed that tumor growth was delayed which points to the importance of CCR5 in the control of antitumor immune responses (42).

Because of their ability to suppress T cell activity, accumulation of Tregs at the tumor site is associated with poor prognosis (42). It has been shown that in hepatocellular carcinoma (HCC), M-MDSCs exert their immunosuppression partially through the induction of functional Tregs when co-cultured with autologous T cells. The induction of Tregs depended on cell-to-cell contact and was abolished when M-MDSCs and T cells were separated (49). Another study

showed a significant increase in Tregs in esophageal, gastric and pancreatic cancer patients compared with healthy controls. And, there was a positive correlation between the increase in MDSC and Treg numbers (4). A direct correlation between high levels of Tregs in tumors, and high tumor grade and stage and poor prognosis has been demonstrated in different cancers (4, 42). Sunitinib, which is multi-tyrosine kinase inhibitor, resulted in significant reduction in MDSC numbers in patients with renal cell carcinoma (RCC). And, this decrease in MDSC numbers significantly correlated with decrease in Tregs (4).

Another population of immune regulatory cells induced by MDSCs is the Th17 cells. The generation of Th17 cells by MDSCs did not depend on cell-to-cell contact but was more dependent on the secretion of various cytokines. It has also been shown that the suppressive activity of MDSCs increased following incubation with IL-17 through the upregulation of Arg1, IDO, and COX-2. Another study showed that MDSCs from tumor-bearing IL-17 knock-out mice were less suppressive and expressed lower levels of Arg1, MMP9, and S100A8/A9 compared with tumor-bearing WT mice (49). These studies suggest that MDSCs and Th17 cells likely upregulate each other's populations through secretion of various cytokines such IL-17.

1.3.6 Programmed death ligand 1/2 (PD-L1/2)

A recent study has shown that most of ImCs and MDSCs expressed PD-L1 and CD80 but not PD-L2 (13). No significant differences were noted in the percentage of PD-L1 or CD80 positive cells within the populations of ImCs from

naïve mice and MDSCs from tumor-bearing mice (13). Further PD-L1 blockade *in vitro* or *in vivo* did not ameliorate MDSC associated T cell suppression (13). Lack of increased expression and no effect of PD-L1 blockade in MDSCs points to the fact that these molecules may have no role in MDSC mediated immune suppression in cancer (3, 13).

1.3.7 Indoleamine 2,3 dioxygenase (IDO)

IDO, an intracellular enzyme is a key regulator of tryptophan metabolism/catabolism (7). Tryptophan is essential for T-cell function and immune regulation (7). IDO expression depends on the pSTAT3 (7). L-tryptophan starvation inhibits T cell proliferation by activating GCN2 kinase and causing cell cycle arrest. Depletion of tryptophan can induce T cell anergy and direct CD4 T-cell differentiation towards Tregs by Foxp3 upregulation (6). IDO was found to be increased in M-MDSCs isolated from both chronic lymphocytic leukemia (CLL) patients and patients after allogeneic hematopoietic stem cell transplantation (allo-HCT) (7).

1.3.8 Inhibition of NK cell activity

MDSCs have also been shown to have potent NK cell inhibitory activity (10). M-MDSCs efficiently block NK cell proliferation, cytokine production, and cytotoxicity (12). Murine studies have demonstrated an inverse correlation between NK cell activation and MDSC frequency (12). NK cell inhibitory activity of MDSCs is not mediated by ARG, iNOS, or IDO, but required MDSC-NK cell

contact involving the NK cell activating receptor NKp30 (12, 19). Furthermore, MDSCs block perforin and NKG2D expression, and IFN-γ production both *in vitro* and *in vivo* (12). *In vitro* studies have demonstrated that blockade of NKp30 and depletion of MDSCs can reverse MDSC suppressive activity on NK cells (19).

1.3.9 Cysteine depletion

MDSCs also deplete cysteine in the TME, another amino acid essential for T cell activation, proliferation, and differentiation (1, 28, 42). Cells are able to import cystine (an oxidized form of cysteine) from exogenous sources either through the cysteine-glutamate (XC) transporter or from the conversion of methionine by cystathionase (6). However, T cells lack both and are entirely dependent on cysteine in the environment which is normally produced by mature DCs and macrophages during antigen presentation (1). During this process, antigen presenting cells (APCs) release reduced cysteine in the extracellular space through the alanine-serine-cysteine (ASC) transporter which can then be taken up by T cells. However, MDSCs express xc-transporter allowing for the uptake of cystine but lack ASC transporter to export cysteine and do not express cystathionase. This results in sequestration of cysteine in the MDSCs, thereby limiting the availability of this essential amino acid required for T cell function (6, 34).

1.3.10 Other mechanisms of T cell suppression

PGE2 produced by the cancer cells via COX-2 has been shown to be an important stimulus for Arg1 expression. COX-2 has also been to shown to be overexpressed in MDSCs. Studies have shown that COX-2 inhibitors *in vitro* and *in vivo* improve anti-tumor T cell immune responses (34).

MDSC also play an important role in tumor progression and angiogenesis through expression of VEGF and MMP9. A recent study has revealed a more direct role of MDSC in tumor vascularization. MDSCs when co-injected with tumor cells lined the endothelial walls of newly formed tumor vasculature and differentiated into cells with endothelial cell characteristics (12).

M-MDSCs isolated from prostate cancer patients expressed high levels of IL-10 while in melanoma patients they expressed high levels of TGF-β (12). TGF-β expression has direct effect on T cell proliferation. It results in cell cycle arrest typically in the G_1 phase through the expression of the cell cycle inhibitors p27Kip1 and p21Cip1 or by inhibiting IL-2 secretion (6). TGF-β has also been shown to inhibit the differentiation of CD4 T cells into Th1 or Th2 cells by suppressing the expression of T-bet and GATA-3 respectively (6). TGF-β-producing MDSCs promote the clonal expansion of antigen-specific natural Treg cells and induce the conversion of naïve CD4 T cells into induced Treg cells (6).

MDSCs also down-regulate the expression of the lymph node homing receptor, CD62L on CD4 and CD8 T cells. As consequence, T cells do not migrate to lymph nodes where they would otherwise undergo activation (1).

1.4 Clinical relevance of increased MDSCs in cancer

Numerous studies have demonstrated an increase in MDSC population in patients with cancer (9, 11, 13, 17). However, significant difference is only observed between patients with advanced tumor and healthy donors while patients with stage I/II cancers have moderately increased percentage and absolute number of circulating MDSCs (13, 22). There is a significant correlation between circulating MDSC, and clinical cancer stage and prognosis (2, 10, 12, 13, 15, 17, 21, 50, 52). Patients with extensive metastatic tumor burden have the highest percent and absolute number of MDSCs (10, 13). MDSCs are increased in patients with different cancers such as breast, bladder, gastrointestinal, head and neck, hepatocellular, non-small cell lung, prostate and thyroid cancers, melanoma, multiple myeloma (MM), ovarian carcinoma, RCC, glioblastoma and sarcoma (**Fig. 5**) (1, 2, 4, 6, 7, 10, 12, 15, 17, 19, 22, 28, 51, 52).

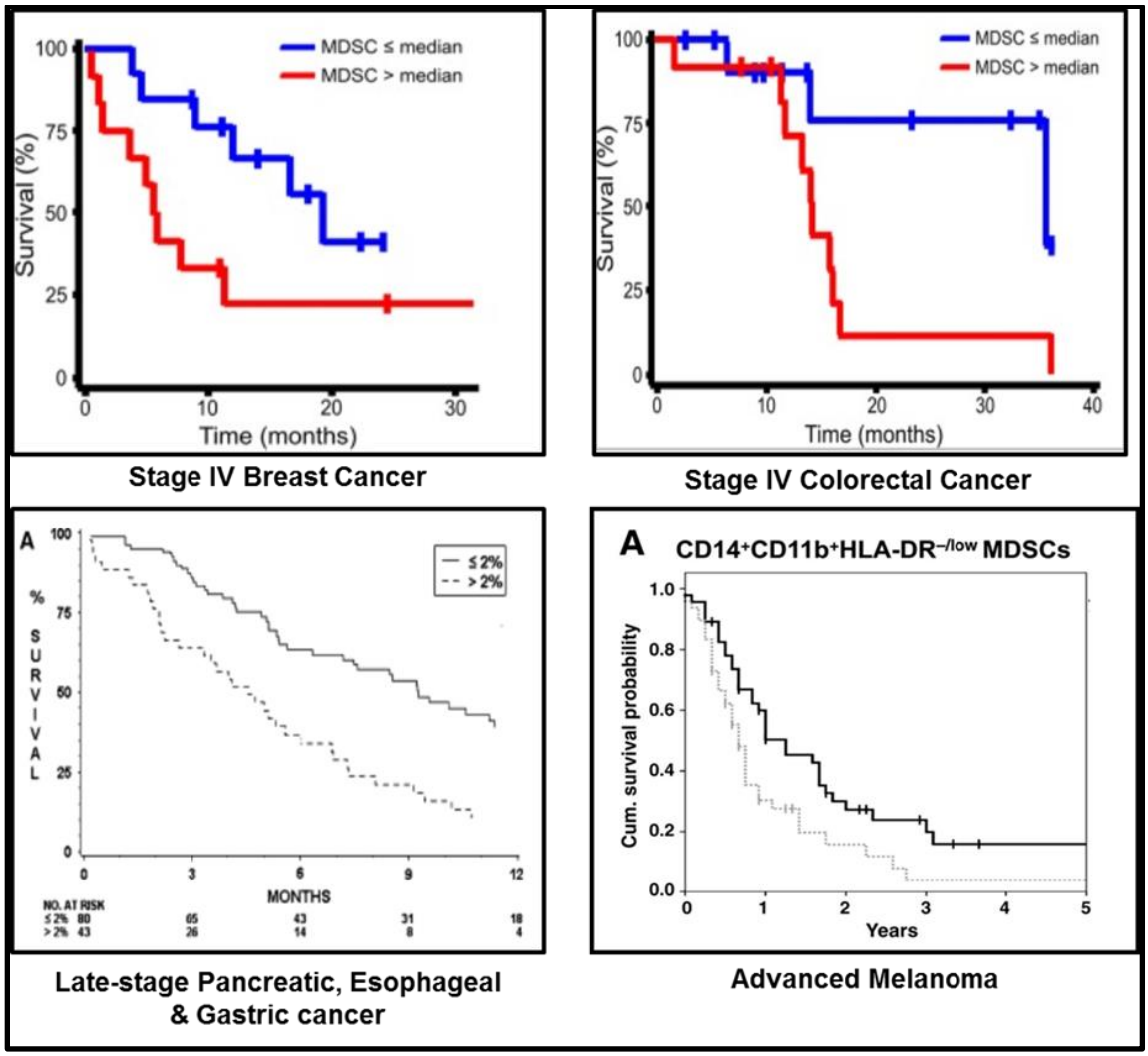

Figure 5. High MDSC count is inversely correlated with overall survival (OS) (2-4)

Studies have shown that if tumor-derived MDSCs were placed in culture conditions without TDSFs or injected into tumor-free recipients, they differentiate into mature functionally competent macrophages (MΦ) and DCs (24). This is consistent with observations that surgical removal of tumors result in elimination or decrease in MDSCs (15, 24). Also, these cells express no suppressive activity compared to MDSCs from patients with active disease (15). It has also been observed that antibody-mediated depletion of MDSCs restores T cell frequency

and function (5). In a study of patients with newly diagnosed stage I-IV solid cancers, circulating M-MDSCs levels prior to the start of treatment were found to correlate both with clinical stage ($p < 0.0001$) and metastatic burden ($p < 0.01$) (28). Also, patients with radiographic evidence of disease progression had increased levels of circulating MDSCs while the patients who responded to treatment had decreased MDSCs (28).

In melanoma, M-MDSCs ($CD14^{pos}HLA\text{-}DR^{low/neg}$) population is expanded in the peripheral blood and is associated with CD4 and CD8 T cell suppression, decreased IFN-γ production and decreased OS (2, 10, 15, 26, 39, 50, 52). Studies have shown that in patients with malignant melanoma, even at the physiologically low MDSC to T cell ratio of 1:4; MDSCs suppressed T cell proliferation and IFN-γ production by 40% (15, 17, 26). Recent studies have also suggested that increased numbers of pretreatment MDSCs and Tregs, and high levels of lactate in patients with advanced melanoma predicts poor response to ipilimumab (Yervoy®) (2, 7, 56).

Studies have reported that the presence of increased number of MDSCs predicted poor OS in breast, colon, esophageal, gastric and pancreatic cancer patients (**Fig. 5**) (12, 22). In another study of patients with pancreatic cancer, high $CD14^{pos}$ cells to CD8 ratio in the tumor infiltrates correlated with a significantly reduced OS (7). In HCC, impaired DC function correlated with the presence of $CD14^{pos}HLA\text{-}DR^{low/neg}$ M-MDSC cell population (19).

Different studies have shown the increased presence of both PMN- and M-MDSCs in patients with RCC (15, 22). This increase was negatively

associated with OS in the retrospective analysis of RCC patients (22). Circulating M-MDSCs and Tregs are increased in patients with metastatic prostate cancer (mPC) compared to healthy donors and negatively correlates with OS (6, 52). Further, M-MDSCs isolated from patients with mPC express significantly high levels of iNOS compared with healthy donors (6, 52).

A recent study reported that the suppressive activity of human MDSCs resides in a $CD14^{pos}S100A9^{pos}$ inflammatory monocyte or M-MDSC population in non-small cell lung cancer (NSCLC) patients (22). Ovarian carcinomas recruit $CD14^{pos}$ cells that inhibit T cell proliferation and negatively correlate with OS and DFS in both primary and metastatic ovarian cancers (10).

In MM, $CD14^{pos}$HLA-$DR^{low/neg}$ M-MDSCs are significantly increased in both PB and bone marrow of patients with active disease compared with healthy donors (15, 52). These cells also possess more pronounced inhibitory capacity compared to cells with similar phenotype from healthy donors (15, 52). Furthermore, studies have demonstrated a bidirectional relationship between MDSCs and MM cells and immune effector cells. MDSCs induce MM growth and suppress T cell activity. While MM cells induce the development of MDSCs from healthy donor peripheral blood mononuclear cells (PBMCs) (45).

In patients with chronic myelogenous leukemia (CML), percentage of M-MDSCs was higher in high risk compared to those with low risk patients and correlated with decreased OS (7). In CLL patients, expansion of M-MDSCs was associated with decreased T-cell proliferation in a dose-dependent manner and

its levels negatively correlated with the absolute number of circulating T-lymphocytes (7).

1.5 Pharmacological interventions targeting MDSCs

In mouse tumor models, it has been shown that T cell function can be restored, and tumor growth and development delayed by blocking MDSC suppression or through their depletion (15). Elimination of MDSC accumulation in tumors can help overcome T cell resistance (intrinsic resistance), improve anti-tumor immunity and further potentiate T cell response to immune checkpoint blockade therapies such as anti-PD1/PD-L1 and anti-CTLA4 mAbs.

To this end, various therapeutic strategies targeting MDSCs as an adjunct to conventional and immune therapies are being studied. These strategies have been broadly placed into four categories (30);

a. Deactivation of MDSC immune suppressive function

Phosphodiesterase-5 inhibitors such as sildenafil deactivate MDSCs by interfering with Arg1 and iNOS expression (30, 57). Nitro-aspirin (NO-aspirin) interferes with MDSC NO metabolism (30). Synthetic triterpenoids deactivate MDSC by reducing ROS. COX2 inhibitors reduce MDSC suppressive function by decreasing expression of Arg1. N-hydroxy-L-Arginine (NOHA) and N(G)-Nitro-L-Arginine Methyl Ester (L-NAME) inhibit MDSC suppressive function by downregulating Arg 1 activity (30). Anti-glycan antibody and inhibitors of colony stimulating factors and their receptors block the migration of MDSC (30). Studies

have shown that histamine may stimulate GMCSF and IL-6 production via H1 and H2 receptors on human PBMC in-vitro. Anti-histamines can block this activity and modulate MDSC suppressive function (30). IL-17 is important for recruitment of MDSCs to tumor sites. In tumor-bearing IL-17R and IFN-γR deficient mice, tumor development was inhibited which was associated with increased CTL infiltration of tumors and lower MDSC levels (30). A recent study showed that murine and human MDSC express Bruton's tyrosine kinase (BTK). BTK inhibitor, ibrutinib (Imbruvica®) was able to inhibit the phosphorylation of BTK in these cells which resulted in impaired NO production, migration, and generation of MDSCs *in vitro* (31).

b. Differentiation of MDSC into mature cells

Agents such as all-trans retinoic acid (ATRA) and vitamins such as vitamin D3 or A enhance maturation of myeloid cells. DNA fragments that contain high frequency of unmethylated deoxycytosine-deoxyguanine dinucleotide (CpG) motifs (common in bacterial and viral DNA) can stimulate maturation of immune cells via Toll-like receptor 9 (TLR9) (30). Anti-microtubular agent, paclitaxel has been recently shown to promote differentiation of MDSCs into DC *in vitro* in a TLR4-independent manner (57).

c. Inhibition of MDSC development

Nitro-Bisphosphonates (N-Bisphosphonates), platinum agents, and STAT3 inhibitors such as sunitinib (Sutent®) have been shown to block the formation of MDSCs.

d. Depletion of MDSC

Pyrimidine analogues like gemcitabine and 5-fluorouracil (5-FU), and anti-microtubule agents like docetaxel and paclitaxel have been found to reduce the number of splenic and tumor MDSCs without affecting the numbers of T cells, NK cells, macrophages, or B cells (5, 30, 57). Paclitaxel has also been shown to reduce Tregs and their inhibitory function (57). Treatment of tumor-bearing mice with ibrutinib resulted in a significant reduction of MDSC and improved the antitumor effect of anti-PD-L1 checkpoint blockade (31).

1.6 Overview of metabolism in cancer and immune cells

Otto Warburg in the early 20^{th} century made an observation that rat hepatoma tissue slices maintained a higher rate of glucose catabolism than normal liver tissues even in the presence of oxygen (58, 59). This phenomenon was then called the “Warburg effect” and provides the basis for 2-[18F]fluoro-2-deoxy-glucose positron emission tomography (PET) imaging (58, 59).

Supporting the energy needs of the cell with glycolysis alone is a wasteful process. Catabolism of 1 mol of glucose to lactate yields only 2 mol of ATP;

however, 38 mol of ATP are produced on complete combustion of glucose to carbon dioxide and water in the presence of oxygen (58, 59). Cancer cells need not only ATP, but also need biosynthetic precursors from glycolytic intermediates in order to proliferate and invade (32). High glycolytic flux to pyruvate/lactate observed in tumors not only provides a ready supply of fructose-6-phosphate (F-6-P) and glyceraldehyde-3-phosphate for shunting into de-novo nucleic acid synthesis but also decreases intracellular and extracellular pH, causing apoptosis in normal cells that express functional p53 (18, 32, 58-60).

Hexokinase (HK) phosphorylates glucose to form glucose-6-phosphate (G-6-P), which can be converted into glycogen, oxidized by the pentose phosphate pathway (PPP) to generate NADPH or F-6-P. HK is the first irreversible but not rate-limiting step of glycolysis (58, 59). However, 6-phosphofructo-1-kinase (PFK-1) is the irreversible and rate-limiting step of glycolysis which dictates the pace of glycolytic flux (**Fig. 6**) (58-60). PFK-1 activity is modulated by several allosteric effectors such as adenosine triphosphate (ATP), citrate and hydrogen (H^+) ions (58-60). ATP is the most potent inhibitor of PFK-1 and can directly inhibit PFK-1 as result of negative feedback when energy is abundant, also called the Pasteur effect (58, 59).

PFK-1 activity is markedly increased in cancer cell lines and primary tumor tissues in situ; and the oncogenes ras and src activate PFK-1 in immortalized cells (58, 59). Fructose-2,6-bisphosphate (F2,6BP) allosterically activates PFK-1 by shifting the conformational equilibrium of PFK-1 from a low to a high affinity state for F6P. F2,6BP can relieve the ATP induced allosteric inhibition of PFK1,

and thus allowing cancer cells to maintain high glycolytic flux despite the presence of physiologic ATP (58, 59).

The steady-state concentration of F2,6BP is maintained by a family of bifunctional enzymes called 6-phosphofructo-2-kinase/fructose-2, 6-bisphosphatases (PFK-2/FBPases), which phosphorylate F6P to F2,6BP or dephosphorylate F2,6BP back to F6P (**Fig. 6**) (58-60). The PFK-2/FBPases are encoded by four genes (PFKFB1–4). The enzymes encoded by the PFKFBi1, PFKFBi2 and PFKFBi4 genes display nearly equal kinase:phosphatase ratios. An inducible PFK2/FBPase encoded by the PFKFBi3 gene was recently identified to be activated by mitogenic, inflammatory and hypoxic stimuli and to display markedly reduced bisphosphatase activity (kinase:phosphatase ratio 740 : 1) (58, 59).

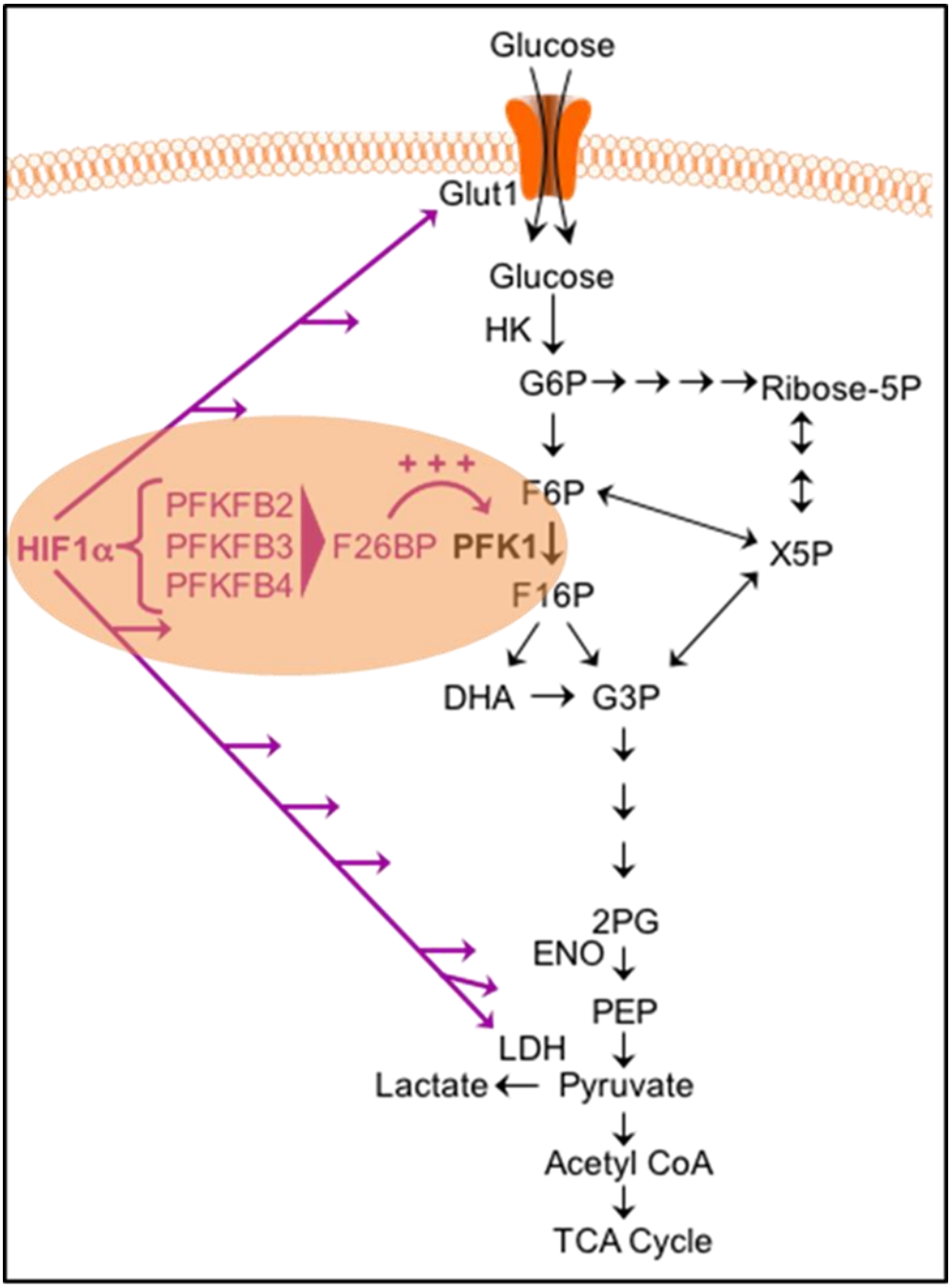

Figure 6. HIF-1α regulates the expression of PFKFB3 which synthesizes F26BP, a potent allosteric activator of PFK1.

Metabolic adaptation to hypoxia in cancer cells is largely mediated through upregulation of transcription factor hypoxia inducible factor 1 alpha (HIF-1α)

which promotes increased expression of various glucose transporters and glycolytic enzymes such as Glut1 glucose transporter, HK2, PFK-1, pyruvate kinase M2 (PKM2) and lactate dehydrogenase A (LDH A) (**Fig. 6**) (32, 58, 59, 61). Past studies have shown that exposure of Hep-3B human hepatoma cells to hypoxia or hypoxia mimics resulted in rapid induction of the PFKFB3 mRNA. This induction of PFKFB3 mRNA was completely abolished in mouse embryonic fibroblasts conditionally nullizygous for HIF-1α. This suggests that the induction of PFKFB3 mRNA may be an essential component to the HIF-1α mediated adaptive response to hypoxia. In addition to stabilization of HIF-1α, loss of tumor suppressor gene phosphatase and tensin homolog (PTEN), and activation of oncogenes such as rat sarcoma (Ras) and PKB/Akt result in increased activity of PFKFB3 in cancers (58-61). The role of PFKFB3 in cancer development and progression is now well established.

Upregulated aerobic glycolysis in immune cells was first reported in neutrophils. Activation of neutrophils resulted in upregulation of glycolysis, increased glucose consumption and increased oxygen consumption which was used primarily to produce ROS (62). It was shown that increased flux through the PPP generates nicotinamide adenine dinucleotide phosphate (NADPH), which is used by NOX enzymes to generate ROS (62-64). Studies evaluating the metabolic profile of macrophages and DCs have shown that inflammatory signals or activation is accompanied by increased glycolysis, lactate production and flux through PPP, and decreased oxygen consumption and TCA cycle activity (63, 65, 66). Enhanced PPP provides biosynthetic precursors for purines and

pyrimidines. In macrophages and DCs stimulated with LPS and IFN-γ, expression of iNOS is increased which inhibits mitochondrial respiration through NO and results in metabolic shift away from oxidative phosphorylation (63, 67, 68).

Bone marrow cells from naïve wild type mice cultured in the presence of GM-CSF and IL-6 result in generation of MDSCs which are functionally and phenotypically similar to tumor derived MDSCs. These BM-MDSCs express high levels of Arg1 and iNOS. This is accompanied by increased L-glutamine and glucose metabolism by anaerobic glycolysis which results in the accumulation of TCA or Kreb cycle intermediates and lactate, and upregulated production of energy-rich nucleotides (69). These data show that MDSC maturation and immunosuppressive potential are associated with an increase in the central carbon metabolism activity level and bioenergetic status (69).

Hammani *et al* showed that the increase in glucose uptake in BM-MDSCs resulted in cell specific concentration of F-6-P that was approximately 60% to 70% that of G-6-P suggesting an upregulation of glycolysis. This was further associated with increased glucose consumption rate at 72 hours and decreased cell respiration. AMP-to-ATP ratio was up to 5-fold higher than in the control culture. The lactate-to-glucose yield started to increase at 32 hours and peaked after 80 hours. Conversely, the lactate-to-glucose yield remained stable (69). This accumulation of glycolysis intermediates may suggest that cells continue producing these intermediates without consuming them which can be observed at the time of initiation of cell death. However, cells were found to be alive. L-Arg

and lactate were continuously produced, suggesting that cells consumed these intermediates to support both the catabolic processes and the sparse synthesis of anabolism-related macromolecules (69). These results support the studies done by Ando *et al.* where it was seen that IL-6 enhances the expression of the glycolytic enzymes HK2 and PFKFB3 in mouse embryonic fibroblasts via the IL-6/STAT3 pathway (69, 70). BM-MDSCs upregulate glycolysis despite non-limiting oxygen conditions and produce lactate rather than obtaining high energy yields from respiration.

Accumulation of TCA cycle intermediates such as fumarate and succinate is associated with the inhibition of HIF hydroxylases resulting in the stable expression of HIF-1α (24, 63). This is in concert with recent findings reported by Corzo *et al* that MDSCs express HIF-1α to adapt to the quasi-hypoxic conditions encountered in tumors (11). Decreased respiration in BM-MDSCs in the presence of GM-CSF and IL-6 is likely related to HIF-1α expression (69). Another study had demonstrated that monocytes exposed to hypoxia rapidly stimulate glycolysis by activating PFKFB3 through phosphorylation of serine (58). In addition, accumulation of fumarate suggests that L-Arginine is being continuously synthesized which supports a permanent immunosuppressive activity (69).

GM-CSF has been shown to induce a rapid glucose-dependent extracellular acidification that is regulated by protein kinase C (PKC) and the sodium/proton antiporter (69, 71). Furthermore, iNOS activity is associated with an increased glucose consumption rate, increased glycolysis and PPP, and the inhibition of oxidative phosphorylation in zymosan (a glucan with repeating

glucose units and aTLR2 agonist) treated macrophages (69). MDSCs tend to behave like tumors when it comes to their bioenergetics and metabolic needs. These findings substantiate the findings that M-MDSCs express and stabilize HIF-1α to help adapt to oxygen poor TME.

Another recent study demonstrated a link between upregulated glucose metabolism and fatty acid oxidation (FAO) to immunosuppressive phenotype of MDSCs (53, 69). Authors showed that this was accompanied by an increase in the mitochondrial mass, upregulation of the enzymes involved in glycolysis and FAO and increase in oxygen consumption rate (53, 69). Authors also demonstrated that pharmacologic inhibition of FAO blocked the immunosuppressive function of PMN-MDSCs resulting in delayed tumor growth and improved T cell activity (53).

Yet another recent study showed that the activation of the inflammatory response is accompanied by a metabolic shift to anaerobic glycolysis for the reasons as described above. Authors reported that mechanistic target of rapamycin complex 1 (mTORC1) -dependent glycolysis is critical for the lineage commitment of M-MDSCs but not PMN-MDSCs. It was observed that mTORC inhibition or deletion resulted in significant decline in glycolysis during MDSC differentiation as evidenced by the lower glucose uptake and glycolysis-related enzymes like HK1, HK2, PFK1, PKM2 and LDHA. 2-DG, which blocks HK activity significantly, inhibited M-MDSC development from bone marrow. On the other hand, metformin which is an enhancer of the glycolytic pathway significantly enhanced M-MDSC differentiation and rescued rapamycin-mediated poor

differentiation of MDSCs *in vitro* and *in vivo*. Thus, rapamycin is able to block M-MDSC differentiation from bone marrow precursors mainly through mTORC1-dependent glycolysis pathway (72).

Glycolysis results in the production of pyruvate and under normoxic conditions; pyruvate is converted to acetyl-CoA by the enzyme pyruvate dehydrogenase (PDH). Acetyl-CoA then enters into the TCA or Krebs cycle and results in the production of more ATP and other biosynthetic precursors. However, under anaerobic conditions, pyruvate is converted to lactic acid by the enzyme lactate dehydrogenase (LDH) (73). Tumors preferentially convert pyruvate into lactate instead of entering into the TCA cycle, even under normoxic conditions (73). In addition, lactate is also produced as a by-product of glutaminolysis where glutamine is converted to glutamate, then to α-ketoglutarate, followed by conversion into malate, which is then oxidized into pyruvate in the cytosol. This pyruvate is then converted to lactate allowing the coupled regeneration of NAD+ and the production of ATP via the glycolysis pathway. This allows cells to produce ATP under hypoxic conditions and places glucose, rather than fatty acids or amino acids, in the unique position of being essential for cells to survive (73-75). LDH-A is induced by different oncogenes, including c-myc and, thus, providing a link between malignant transformation and metabolic pathways (73, 76).

Lactate generation contributes to the acidic TME that increases the frequency of MDSC accumulation, induces tolerogenic T cells and decreased CTL and NK cell activity, stimulates angiogenesis and promotes metastasis (18,

32, 73). Lactic acid can also be actively produced in immune-regulatory myeloid cells by cytokine-activated, anaerobic glycolysis (33). Lactate accumulation affects DC maturation and results in the arrested development of APCs from myeloid progenitors (18, 32, 73). Further, it affects CTL activity through polarization of immune responses to a more pro-inflammatory profile consisting of Th17 and Th23 phenotypes (18, 32). Lactate can also induce transcription of Arg1 gene leading to increased arginase expression and suppressed T cell activity (73). Studies have also shown that when mice are subjected to a ketogenic diet, essentially a suboptimal surrogate for LDH-A inhibition, tumors have higher frequency of T effector cell infiltration further providing evidence that high lactate levels can effect T cell recruitment (77). Lactate has also been shown to be an endogenous inhibitor of histone deacetylases (HDAC), regulating the transcription of genes involved in metabolism and immune responses, such as natural cytotoxicity triggering receptor 1 (NCR1), which encodes NK-cell activating receptor (77). High levels of LDH or lactate in the peripheral blood of patients with advanced melanoma have been shown to predict poor outcome with ipilimumab (2, 56, 73).

1.7 Hypoxia

Hypoxia is one of the hallmarks of the tumor microenvironment (TME). It is the consequence of insufficient blood supply and rapid tumor growth. Subsequently, cells adapt to the low oxygen environment and upregulate the transcription of genes required for cell survival and metabolism under these

conditions. HIF-1α promotes the metabolic switch to glycolysis so cells can continue to produce ATP when oxygen is limited. HIF plays a critical role in the modulation of cellular responses, and recently, also the anti-tumor immune responses (37).

HIF-1α is a predominant oxygen sensing subunit in hematopoietic cells. HIF-1α activity is regulated by post-translational modification of oxygen-dependent degradation domain (ODD). When oxygen levels are above 5%, hydroxylation of the proline residues at positions 402 and 564 in the ODD enable binding of the ubiquitination ligase von Hippel-Lindau (VHL) tumor suppressor protein leading to the degradation of HIF-1α by the proteosome. However, at oxygen levels below 5%, hydroxylation is inhibited resulting in stabilization of HIF-1α allowing it to translocate to the nucleus, bind to HIF-1β and regulate transcription (37). In activated macrophages, it has been shown that mTOR helps cells meet high metabolic needs by increasing expression of HIF- 1α which then increases the expression of glycolytic and inflammatory genes (78, 79).

In anaerobic glycolysis, pyruvate, which is an end product of glycolysis is metabolized to lactate instead of feeding into the TCA cycle to boost subsequent oxidative phosphorylation (80). HIF-1α induces the expression of genes such as the glucose transporter GLUT1 and enzymes involved in glycolysis by binding to their hypoxia response elements (HRE) (81-83). It also induces the expression of LDH which catalyzes the production of lactate from pyruvate limiting the supply of acetyl-CoA for the TCA cycle (84). It has also been shown to suppress oxidative phosphorylation in mitochondria. (11). HIF-1α expression is also stabilized by the

lactic acid produced by anaerobic glycolysis in cancer cells (85). In macrophages, Colegio *et al* showed that lactic acid can stabilize HIF-1α even under normoxic conditions and stimulate the transcription of VEGF and Arg1 genes (85). Also in macrophages, it has been shown that iNOS is a hypoxia-inducible gene (86). Hypoxia induced iNOS-HRE activity and activated the iNOS promoter and induced iNOS transcription and mRNA expression (86). Based on data from studies done in macrophages, hypoxia appears to be a common denominator for the metabolic shift to glycolysis and production of lactic acid and ultimately upregulation of inflammatory genes such as Arg1 and iNOS (**Fig. 4**).

Hypoxia in the TME plays a critical role in the regulation of MDSC function via upregulation of HIF-1α. Exposure of splenic MDSCs to hypoxia can mimic the effects of the TME on these cells by inducing a dramatic up-regulation of iNOS and Arg1 expression and downregulation of NOX2 and ROS (10, 11, 15, 17, 21, 24, 25, 37, 42, 51, 55). Further, these cells functionally differentiate from antigen-specific to antigen-nonspecific T cell suppressors (Fig. 7) (10, 11, 15, 17, 21, 24, 25, 37, 42, 51, 55). TME due to hypoxia and low pH does not support the survival of PMN-MDSCs (24).

Further, under hypoxic conditions and in the presence of TDSFs, splenic M-MDSCs differentiate to tumor associated macrophages (TAMs) which express F4/80 in mice and CD68 in humans resulting in further immune suppression and a tolerogenic state (Fig. 7) (1, 11, 16, 17, 20, 24, 37). These macrophages do not show preferential polarization to either the M1 or M2 subtype and express high levels of genes associated with both such as CXCL10 and CD206 typical of M1

and M2 activation, respectively. HIF-1α-deficient MDSCs have reduced ability to differentiate in to macrophages and instead acquire markers of DC (8, 37).

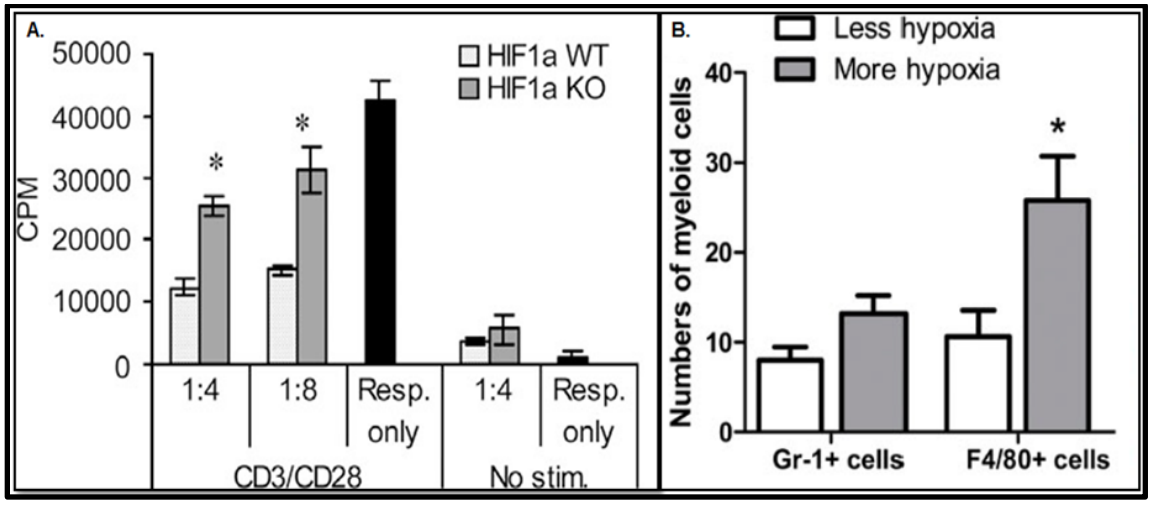

Figure 7. Hypoxia and MDSC. (A) MDSCs from HIF-1α knock-out mice result in reduced antigen non-specific suppression of T cells as compared to MDSCs from WT mice. (B) Hypoxia results in further expansion of MDSCs and macrophages (11).

Upregulation of HIF-1α inhibits effector functions of tumor-infiltrating lymphocytes (TILs), promotes development of Th17 cells and Treg recruitment to the tumor site (37). HIF-1α also regulates the expression of genes involved in angiogenesis, apoptosis, proliferation, cell cycle progression, cancer stem cell self-renewal and metastasis (37).

1.8 MDSCs – *in vitro* models

One of the major difficulties with MDSC studies is the ability to obtain adequate number of cells from *in vivo* models. Studies by Marigo *et al.* have demonstrated that the combination of GM-CSF and IL-6 can allow for a rapid

generation of MDSCs from mice and human bone marrow (14). In mice, these bone marrow derived MDSCs (BM-MDSCs) are highly tolerogenic, suppress T cell activity and have a functional phenotype similar to tumor MDSCs (14, 26, 69). In another study, GM-CSF and IL-6 combination was used to generate suppressive human $CD33^{pos}$ myeloid cells *ex vivo*. Following adoptive transfer, BM-MDSCs generated from mouse embryonic stem cells and bone marrow hematopoietic progenitor cells prevented alloreactive T-cell-mediated GVHD (87). LPS has also been shown to induce BM-MDSCs from bone marrow progenitor cells and on adoptive transfer suppressed allergen-induced airway inflammation in recipient mice (24). Mouse bone marrow-derived $IL4R\alpha^{pos}$ MDSC induced following incubation with GM-CSF+G-CSF or GM-CSF+IL-6 or IL-13 consist of a mixture of immature cells and exhibit immune suppressor activity (19). Human MDSCs induced following incubation of PBMC with GM-CSF+IL-6 or GM-CSF+IL-1β, PGE2, TNF-α and VEGF resulted in immune suppressive cells that were CD33, CD11b and CD66b positive and HLA-DR negative, and inhibited the proliferation and IFN-γ production by autologous human T cells after anti-CD3/CD28 stimulation (3, 19).

BM-MDSCs obtained following incubation with GM-CSF and IL-6 resulted in a significant upregulation of ARG1 and iNOS activity after 16 and 24 hours, respectively (69). This was followed by changes in glycolytic intermediates and cell respiration levels at 32 hours. BM-derived MDSCs exhibit immunosuppressive potential only after 48 to 72 hour exposure to cytokines (69).

Co-culture of $CD14^{pos}$ cells obtained from normal donor PBMCs with melanoma cell lines such as A375 or EST can allow for rapid generation of MDSCs *in vitro* (26, 50). On multicolor flow cytometry analysis, the percentage of $CD14^{pos}CD11b^{pos}CD33^{pos}HLA\text{-}DR^{low}$ cells was substantially increased in melanoma-monocyte co-cultures compared with that in monocytes cultured in the absence of melanoma cells (26, 50). $CD11b^{pos}$ cells purified from the melanoma-monocyte co-cultures exhibited a significant reduction in HLA-DR and increase in CD14, CD33, PD-L1, CD86 and DC-SIGN (CD209) markers (26, 50). Phenotype of A375-MDSCs was similar to circulating M-MDSCs obtained from late-stage malignant melanoma patients (26, 50). Separation of melanoma cells and monocytes in a transwell system did not result in the upregulation of CD14 or CD11b as compared with control cultured monocytes, which points to the fact that cell-to-cell contact or mechanisms that require close proximity to tumor cells were necessary (26).

Importantly, it should be noted that cryo-preservation can affect not only MDSC phenotype but also their functional activity. Studies have shown that MDSCs sorted from fresh blood samples of cancer patients suppressed the proliferation of autologous T cells. However, when MDSCs were isolated from frozen PBMCs, they failed to suppress T cell activity (7).

1.9 MDSCs in other disease states

MDSC are present in a low frequency in healthy individuals, but are increased in bacterial, viral and parasitic infections, and trauma to facilitate

wound healing (26). There is growing evidence that MDSCs play a central role in different models of autoimmune diseases such type 1 diabetes mellitus, auto-immune arthritis, colitis, alopecia areata, myocarditis, GVHD or experimental autoimmune encephalomyelitis (EAE) (19, 27).

Chronic infections such as trypanosomiasis, toxoplasmosis, candidiasis, and leishmaniasis results in expansion of M-MDSCs and mediates suppression through NO secretion (6, 49). In lupus-prone MRL-Faslpr mice, MDSC suppressive effect on CD4 T cell proliferation was blocked by an Arg1 inhibitor (49). Sepsis results in MyD88-dependent expansion of MDSCs, T cell suppression and Th2 polarization (49).

In an inflammatory bowel disease model, the repeated transfer of antigen-specific T cells resulted in an increase in the frequency of iNOS and Arg1-expressing MDSCs in spleen and intestine (49). However, co-transfer of MDSCs with specific CD8 T cells ameliorated enterocolitis suggesting a direct immunoregulatory effect of MDSCs (49). In a Theiler's murine encephalomyelitis virus mouse model of multiple sclerosis (MS), M-MDSC depletion resulted in an increase of virus specific CD4 and CD8 T cell responses, and an increased expression of IFN-γ and IL-17, and a decreased expression of IL-10 in the CNS (49). *In vivo* transfer of MDSCs ameliorated EAE which was followed by significantly decreased demyelination, and delayed disease onset through the inhibition of Th1 and Th17 immune responses (49). In obese mice, MDSCs have been shown to counter proinflammatory immune responses in the liver and adipose tissue through suppression of CD8 T cell proliferation, induction of

apoptosis, and skewed differentiation of macrophages into insulin-sensitizing, alternatively activated M2 macrophages (49). MDSCs together with Tregs are also involved in the regulation of immune response during organ transplantation and GVHD (49). MDSCs, generated *in vitro* or *in vivo*, alleviate GVHD in murine allogeneic bone marrow transplantation models (49). Studies have shown a significant correlation between the MDSC levels, disease progression, and the response of patients to antiviral therapy in patients with chronic Hepatitis C (49). In HIV, the presence of M-MDSCs in peripheral blood correlated with prognostic HIV-1 disease markers such as HIV-1 viral load and CD4 T cell loss. M-MDSCs from HIV-1 positive patients suppressed T cell responses in both HIV-1–specific and -nonspecific manners (49).

2.0 METHODS AND MATERIALS

2.1 Media and reagents

Tumor cell lines were cultured in Dulbecco's Modified Eagle Medium (DMEM) supplemented with 100 mg/ml penicillin and streptomycin (Gibco, Carlsbad, CA), 1% sodium glutamate (Gibco, Carlsbad, CA) and 10% heat-inactivated FBS (Life Technologies, Carlsbad, CA). Splenic MDSCs were cultured in Roswell Park Memorial Institute medium (RPMI) 1640 medium supplemented with 100 mg/ml penicillin and streptomycin, 1% sodium glutamate, 50 mM beta-mercaptoethanol (BME) (Gibco, Carlsbad, CA), and 10% heat-inactivated FBS. Bone marrow-derived MDSCs were cultured in the same media as for splenic MDSCs but with the addition of 50 µM HEPES. Human MDSC and $CD14^{pos}$ cells were cultured in Iscove's Modified Dulbecco's Medium (IMDM) supplemented with 100 mg/ml penicillin and streptomycin, 1% sodium glutamate, and 10% human AB sera (Sigma-Aldrich, St. Louis, MO).

2.2 Patient samples and cell lines

Peripheral blood was collected from 33 patients with stage III-IV melanoma, and from eight normal donors. Melanoma patients included in the study were treatment naïve or had not received any active treatment in the six months prior to when their samples were collected. Informed consent was obtained prior to patient sample collection by the staff of the JG Brown Cancer Center Biorepository and covered under University of Louisville IRB protocol number 08.0388. Peripheral blood mononuclear cells (PBMC) were isolated from the melanoma patients using cell preparation tube (BD Vacutainer® CPT™). For *in vitro* induction of human MDSC experiments, PBMC were isolated from normal donors by density gradient centrifugation (Ficoll-Hypaque, GE) within 2 hours of sample collection.

The melanoma cell lines A375 (ATCC® CRL-1619™) and B16-F10 (ATCC® CRL-6475™) were purchased from the ATCC and maintained in complete DMEM as described above. Cell lines were never cultured for longer than six to eight weeks. All of cell line stocks came from thawed vials that were frozen at passage two after they were received from the ATCC. A375 and B16-F10 cell lines were authenticated by the ATCC cell bank using short tandem repeat profiling.

2.3 Mice

Wild-type (WT) male C57BL/6 mice were purchased from Envigo (Dublin, VA) and the Jackson Laboratory (Bar Harbor, ME). Mice were six-eight weeks

old. OT-II CD4 ovalbumin TCR-Tg mice were purchased from the Jackson Laboratory. All mice were kept in pathogen free conditions and handled with the approval of the Institutional Animal Care and Use Committee at the University of Louisville (Louisville, KY).

2.4 Tumor models

C57BL/6 WT mice were injected subcutaneously (s.c.) with B16-F10 melanoma cell line (1×10^5/mouse) in to their left flanks. Tumor measurements were performed with digital calipers every three to four days. Mice were sacrificed at 18-21 days after tumor challenge or when the tumor diameter reached 15-18 mm in size. Tumor volumes were calculated based on the formula=length × width^2/2. Starting day 11 post-implantation, mice were given intra-peritoneal injections of PFK-158 (60 mg/kg) for a total of four doses at day 11, 13, 16 and 18. On day 19, spleens from vehicle control and PFK-158 treated mice were harvested and splenic M-MDSCs were sorted by magnetic bead separation for functional assay as described below.

2.5 Isolation of Splenic Myeloid Derived Suppressor cells (MDSCs)

Tumor-bearing C57BL/6 WT mice were sacrificed 18–21 days after tumor challenge. To collect MDSCs, single cell suspensions were prepared from spleens, and red cells were removed using ammonium chloride (ACK) lysis buffer. Post-ACK lysis, cells were washed twice with RPMI 1640 medium containing 10% FBS. Single-cell suspensions were then treated with Fc-blocker

for 10 minutes on ice. $GR1^{high}Ly\text{-}6G^{pos}$ PMN- and $GR1^{dim}Ly\text{-}6C^{pos}$ monocytic-MDSCs were isolated from the spleens using the mouse MDSC isolation kit (Miltenyi Biotec, San Diego, CA). The purity of cell populations was confirmed by flow cytometry and was >98%.

2.6 Hypoxic cell culture conditions

Freshly isolated M-MDSCs from the spleens of tumor-bearing mice were cultured for 16, 24 and 48 hours in 25% B16-F10 tumor cell conditioned media (TCCM) under normoxic and hypoxic conditions (1% oxygen with 5% carbon dioxide) as described previously (11). For functional assays, cells were cultured under normoxia, and hypoxia with and without addition of PFK-158 (5 µM) for 48 hours.

2.7 Mouse bone marrow–derived MDSCs (BM-MDSCs)

Tibias and femurs from C57BL/6 WT mice were removed using sterile techniques, and bone marrow was flushed with cold PBS. To obtain bone marrow–derived MDSCs, bone marrow cells were cultured for four days with GM-CSF (40 ng/mL) (Peprotech, Rocky Hill, NJ), and IL6 (40 ng/mL) (Peprotech, Rocky Hill, NJ), as previously described (14). Bone marrow cultures were treated with 0.1% DMSO (vehicle control) and PFK-158 on day zero and day three of the culture period. The dose of PFK-158 was 5 µM on day zero and 2.5 µM on day three. For functional assays, whole bone marrow-derived MDSCs were used.

Using mouse MDSC isolation kit (Miltenyi) both PMN- and M-MDSCs were sorted from these bone marrow cultures. Sorted cells were then treated with vehicle control (0.1% DMSO) and PFK-158 (5 μM) overnight and then used for functional assays and other mechanistic studies.

2.8 Melanoma patient MDSC

$CD14^{pos}$ monocytic MDSCs from melanoma patients were isolated from PBMC using anti-CD14 magnetic microbeads and the autoMACS Pro Separator (Miltenyi Biotec, San Diego, CA), per manufacturer's protocol. One million M-MDSCs were plated in complete IMDM per well in a six-well plate (BD Falcon) and treated with PFK-158 (5 μM) and DMSO (0.1% vehicle control) for 16-18 hours. For functional experiments, autologous T cells were isolated from PBMCs using the Pan T-cell Isolation Kit (Miltenyi Biotec).

2.9 *In vitro* generation of human MDSCs

One million $CD14^{pos}$ cells isolated from PBMCs from normal donors were co-cultured with 5×10^5 A375 melanoma cells in 3.5 mL complete IMDM per well in a six-well plate for three days (26). Tumor/monocyte co-cultures were treated twice with PFK-158 (5 μM on day zero and on day two) or 0.1% DMSO (vehicle control). A375 co-cultured monocytes (both vehicle control and PFK-158 treated) and control monocytes cultured without tumor cells were harvested by gently scraping after three days of culture and $CD11b^{pos}$ cells were purified by anti-$CD11b^{pos}$ microbeads and MS columns (Miltenyi Biotec). Further, A375

melanoma and $CD14^{pos}$ cells were co-cultured for three days without the addition of PFK-158. $CD11b^{pos}$ cells were purified as above and then treated with PFK-158 (5 μM) and vehicle control for 16-18 hours in 2 mL complete IMDM in six-well plates. Following day, cells were harvested and washed prior to functional assays and other mechanistic studies.

2.10 Functional Assays

Freshly isolated PMN- and M-MDSCs (1×10^6 cells/well) from the spleens of B16-F10 tumor bearing C57BL/6 WT mice were cultured in 1 mL complete RPMI and treated with PFK-158 (5 μM) or DMSO (vehicle control) for 16-18 hours in flat-bottom 24-well plate. Cells were harvested, washed and then co-cultured with splenocytes from OT-II mice in triplicates in flat-bottom 96-well plates in the presence of the ovalbumin (200 μg/mL; Sigma-Aldrich) at 1:2, 1:4 and 1:8 ratios for an additional 72 hours. Eighteen hours before harvesting, co-cultures were pulsed with [3H]-thymidine (1 uCi/well; MP Bioscience). [3H]-thymidine incorporation was counted using a liquid scintillation counter and relative counts per minute (cpm) were used to determine percent inhibition of proliferation. Similarly, whole bone marrow-derived MDSCs were co-cultured with splenocytes from OT-II mice in the presence of ovalbumin at 1:4, 1:8 and 1:16 ratios for 72 hours and then pulsed with [3H]-thymidine eighteen hours prior to harvesting. Percent inhibition of proliferation was determined as above.

To determine the suppressive activity of PMN- and M-MDSCs sorted from bone marrow-derived MDSCs, and splenic M-MDSCs cultured under hypoxic

conditions, both treated and non-treated cells were co-cultured with 5 mmol/L carboxyfluorescein succinimidyl ester (CFSE, Invitrogen) labelled splenocytes from C57BL/6 WT mice in an anti-CD3 coated flat-bottom 96-well plate for 72 hours with addition of anti-CD28. Cells were then harvested and stained with CD4 and CD8 APC flourochrome (Biolegend, San Diego, CA), and proliferation was measured using flow cytometry.

To evaluate the suppressive functions of melanoma patient–derived MDSCs and A375-MDSCs, autologous T cells were labeled with 5 mmol/L CFSE and seeded at 100,000 cells per well in a 96-well U-bottom plate. For melanoma patient samples, $CD14^{pos}$ cells pretreated with vehicle control and PFK-158 (5 μM) for 16-18 hours were added to T cells at 2:1 and 1:1 ratios. T cells were activated by the addition of anti-CD3/CD28 monoclonal antibody (mAb) coated beads (Invitrogen) per well for four days. T-cell activation was measured by flow cytometry, and IFN-γ concentrations in the supernatants were determined by ELISA. Controls included non-activated T cells or T cells activated with beads alone. For A375-MDSCs, $CD11b^{pos}$ cells purified from tumor co-cultures with vehicle control and PFK-158 treatment or $CD11b^{pos}$ cells treated with PFK-158 post-purification were added to T cells at ratios of 1:1 and 1:2, and T-cell activation was measured as above.

2.11 Arginase assay

Arginase activity was quantified in cell lysates by measuring the production of urea using the QuantiChrom™ arginase assay kit as per

manufacturer's instructions (DARG-200, BioAssays Systems). One million cells per condition were lysed for 10 minutes in 100 µL of 10 mM Tris-HCl (pH 7.4) containing 1 µM pepstatin A, 1 µM leupeptin, and 0.4% (w/v) Triton X-100. Cell lysates were centrifuged at 14,000 g at 4˚C for 10 min. Supernatants were used to measure arginase activity following incubation with arginase reaction mix and urea reagent. OD was measured at 430 nm.

2.12 Nitric oxide assay

Supernatants from PFK-158 and vehicle control treated cell cultures were collected. To detect nitric oxide (NO), equal volumes of culture supernatants (100 µl) were incubated with Greiss reagent (Sigma Aldrich) at room temperature (RT) for 15 minutes in a 96-well plate. Absorbance at 550 nm was measured using a microplate plate reader (BioTek, Winooski, VT). NO concentrations were determined by comparing the absorbance values for the test samples to a standard curve generated by serial dilution of 0.25 mM sodium nitrite.

2.13 ROS detection

Oxidation-sensitive dye dichlorodihydrofluorescein diacetate (DCFDA, Molecular Probes/Invitrogen, Carlsbad, CA), was used to measure ROS production by MDSCs. Cells were incubated at 37°C in RPMI in the presence of 5 µM DCFDA for 30 min. For induced activation, cells were simultaneously cultured, along with DCFDA, with 30 ng/ml phorbol 12-myristate-13-acetate

(PMA) (Sigma, St. Louis, MO). The mean fluorescence intensity (MFI) of intracellularly retained DCF in $CD14^{pos}$ cells was determined by flow cytometry.

2.14 Lactate assay

Lactate production was measured using colorimetric assay (Biovision, CA). Supernatants collected from the PFK-158 and vehicle treated groups were filtered through a 10 kDa molecular weight spin filter (Amicon Ultra) to deproteinize and remove LDH present in FBS containing medium and diluted in dH_2O. Equal volumes (50 µL) of the supernatants were incubated with reaction mix containing the assay buffer, enzyme mix and probe at RT for 30 min. Absorbance at 570 nm was measured using a microplate plate reader (BioTek).

2.15 F-2,6-BP assay

Intracellular concentration of F-2,6-BP was determined based on previously described protocol (88). Briefly, cells were washed in PBS and lysed in NaOH/Tris acetate by heating at 80°C for 5 minutes. Lysates were neutralized to pH 7.2 by adding ice-cold acetic acid and HEPES. Samples were incubated at 25°C for 2 minutes in the following assay mixture: 50 mM Tris, 2 mM Mg^{2+}, 1 mM F6P, 0.15 mM NAD, 10 U/l PPi-dependent PFK-1, 0.45 kU/l aldolase, 5 kU/l triosephosphate isomerase and 1.7 kU/l glycerol-3-phosphate dehydrogenase (Sigma). In total, 0.5 mM pyrophosphate was added and the rate of change in absorbance (OD=339 nm) per minute was followed for 5 minutes. F-2,6-BP was

calculated based on a calibration curve produced by measuring 0.1 to 1 pmol of F-2,6-BP (Sigma) and normalized to total cellular protein.

2.16 Glucose uptake assay

Glucose uptake in cells was measured using cell-based glucose uptake assay kit (Abcam, ab204702). Bone marrow-derived M-MDSC (2×10^6 cells) were cultured in 400 µL of RPMI medium with 0.5% FBS with vehicle control and PFK-158 for one hour at 37˚C with 5% CO_2. Cells were then centrifuged at 400 x g for 5 minutes, media was removed and 400 µL of glucose uptake mix containing 376 µL of RPMI with 0.5% FBS, 4 µL of glucose tracker reagent, 20 µL of glucose tracker enhancer, and PFK-158 and vehicle control was then added and cells incubated for additional 30 minutes under same conditions. Cells were then washed with ice cold analysis buffer and flow cytometry analysis was performed where MFI was quantified in FL1 channel.

2.17 Bioenergetic analysis

The Seahorse XF96e Extracellular Flux Analyzer (Seahorse Bioscience, North Billerica, MA) was used to perform bioenergetic analysis of MDSCs. The Extracellular Flux Analyzer enables simultaneous live cell measurement of oxygen consumption rate (OCR) which is an indicator of mitochondrial respiration, and extracellular acidification rate (ECAR) which is an indicator of net proton loss during glycolysis. Bioenergetic analysis was performed comparing fresh bone marrow cells and fresh $CD14^{pos}$ monocytes to their respective *in vitro*

induced MDSC counterparts and between vehicle and PFK-158 treated MDSCs. Cells were seeded in growth media (1×10^5 cells/well) into the XF96e cell culture plate and allowed to loosely attach for 1-2 hours. Cell culture media was then gently replaced with XF media (Seahorse Bioscience), lacking sodium bicarbonate and FBS, after prior washing with XF media. Cell culture plate was placed in a non-CO_2 37°C incubator for 1 hour, prior to start of the experiment. OCR and ECAR were measured over a 3 or 5 minute periods, followed by 3 or 5 minute mixing and re-oxygenation of the media. Basal rate measurements were taken prior to injection of pharmacological manipulators of mitochondrial respiratory chain proteins. Following the determination of basal OCR reading, oligomycin A is applied to inhibit proton (H^+) flow through ATP synthase, essentially blocking all ATP-linked oxygen consumption. Maximal respiration is initiated by exposing cells to carbonyl cyanide-ptrifluoromethoxyphenyl hydrazone (FCCP), an ionophore that transports H^+ across the mitochondrial membrane leading to collapse of membrane potential and rapid consumption of O_2. Antimycin A prevents mitochondrial respiration by blocking complex III (Ubiquinone:Cytochrome b-c complex). Program was set to first inject 1 µM oligomycin A (Sigma), followed by 750 nM FCCP (Sigma) and at last, 1 µM antimycin A (Sigma) was injected. Three measurements of OCR/ECAR were obtained following injection of each drug.

2.18 Western blotting

Cells were lysed with radioimmunoprecipitation assay (RIPA) buffer in the presence of protease and phosphatase inhibitors. Protein lysates were subjected to 8-20% gradient SDS-PAGE gel (BioRad) and transferred to PVDF membranes. Membranes were probed with appropriate specific antibodies overnight at 4°C. Membranes were washed and incubated for 2 hours at RT with secondary antibody conjugated with peroxidase. Results were visualized by chemiluminescence detection using Amersham ECL Prime western blotting detection reagent (GE Healthcare Life Sciences). To confirm equal loading, membranes were stripped and reprobed with antibody against β-actin (Santa Cruz Biotechonology, Santa Cruz, CA). Anti-arginase 1 antibody was obtained from Santa Cruz Biotechnology, anti-NOX2 and NOX4 antibodies were obtained from Cell Signaling Technology (Boston, MA), anti-HIF-1α antibody was obtained from Novus Biologicals (Littleton, CO) and anti-PFKFB3 antibody was obtained from Proteintech (Rosemont, IL).

2.19 ELISAs

IFN-γ concentration was measured using ELISA in the supernatants from T-cell:MDSC co-cultures using instructions as per the manufacturer. ELISA kit used was the human IFN-γ kit obtained from R&D Systems.

2.20 RNA extraction and quantitative real-time PCR

RNA was extracted from MDSCs using Trizol (Invitrogen, Frederick, MD) as per manufacturer's protocol. cDNA was synthesized using iScript cDNA synthesis kit (BioRad). Quantitative real-time PCR (qRT-PCR) was performed using TaqMan Universal PCR Master Mix (Applied Biosystems, Foster City, CA), and target gene assay mix containing sequence-specific primers and 6-carboxyfluorescein (6-FAM) dye–labeled TaqMan minor groove binder (MGB) probe (Applied Biosystems, Foster City, CA). Amplification with an 18S (Hs99999901.s1; VIC; Applied Biosystems) endogenous control assay mix was used for controls. qRT-PCR was carried out in triplicates for each sample. Data quantitation was performed using the relative standard curve method. Expression levels of the genes were normalized by 18S mRNA. The change in gene expression was measured by calculating the fold change in threshold (ΔΔCt), where $\Delta Ct = Ct_{\text{target gene}}$ minus $Ct_{\text{housekeeping gene}}$, $\Delta\Delta Ct = \Delta Ct_{\text{induced}}$ minus $\Delta Ct_{\text{reference}}$ and fold change = $2(-\Delta\Delta Ct)$. All primers used are listed in **Table 1**.

Table 1. Primers used in qRT-PCR analysis of different gene expressions in this study.

Genes	Primer ID	Dye
Mouse Arginase 1	Mm00475988_m1	FAM-MGB
Mouse iNOS/Nos2	Mm00440502_m1	FAM-MGB
Mouse LDHA	Mm01612132_g1	FAM-MGB
Human Arginase 1	Hs00163660_m1	FAM-MGB
Human iNOS/NOS2	Hs01075529_m1	FAM-MGB
18s	Hs99999901.s1	VIC-MGB_PL

2.21 Antibodies and flow cytometry

Untreated or PFK-158–treated murine and human MDSCs were stained using anti-mouse and anti-human antibodies according to the manufacturer's recommendations. Details on flow cytometry antibody panels are provided in Tables 2 and 3. We assessed the frequency and phenotype of MDSCs in all the models described above both in mice and humans. Cells were harvested, washed, counted and resuspended in FACS buffer. 0.5 million cells live cells (by trypan exclusion) were stained with multi-color Ab panel. Following the initial FSC/SSC discrimination to exclude dead cells and aggregates, the gate was set on $CD45^{pos}$ leukocytes to exclude the tumor cells and then on $CD11b^{pos}$ cells. Next, we gated on the subpopulations defined as MDSC in humans: CD14, CD33 and HLA-DR cells and their combinations (**Table 2**), and in mice: GR1 (**Table 3**). Gates were set based on isotype controls.

Table 2. Human MDSC flow antibody panel

Antibody Specificity/Marker Stained	Flurochrome	Source
CD4	APC	Biolegend
CD8	APC	Biolegend
CD11b	FITC	Biolegend
CD14	PE	Biolegend
CD33	PerCP-Cy5.5	Biolegend
HLA-DR	APC	Biolegend
CD45	APC-Cy7	Biolegend

Table 3. Mice MDSC flow antibody panel

Antibody Specificity/Marker Stained	Flurochrome	Source
CD11b	FITC	Biolegend
GR1	APC	Biolegend

2.22 Statistical analysis

GraphPad Prism 5.0 software (GraphPad Prism Software, Inc., La Jolla, CA) was used for all statistical analyses. Comparisons between groups were done by two tailed Student's *t* tests. For all tests, statistical significance was assumed where $p \leq 0.05$.

3.0 WORKING HYPOTHESIS AND RATIONALE

Immune checkpoint inhibitor therapies have shown great results in the treatment of malignant melanoma and lung cancer. However, immune suppressive cells such as Th17 cells, TAMS and MDSCs attenuate effective anti-tumor responses in many patients. MDSCs provide an important therapeutic target as they are responsible for T cell tolerance, angiogenesis and increased risk of metastasis.

Targeting of MDSCs has been very challenging especially due to lack of a unique marker and plasticity of MDSCs. Despite these limitations, numerous studies have demonstrated the varying degree of efficacy of different agents in modulating MDSC suppressive phenotype. Based on recent studies, it has been identified that HIF-1α is important for MDSC differentiation and function (11). In addition, it has been reported that monocytic MDSCs upregulate glycolysis for their metabolic and biosynthetic needs (72). These data provide substantial evidence that glucose metabolism in monocytic MDSCs can be targeted to modulate their immune suppression and improve anti-tumor responses.

We believe that MDSCs upregulate the expression of 6-phosphofructo-2-kinase/fructose-2,6-biphosphatase 3 (PFKFB3), and ultimately glycolysis (Fig. 8). This maintains a functional phenotype of MDSCs that suppress CD4 and CD8 T cell responses and result in poor anti-tumor responses (**Fig. 8**). We hypothesize that PFKFB3 blockade with small molecule inhibitor PFK-158 can modulate immune suppressive phenotype of MDSCs and result in improved anti-tumor immunity (**Fig. 9**).

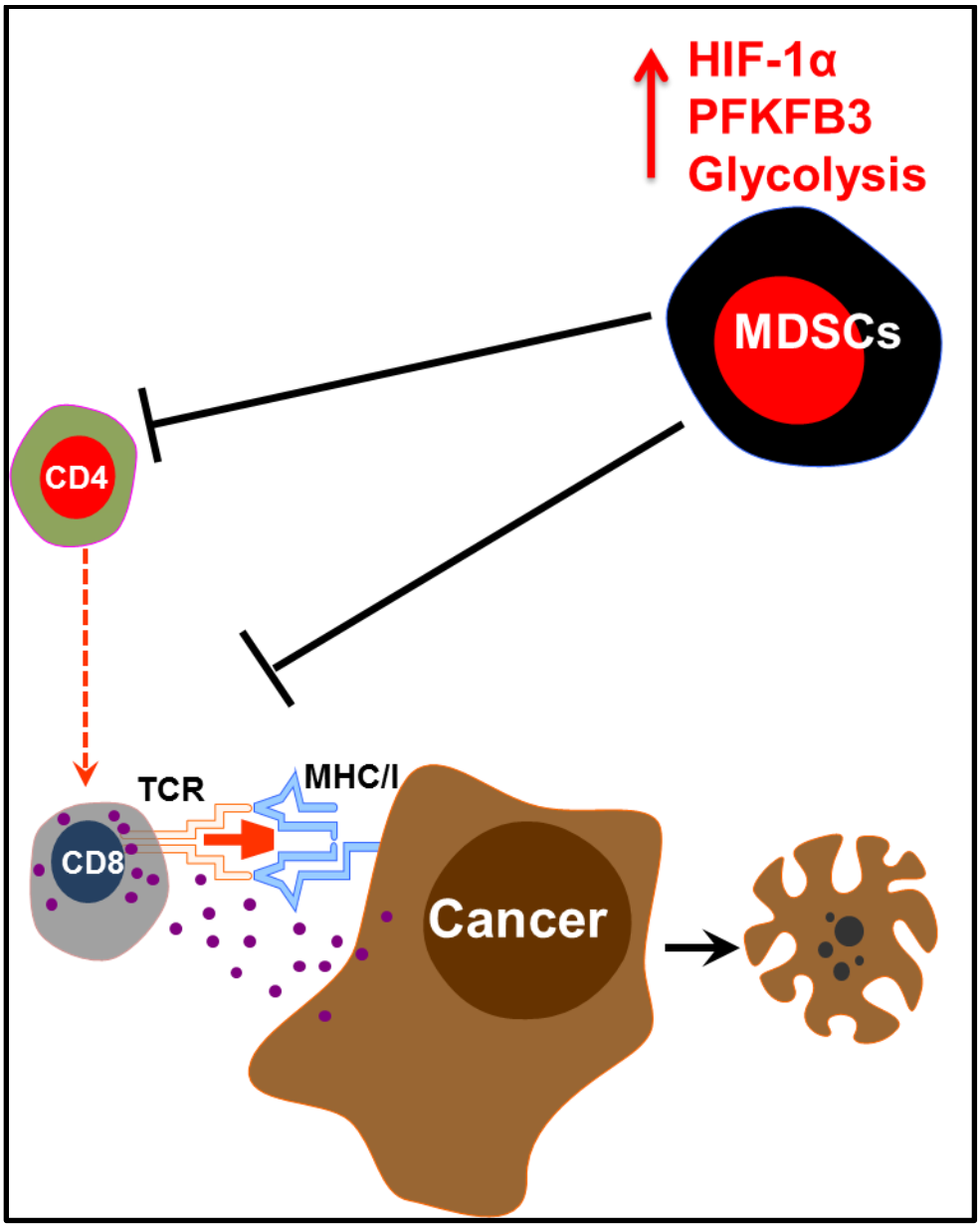

Figure 8. MDSCs upregulate the expression of PFKFB3 that results in an increased rate of glycolysis. This maintains a functional phenotype of MDSCs that suppress anti-tumor CD4 and CD8 T cell responses.

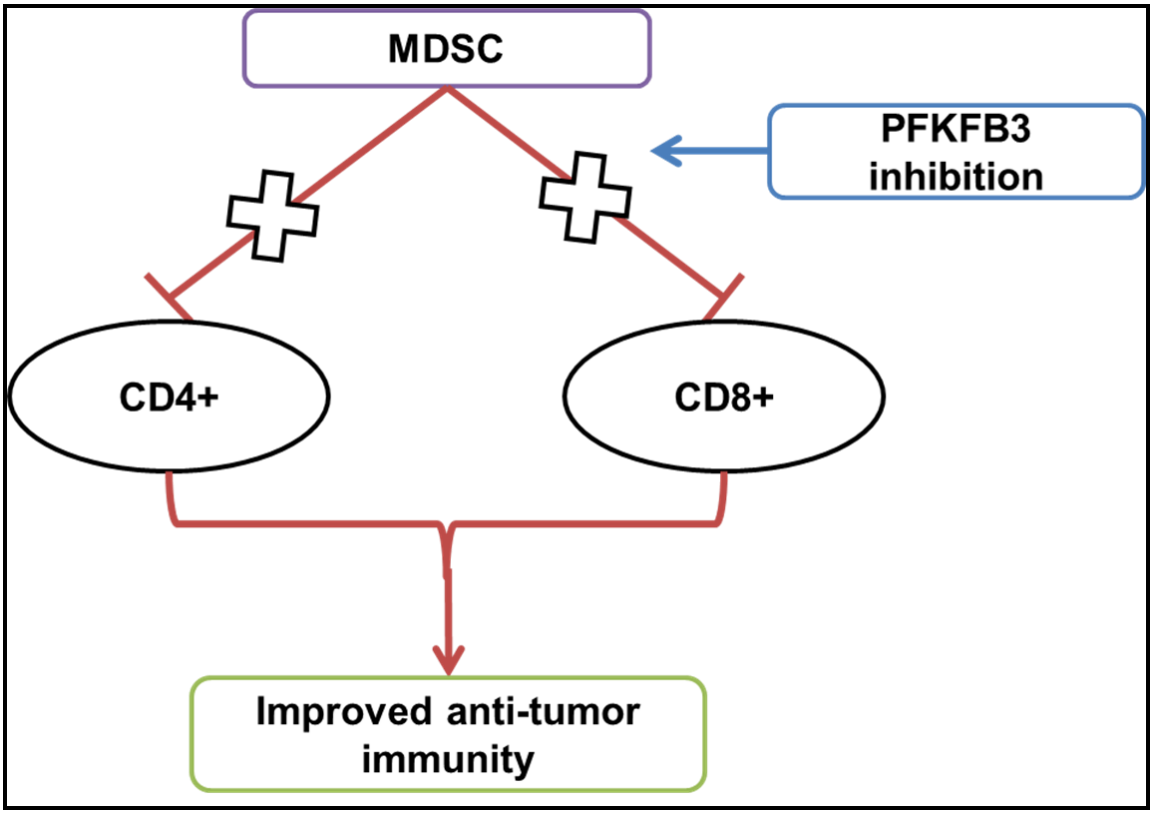

Figure 9. PFKFB3 inhibition will result in reduced MDSC mediated CD4 and CD8 T cell suppression and improved anti-tumor immunity in a tumor-bearing host.

4.0 RESULTS – MOUSE STUDIES

4.1 Both MDSC subsets, PMN- and M-MDSC expand in the spleens of tumor-bearing mice

In order to study the functional characteristics of MDSCs – both PMN- and M-MDSCs and perform mechanistic studies, C57BL/6 WT mice were subcutaneously injected with B16-F10 melanoma cells (1×10^5 cells per mouse) in their left flanks. Spleens from tumor-bearing mice were harvested at 18-21 days or when the tumor diameter reached 15-18 mm in size (**Fig. 10**). We then assessed and compared the frequency of both MDSC subsets in the spleens of naïve and tumor-bearing mice. Both MDSC subsets differentially expanded in the spleens of tumor-bearing mice compared with naïve mice (Fig. 11). Murine PMN-MDSCs are defined as $SSC^{high}CD45^{pos}CD11b^{pos}Ly6\text{-}G^{pos}$ and M-MDSCs are defined as $SSC^{low}CD45^{pos}CD11b^{pos}Ly6\text{-}C^{pos}$ (**Fig. 10**).

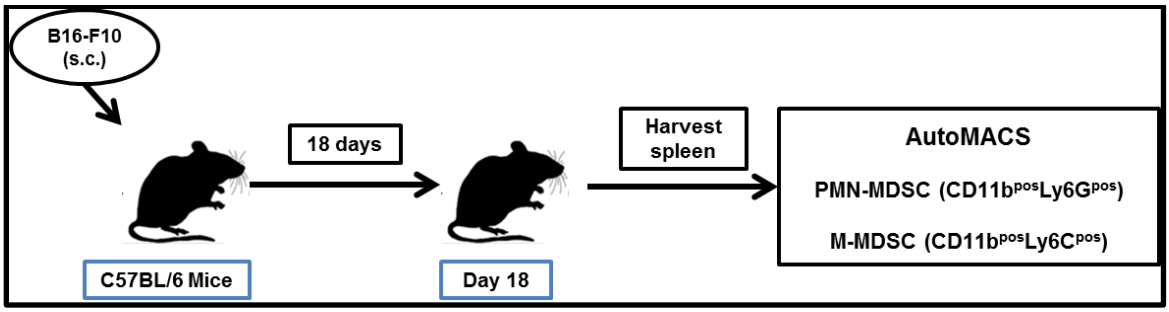

Figure 10. Schematic representation of the steps involved in the sorting of PMN- and M-MDSCs from the spleens of B16-F10 tumor bearing mice. Six-eight week old male C57BL/6 WT mice were injected subcutaneously with 1 × 10^5 B16-F10 melanoma cells. After 18 days or when the tumor diameter reached 15-18 mm in size, spleens from these tumor bearing mice were harvested. PMN- and M-MDSCs were sorted using mouse MDSC isolation kit as per manufacturer's protocol (Miltenyi Biotec).

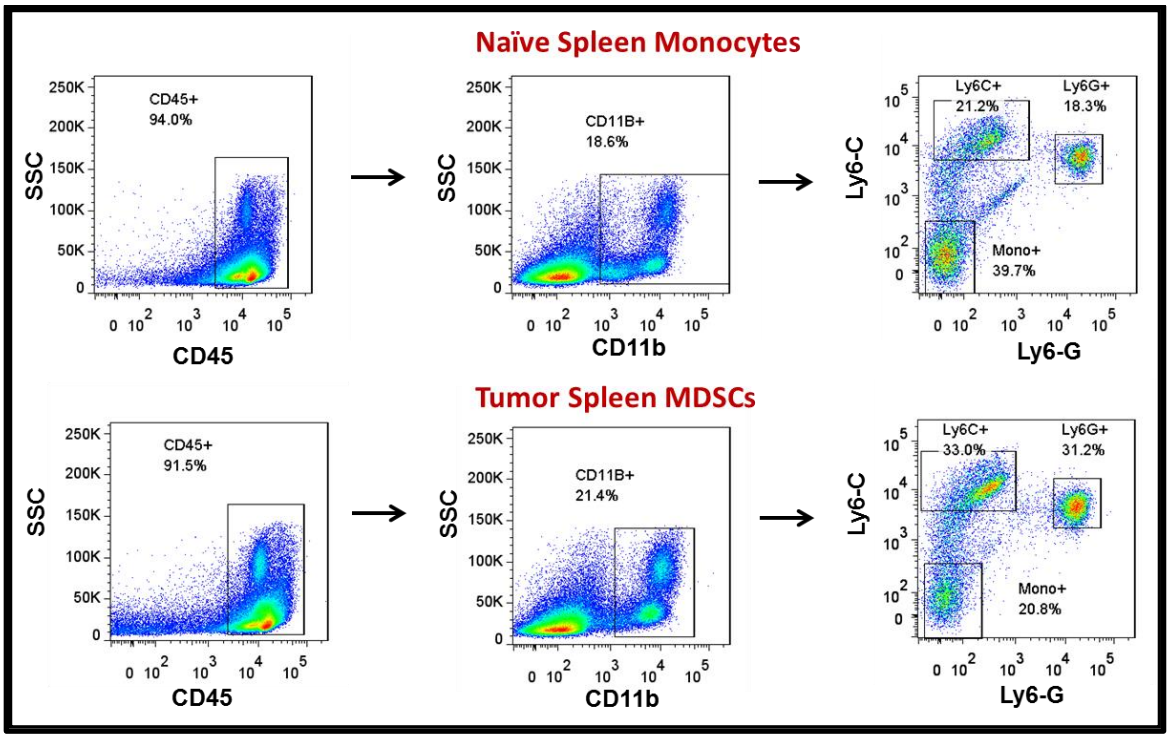

Figure 11. MDSC subsets differentially expanded in the spleens of tumor-bearing mice compared with naïve mice. C57BL/6 WT mice were subcutaneously implanted with B16-F10 melanoma (1×10^5 cells per mouse) and spleens were harvested at day 18 or when the tumor diameter reached 15-18 mm in size. Representative dot plots of the frequencies of PMN-($SSC^{high}CD11b^{pos}Ly6\text{-}G^{pos}$) and M-MDSCs ($SSC^{low}Cd11b^{pos}Ly6\text{-}C^{pos}$) in naïve and tumor-bearing mice spleens.

4.2 PFKFB3 is over-expressed in splenic M-MDSCs from B16-F10 tumor bearing mice

Western blot was performed to determine the expression of PFKFB3 in both MDSC subsets from both naïve and tumor-bearing mice. We found that PFKFB3 is significantly over-expressed in M-MDSCs sorted from the spleens of B16-F10 tumor-bearing mice compared with M-MDSCs sorted from the spleens of naïve mice (**Fig. 12A and B**). However, in PMN-MDSCs there was no difference in PFKFB3 expression between the naïve and tumor-bearing mice (**Fig 12C**).

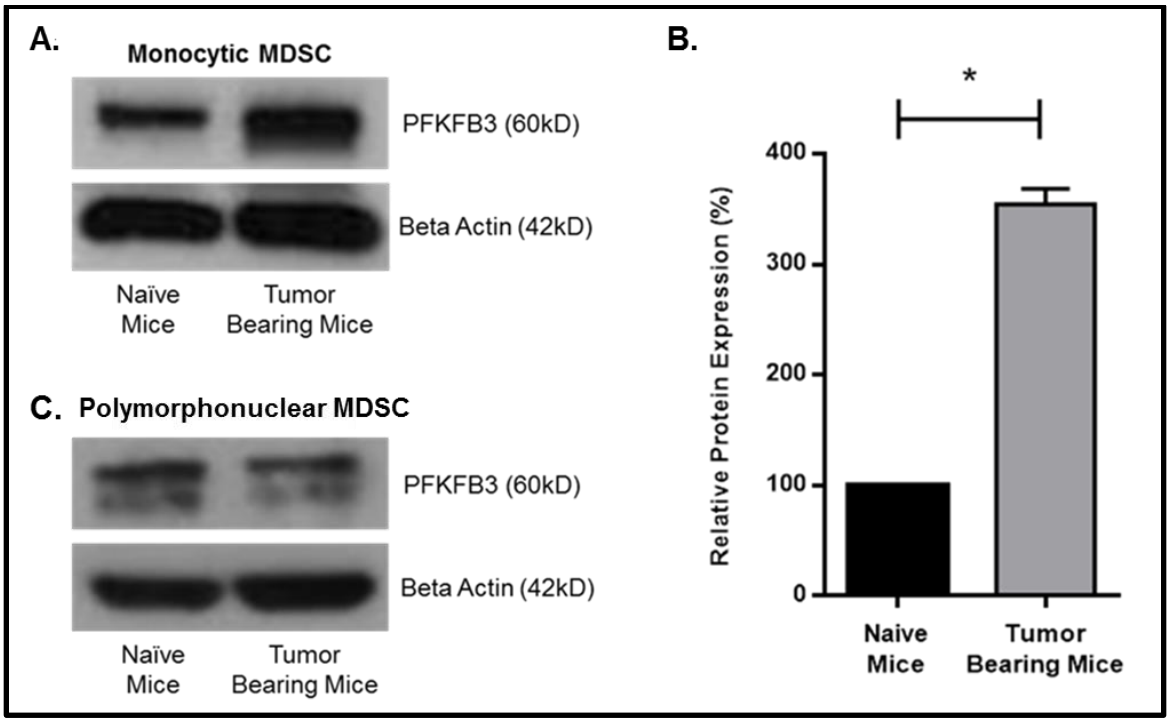

Figure 12. PFKFB3 is over-expressed in splenic M-MDSCs from tumor-bearing mice. PMN- and M-MDSCs were sorted from the spleens of naïve and B16-F10 tumor-bearing mice using magnetic bead sorting as per manufacturer's protocol (Fig. 9). Using western blot, expression of PFKFB3 was determined in (A) M- and (C) PMN-MDSCs from the spleens of naïve and B16-F10 tumor-bearing mice. (B) Representative bar graph of relative expression of PFKFB3 in M-MDSCs from naïve and B16-F10 tumor bearing mice determined using ImageJ® software. Results are representative of three independent experiments.

4.3 PFKFB3 inhibition with PFK-158 reduces M-MDSC suppressive activity

MDSCs circulating in the peripheral blood or in the peripheral lymphoid organs such as spleen result in antigen specific T cell suppression. To this end, we first wanted to determine if PMN- or M-MDSCs sorted from the spleens of B16-F10 tumor-bearing mice suppressed OVA-specific T cell proliferation. Next, we wanted to determine if PFKFB3 inhibition with PFK-158 resulted in reduced MDSC antigen specific T cell suppression (**Fig. 13**). M-MDSCs sorted from the spleens of B16-F10 tumor-bearing mice suppressed OVA-specific T cell proliferation and this suppression was significantly reduced following PFKFB3 inhibition with PFK-158 (**Fig. 14**). However, PMN-MDSCs did not suppress OVA-specific T cell proliferation and the functional profile of these cells did not change following PFKFB3 inhibition with PFK-158 (**Fig. 15**). This provides evidence that in B16-F10 melanoma model, M- and not PMN-MDSCs are suppressive. Furthermore, M-MDSCs express high PFKFB3 and inhibition with PFK-158 resulted in reduced suppressive activity.

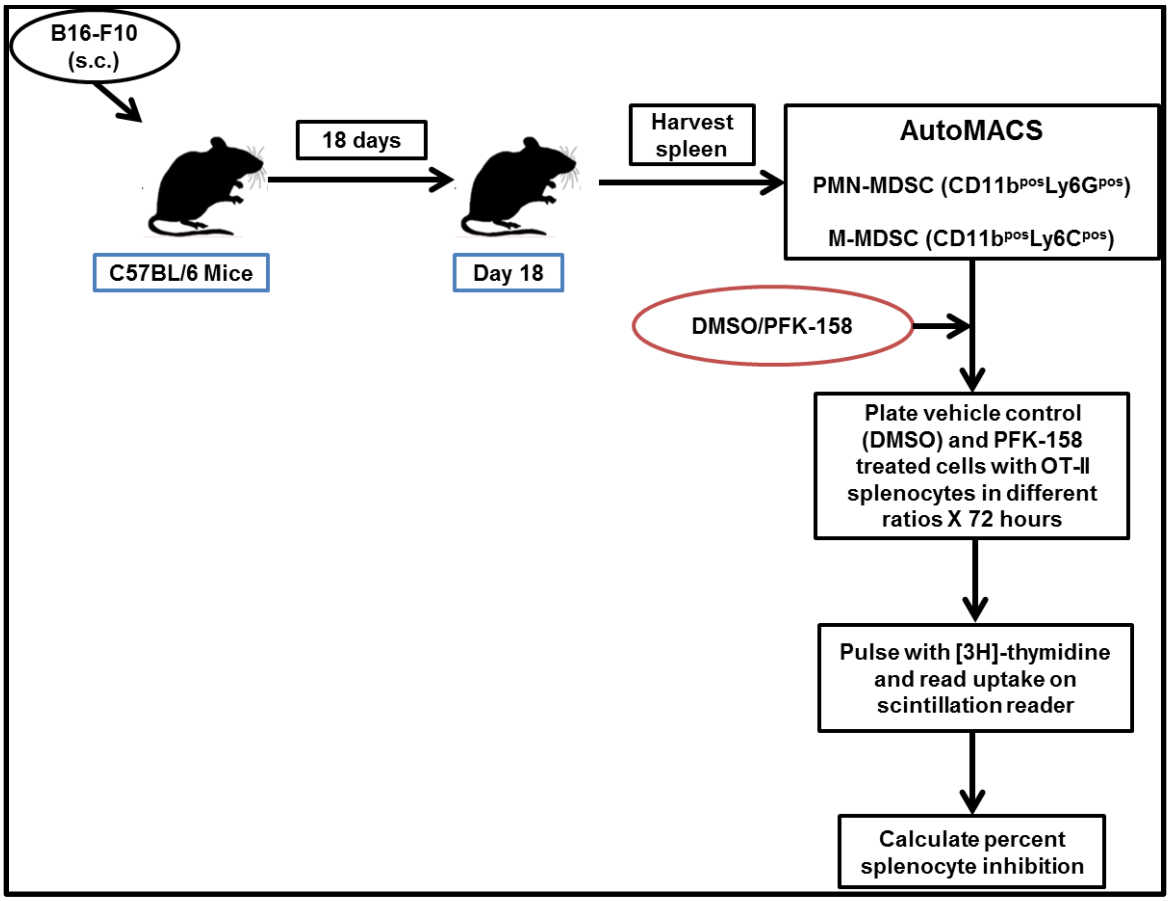

Figure 13. Schematic representation of the steps involved in set-up of functional assay using splenic MDSCs. PMN- and M-MDSCs from the spleens of B16-F10 tumor-bearing mice were sorted using magnetic bead separation as per manufacturer's protocol. MDSCs were then cultured overnight with vehicle control or PFK-158 (5 µM). The following day, cells were washed and plated with OT-II splenocytes in a 96-well flat-bottom plate in different ratios for 72 hours in the presence of ovalbumin (200 µg/ml). Cells were pulsed with [3H]-thymidine 12-16 hours before harvesting. Uptake of [3H]-thymidine was measured using scintillation reader and percent splenocyte inhibition was calculated to evaluate the difference in suppressive activity of MDSCs treated with vehicle control and PFK-158.

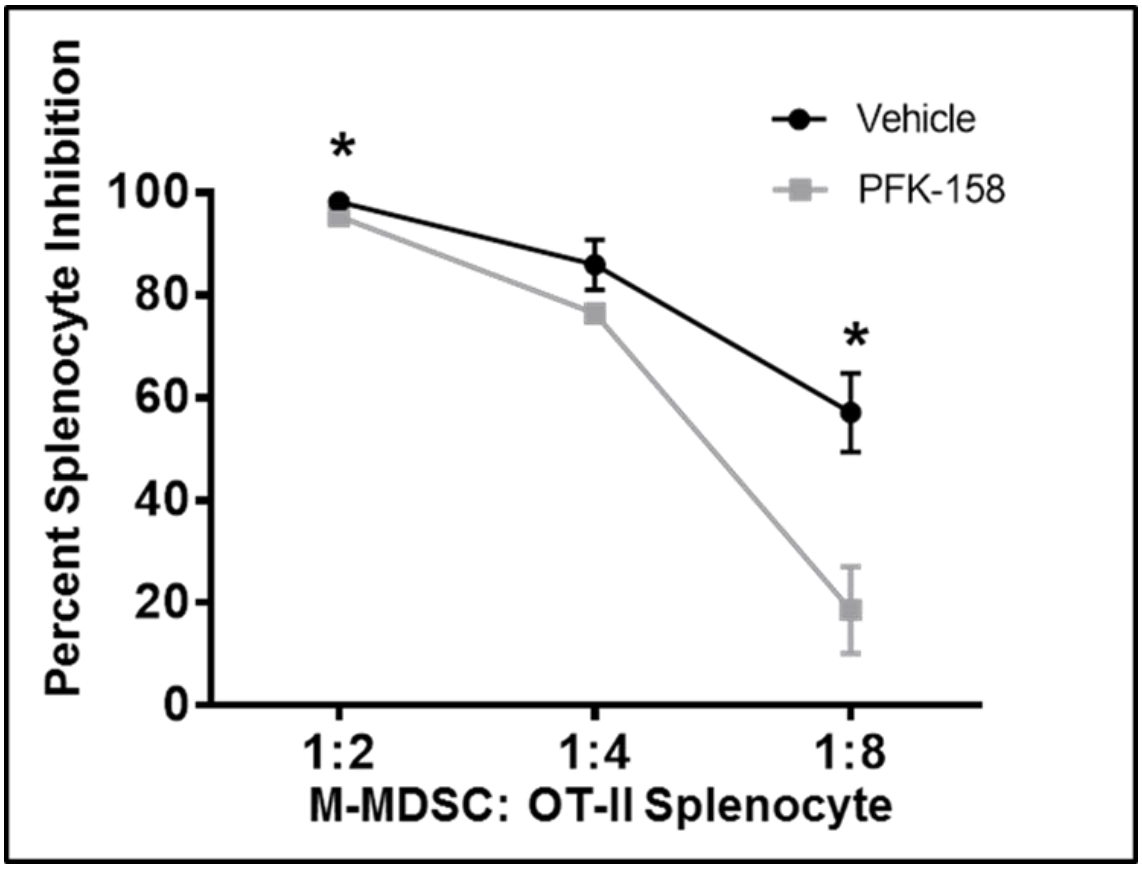

Figure 14. PFKFB3 inhibition with PFK-158 reduces M-MDSC suppressive activity. M-MDSCs pretreated with vehicle control and PFK-158 (5 µM) were co-cultured with OT-II splenocytes in the presence of ovalbumin (200 µg/mL) for 72 hours at 1:2, 1:4 and 1:8 ratio. Percent splenocyte inhibition was calculated. Line graph of percent splenocyte inhibition following treatment of splenic M-MDSCs with vehicle control and PFK-158. Results are representative of three independent experiments. *p≤0.05.

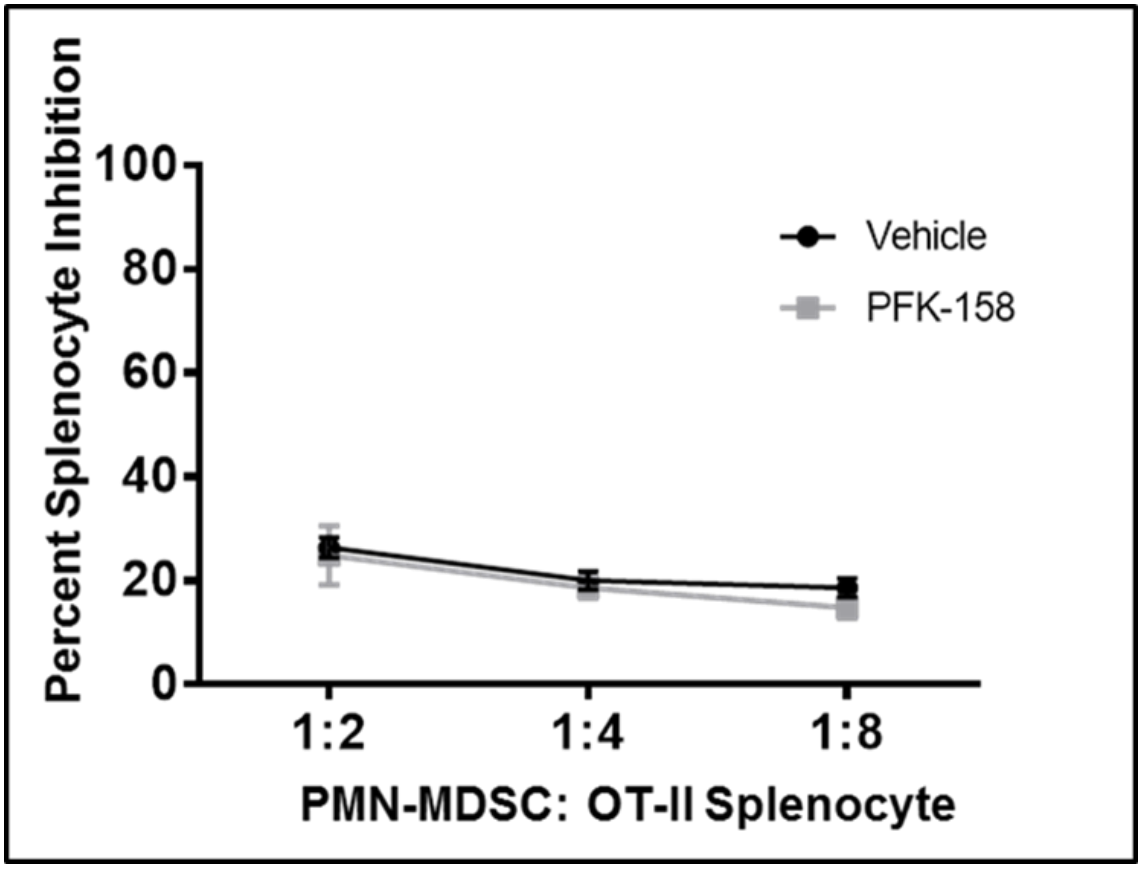

Figure 15. Splenic PMN-MDSCs do not suppress T cell activity in B16-F10 tumor model. PMN-MDSCs pretreated with vehicle control and PFK-158 (5 µM) were co-cultured with OT-II splenocytes in the presence of ovalbumin (200 µg/mL) for 72 hours at 1:2, 1:4 and 1:8 ratio. Percent splenocyte inhibition was calculated. Line graph of percent splenocyte inhibition following treatment of splenic PMN-MDSCs with vehicle control and PFK-158. Results are representative of three independent experiments.

4.4 PFKFB3 inhibition with PFK-158 reduces markers of suppression in splenic M-MDSCs

Arginase 1 and iNOS are important markers of suppression in monocytic MDSCs. We have clearly demonstrated that PFKFB3 is over-expressed in monocytic MDSCs from the spleens of B16-F10 tumor bearing mice and its inhibition reduces M-MDSC suppressive activity (**Fig. 12A and 14**). In order to determine the mechanistic link for reduced M-MDSC suppressive activity following PFKFB3 inhibition with PFK-158, we first determined baseline expression of arginase 1 and iNOS mRNA in naïve and tumor-bearing mice. Both arginase 1 and iNOS were highly expressed in splenic M-MDSCs from tumor-bearing mice compared to naïve mice (**Fig, 16A and 17A**). Then we sought to evaluate the expression of arginase 1 and iNOS mRNA following treatment with vehicle control and PFK-158. Both arginase 1 and iNOS mRNA expression decreased significantly following treatment with PFK-158 compared to treatment with vehicle control (**Fig. 16B and 17B**). Using arginase activity assay, we saw a significant decrease in arginase activity following PFKFB3 inhibition with PFK-158 both with and without the addition of lipopolysaccharide (LPS) (**Fig. 16C**). Splenic M-MDSCs did not produce NO without LPS stimulation. However, LPS stimulation resulted in the production of NO which was completely abrogated following PFKFB3 inhibition with PFK-158 (**Fig. 17C**).

PFKFB3 inhibition with PFK-158 reduced splenic M-MDSC suppressive activity and markers of suppression such as arginase and iNOS. Next, we sought to determine if treatment with PFK-158 resulted in phenotypic change in the M-

MDSCs. On flow cytometry, no change in the frequency or phenotype of splenic M-MDSCs was noted following treatment with vehicle control and PFK-158 (**Fig. 18**). This provides evidence that PFKFB3 inhibition results in reduced suppressive activity primarily through decreased expression of arginase 1 and iNOS, and not through the induction of phenotypic change in these cells to antigen presenting cells such as dendritic cells (DCs).

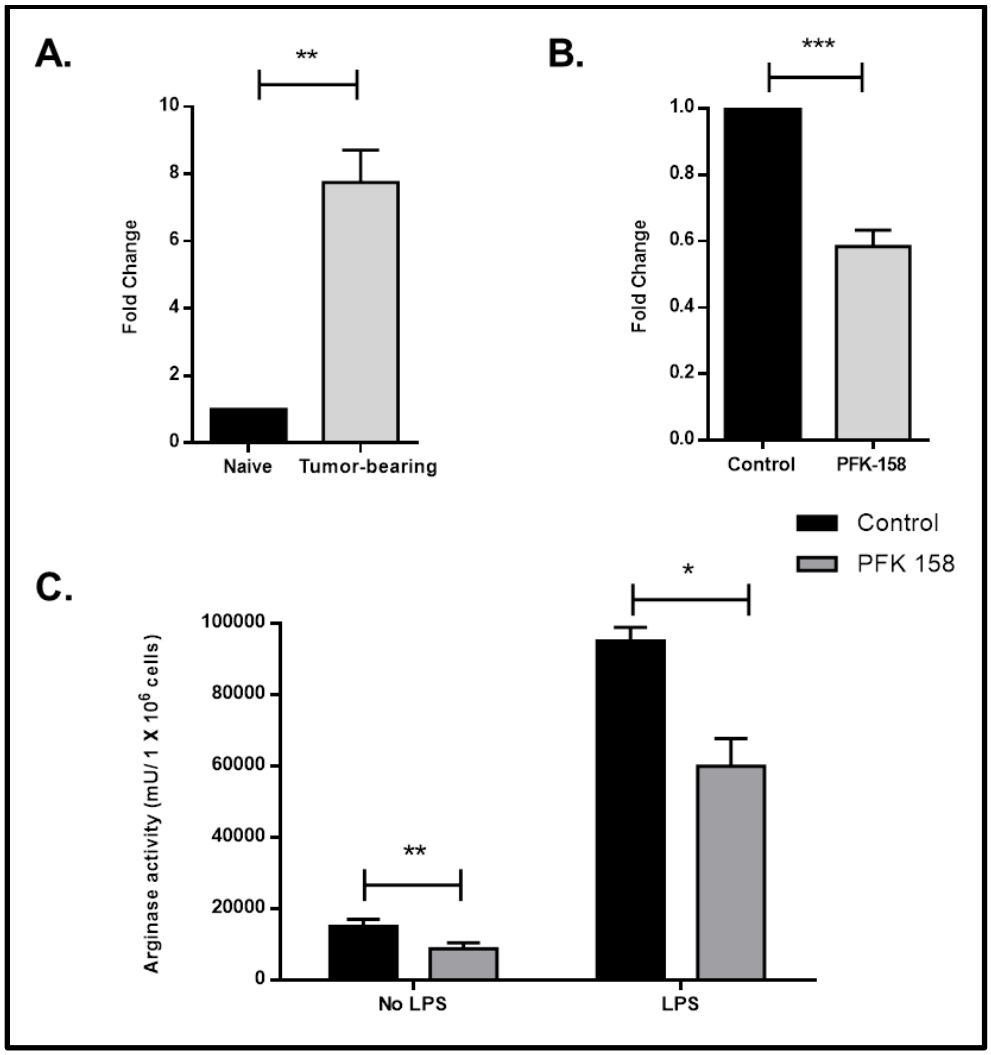

Figure 16. PFKFB3 maintains arginase expression in splenic M-MDSCs from B16-F10 tumor-bearing mice. (A) qRT-PCR analysis of arginase 1 mRNA expression in fresh M-MDSCs sorted from the spleens of naïve (n=3) and tumor-bearing mice (n=3). (B) Arginase 1 mRNA expression was determined in splenic M-MDSCs following treatment with vehicle control (n=4) and PFK-158 (5 µM) (n=4). (C) Arginase activity was determined following treatment with vehicle control (n=4) and PFK-158 (5 µM) (n=4) both with and without the addition of lipopolysaccharide (LPS, 200 ng/mL). Results are representative of three independent experiments. *p≤0.05, ***p≤0.0005.

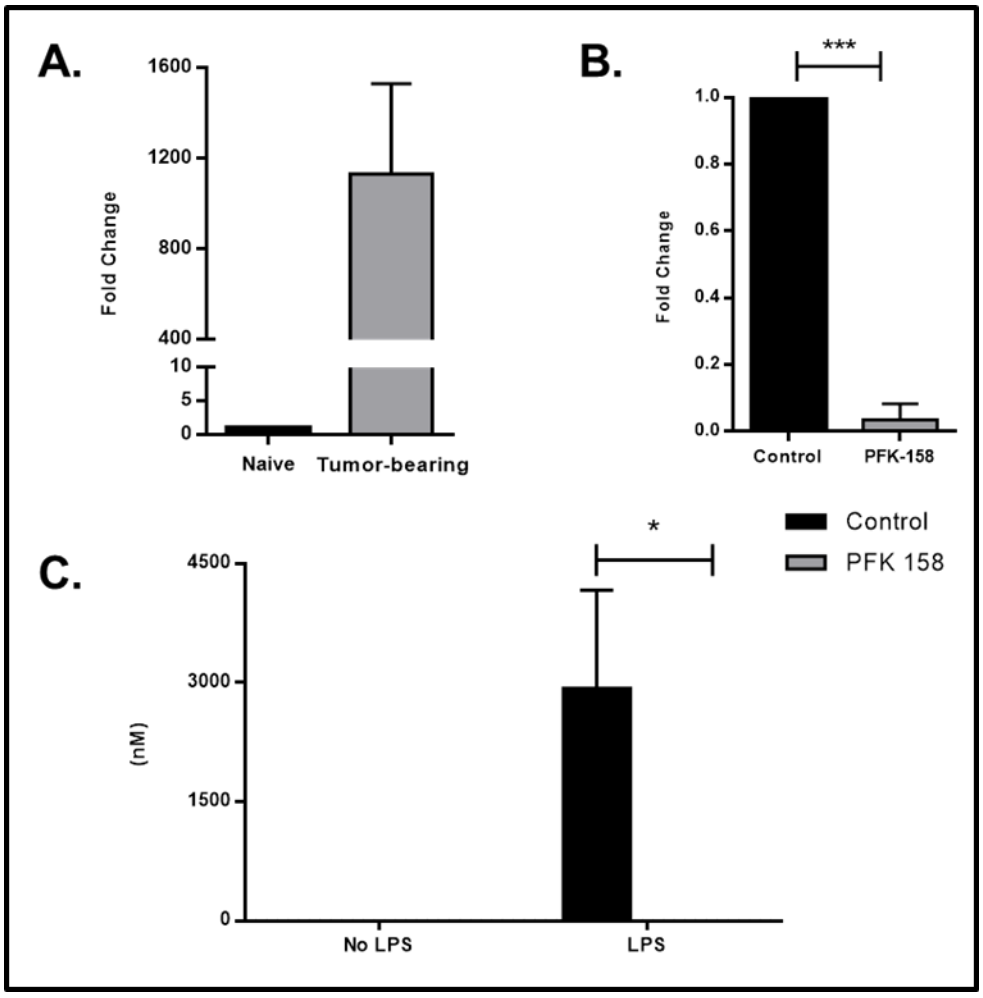

Figure 17. PFKFB3 maintains iNOS expression in splenic M-MDSCs from B16-F10 tumor-bearing mice. (A) qRT-PCR analysis of iNOS mRNA expression in fresh M-MDSCs sorted from the spleens of naïve (n=3) and B16-F10 tumor-bearing mice (n=3). (B) iNOS expression in splenic M-MDSCs following treatment with vehicle control (n=4) and PFK-158 (5 µM) (n=4). (C) NO production was determined following treatment with vehicle control (n=4) and PFK-158 (n=4) both with and without the addition of LPS (200 ng/mL). Results are representative of three independent experiments. *p≤0.05, ***p≤0.0005.

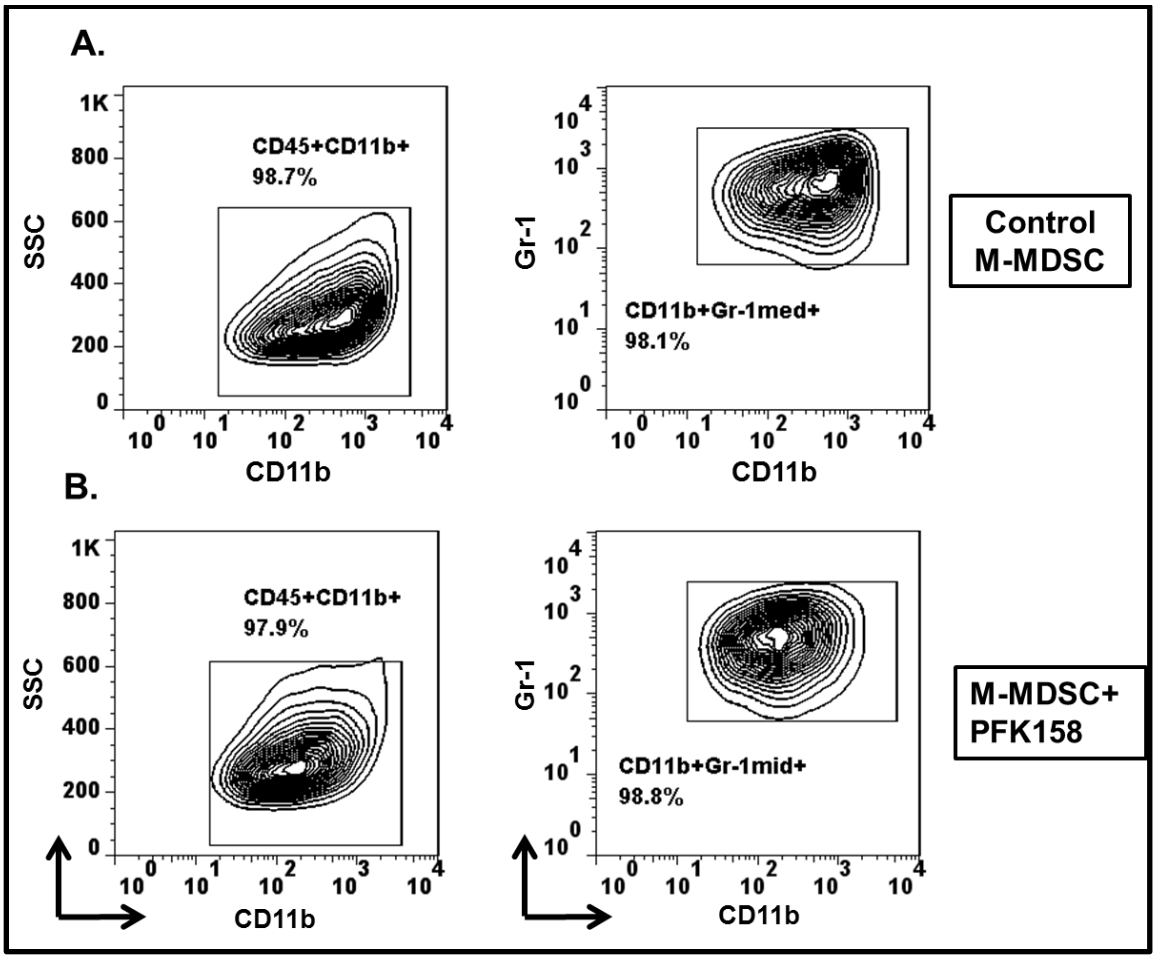

Figure 18. Phenotype of splenic M-MDSCs from B16-F10 tumor-bearing mice does not change following PFKFB3 inhibition with PFK-158 (5 μM). Representative contour plots of (A) splenic M-MDSCs treated with vehicle control and (B) splenic M-MDSCs treated with PFK-158.

4.5 Bone-marrow derived MDSCs express high PFKFB3

Sorting of tumor MDSCs using magnetic bead separation has limitations especially with significant tumor cell contamination. In order to overcome this limitation and study the functional and mechanistic characteristics of tumor MDSCs, we used bone marrow MDSC model as described by Marigo *et al* (**Fig. 19**) (14). Bone marrow cells from C57L/B6 WT mice are cultured in the presence of GM-CSF and IL6 for four days. MDSCs induced subsequently provide an ex-vivo correlate of tumor MDSCs.

We first sought to determine if bone marrow-derived MDSCs using this model has high expression of PFKFB3. Western blot analysis showed that bone marrow cells cultured in the presence of GM-CSF and IL6 expressed high PFKFB3 compared with fresh bone marrow cells and bone marrow cells cultured in the presence of GM-CSF alone (**Fig. 20A and B**). On flow cytometry, the frequency of $CD11b^{pos}GR1^{pos}$ cells increases significantly when fresh bone marrow cells are cultured in the presence of GM-CSF and IL6 (**Fig. 20C**).

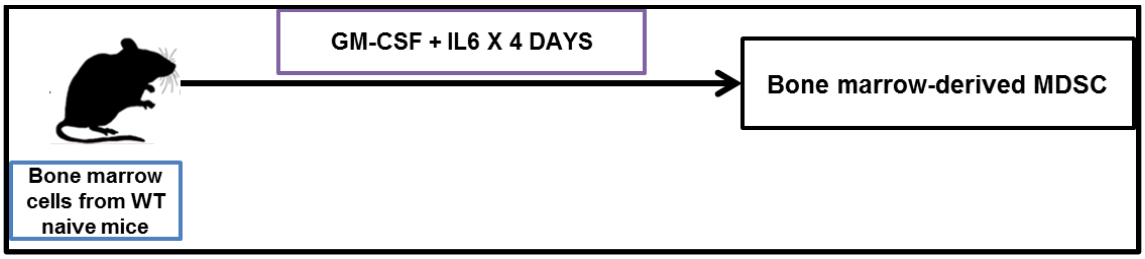

Figure 19. Schematic representation of the steps involved in the induction of bone marrow-derived MDSCs. Bone marrow cells obtained from the tibias and fibulas of C57BL/6 WT mice were cultured in the presence of GM-CSF (40 ng/mL) and IL6 (40 ng/mL) for four days. MDSCs obtained subsequently provide an *ex-vivo* correlate for tumor MDSCs.

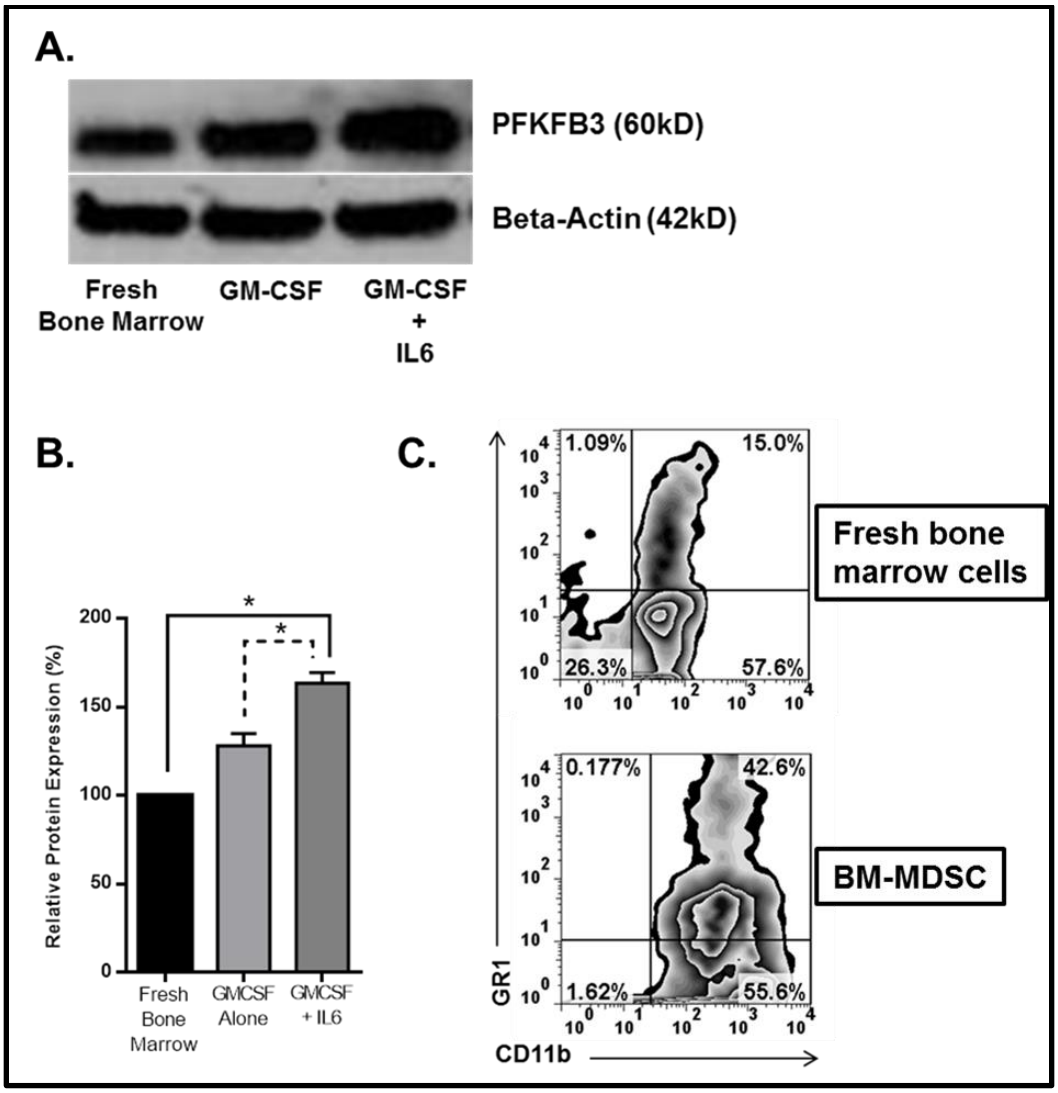

Figure 20. PFKFB3 is over-expressed in bone marrow-derived MDSCs (BM-MDSC). Bone marrow cells from C57BL/6 WT mice were cultured in the presence of GM-CSF (40 ng/mL) and IL6 (40 ng/mL) for four days. (A) western blot and (B) bar graph of relative expression of PFKFB3 in BM-MDSC compared with fresh bone marrow cells and bone marrow cells cultured in the presence of GM-CSF alone. (C) Representative greyscale density plot of fresh bone marrow cells and BM-MDSCs ($CD11b^{pos}GR1^{pos}$). Results are representative of three independent experiments.

4.6 PFKFB3 inhibition with PFK-158 reverses bone marrow-derived MDSCs suppressive activity

Next, we sought to determine if bone marrow-derived MDSCs were suppressive and if suppressive activity can be reversed following PFKFB3 inhibition with PFK-158. Bone marrow cells obtained from C57BL/6 WT mice were cultured in the presence of GM-CSF and IL6 for four days. PFK-158 at 5 µM dose or vehicle control (DMSO) was added to the cultures on day zero and then 2.5 µM dose or vehicle control was added again on day three. On day four, cells were harvested and then co-cultured with OT-II splenocytes in different rations in a 96-well flat-bottom plate in the presence of ovalbumin for 72 hours. 12-16 hours before harvesting the plates, cells were pulsed with [3H]-thymidine and percent splenocyte inhibition was calculated (**Fig. 21**). We found that the bone marrow-derived MDSCs suppressed the T cell proliferation which was reversed following PFKFB3 inhibition with PFK-158 at all the ratios that were tested (**Fig. 22**).

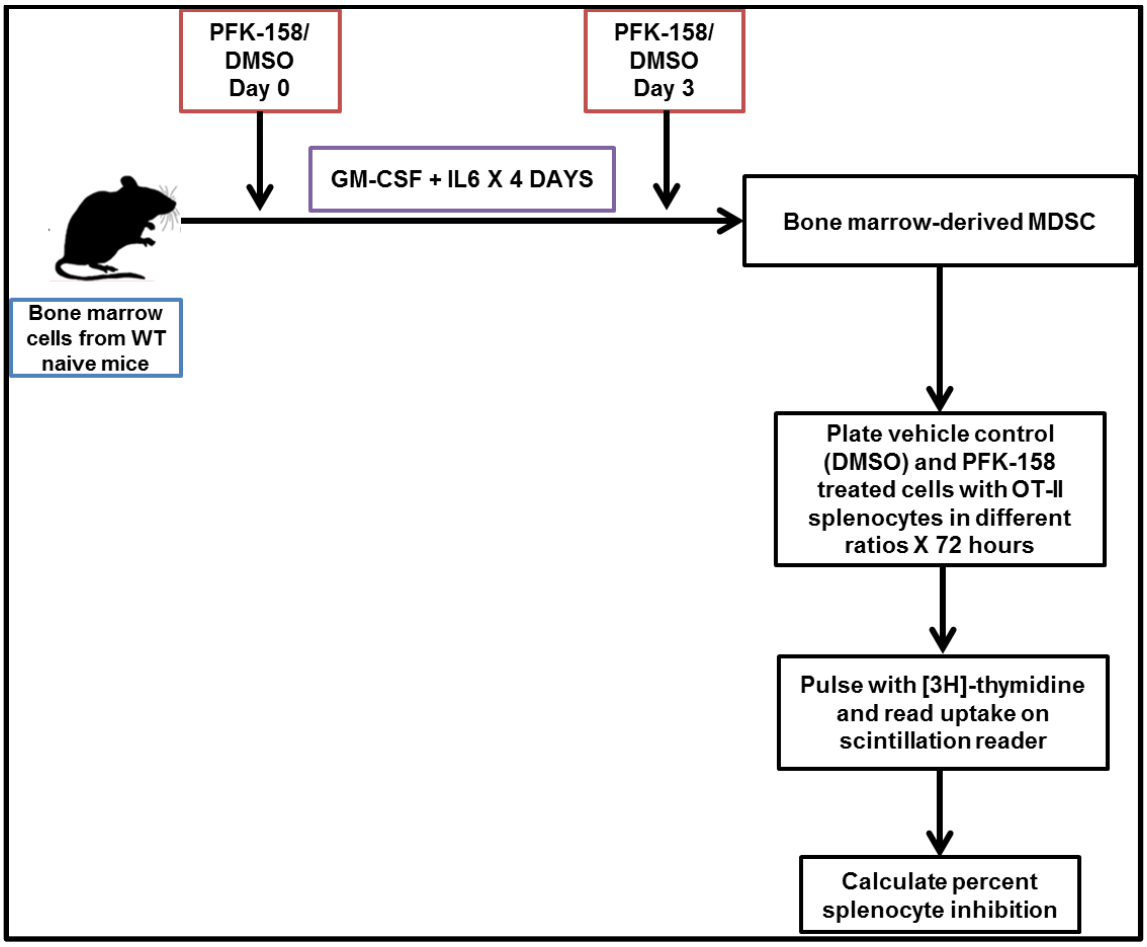

Figure 21. Schematic representation of the steps involved in functional assay with BM-MDSC. PFK-158 (5 µM) or vehicle control was added on day zero and then again on day three (PFK-158, 2.5 µM) to the bone marrow cells co-cultured with GM-CSF and IL6. On day four, cells were harvested, washed and then plated with OT-II splenocytes in a 96-well flat-bottom plate in different ratios for 72 hours in the presence of ovalbumin. Cells were pulsed with [3H]-thymidine 12-16 hours before harvesting. Incorporation of [3H]-thymidine was measured using scintillation reader and percent splenocyte inhibition was calculated to evaluate the difference in suppressive activity of BM-MDSCs treated with vehicle control and PFK-158.

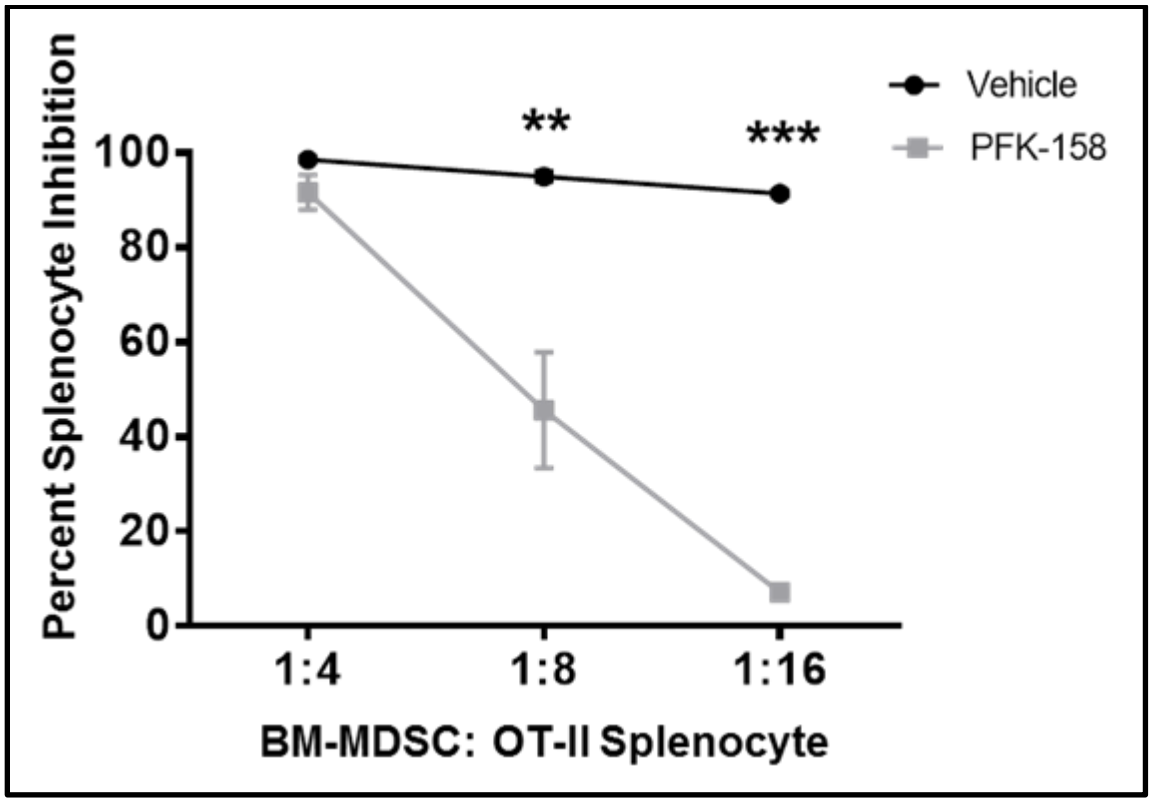

Figure 22. PFKFB3 inhibition with PFK-158 reduces bone marrow-derived MDSC suppressive activity. Bone marrow-derived MDSCs treated with vehicle control and PFK-158 were co-cultured with OT-II splenocytes in the presence of ovalbumin at 1:4, 1:8 and 1:16 ratios. Line graph showing the suppressive activity of vehicle control and PFK-158 treated bone marrow-derived MDSCs. Results are representative of three independent experiments. **p≤0.005, ***p≤0.0005.

4.7 PFKFB3 inhibition reduces markers of suppression in bone marrow-derived MDSCs

Bone marrow-derived MDSCs suppress T cell proliferation primarily through the upregulation of arginase 1 expression and NO production. Inhibition of PFKFB3 during the induction of bone marrow-derived MDSCs resulted in complete loss of arginase 1 expression on western blot and reduced activity on arginase assay (**Fig. 23A and B**). We also sought to analyze if NADPH-oxidase (NOX)/ROS pathway contributed to immune suppressive phenotype of these cells. On western blot analysis, there was no difference in the expression of NOX2 and NOX4 enzymes between the vehicle control and PFK-158 treated BM-MDSCs (**Fig. 23A**). Similarly, on flow cytometry analysis, there was no detectable difference noted in DCF-detectable ROS between the two (**Fig. 24B**).

We also assessed NO production using Griess assay both during induction and following differentiation of BM-MDSCs. To evaluate the NO production during the induction process, PFK-158 was added as described previously, on day zero and then on day three. In the post-differentiation condition, bone marrow cells were cultured with GM-CSF and IL6 for four days and then treated with vehicle control or PFK-158 for 16-18 hours. NO production was stimulated by the addition of LPS. Supernatants from these conditions were used to determine NO level as per manufacturer's protocol. PFKFB3 inhibition with PFK-158 both during induction and post differentiation resulted in significantly reduced production of NO compared with control (**Fig. 24A**).

We next performed flow cytometry analysis of bone marrow-derived MDSCs following treatment with vehicle control and PFK-158 to assess if PFKFB3 inhibition resulted in phenotypic transformation of these cells to APCs. No change in the phenotype of these cells was seen with or without treatment with PFK-158 (**Fig. 25 B and C**). These experiments provide further evidence that PFK-158 modulates immune suppressive phenotype of bone marrow-derived MDSCs through reduced arginase 1 expression and NO production, and not through ROS or through induction of phenotypic change.

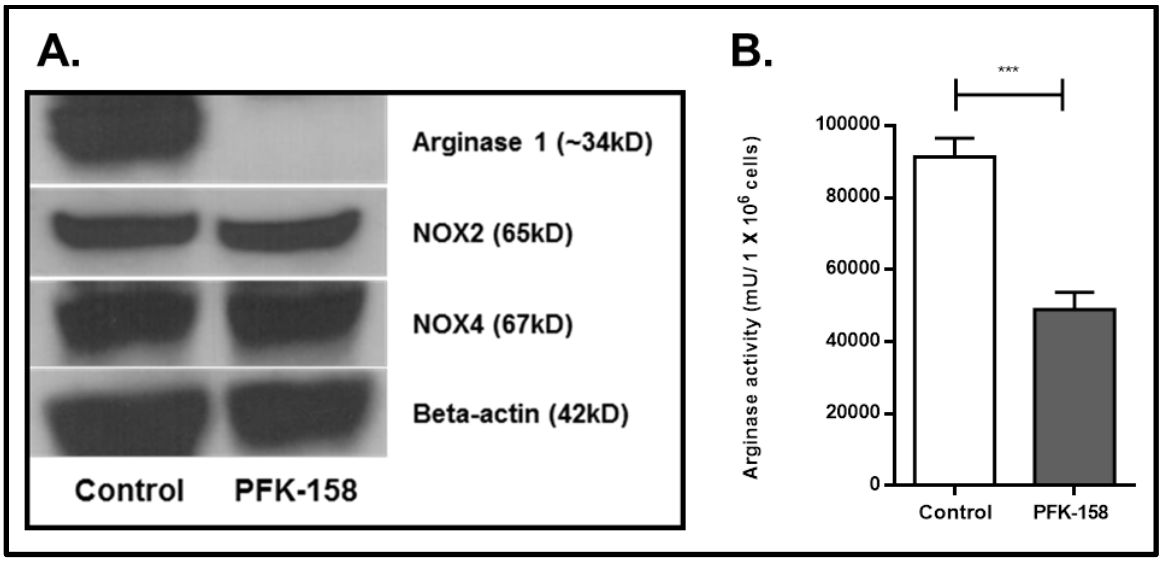

Figure 23. PFKFB3 maintains arginase 1 expression in BM-MDSCs. (A) Western blot analysis of arginase 1, NOX2 and NOX4 expression relative to beta-actin in vehicle control and PFK-158 treated bone marrow-derived MDSCs. (B) Arginase activity was assessed using Quantichrom^{TM} arginase assay – Darg 100 as per manufacturer's protocol. Bar graph of arginase activity between the vehicle control and PFK-158 treated groups. Results are representative of three independent experiments. ***p≤0.0005.

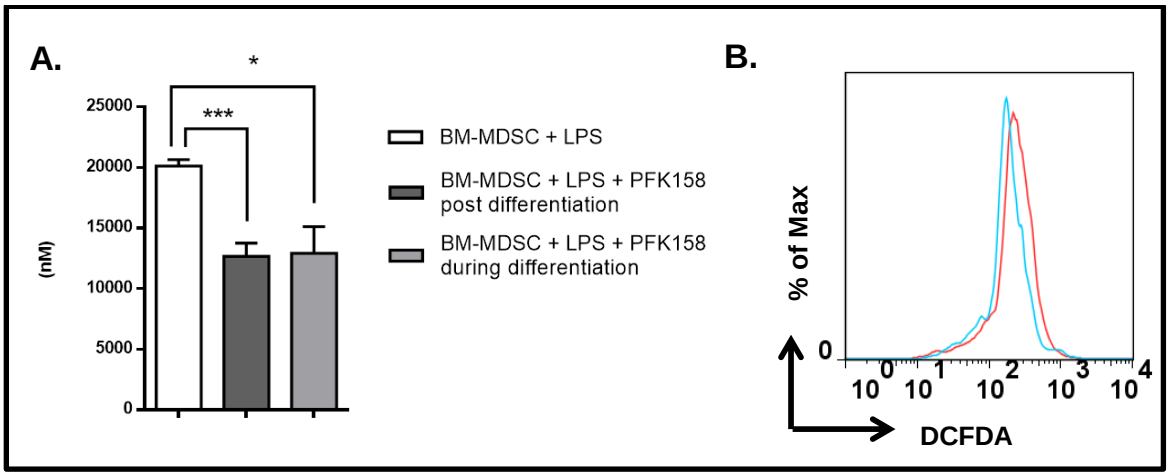

Figure 24. PFKFB3 maintains NO production in BM-MDSCs. (A) NO production was stimulated using LPS. Using Griess assay, NO production was determined in the supernatants from the vehicle control treated group and bone marrow-derived MDSC groups treated with PFK-158 during induction and post-differentiation. (B) DCF-detectable ROS levels in bone marrow-derived MDSCs treated with vehicle control and PFK-158 (5 µM). Results are representative of three independent experiments. *p≤0.05, ***p≤0.0005.

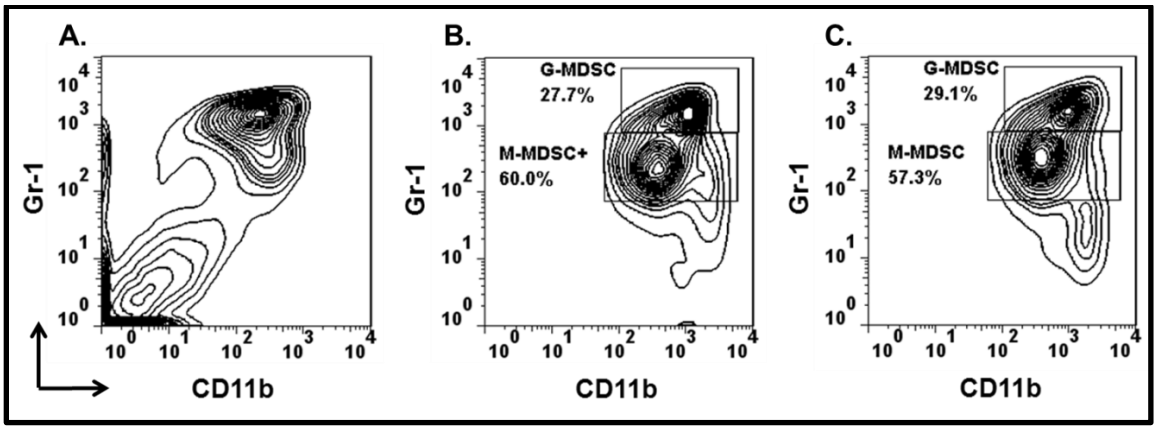

Figure 25. PFKFB3 inhibition does not change phenotype of BM-MDSCs. (A-C) Flow cytometry analysis of fresh bone marrow cells, BM-MDSCs and BM-MDSCs + PFK-158. Representative contour plots of (A) fresh bone marrow cells (B) BM-MDSCs (C) BM-MDSCs following PFKFB3 inhibition with PFK-158. Bone marrow-derived PMN or G-MDSCs are $SSC^{high}CD11b^{pos}GR1^{high}$ and M-MDSCs are $SSC^{low}CD11b^{pos}GR1^{low}$.

4.8 Bone marrow-derived monocytic MDSCs express high PFKFB3 and cause antigen non-specific T cell suppression

Tumor MDSCs result in antigen non-specific T cell suppression. Bone marrow derived MDSCs provide an ex-vivo model to study tumor MDSCs. To this end, we then sought to determine the functional and mechanistic characteristics of monocytic subset sorted from bone marrow-derived MDSCS. Bone marrow cells from C57BL/6 WT mice were cultured with GM-CSF and IL6 for four days (14). At the end of four day culture, monocytic and granulocytic subsets were sorted using mouse MDSC isolation kit as per manufacturer's protocol (Miltenyi Biotec) (**Fig. 26**). We first assessed the expression of PFKFB3 in the monocytic subset. Using western blot analysis, bone marrow-derived M-MDSCs had high expression of PFKFB3 compared with fresh bone marrow cells (**Fig. 27**).

In order to study the suppressive function, both granulocytic and monocytic subsets were then treated with vehicle control and PFK-158 (5 μM) for 16-18 hours. The following day, cells were harvested, washed and co-cultured with CFSE labeled splenocytes from WT mice in an anti-CD3 coated 96-well flat-bottom plate in the presence of anti-CD28 in different ratios for 72 hours. Cells were then stained for CD4 and CD8, and T cell proliferation was determined using flow cytometry (**Fig. 26**). M-MDSC induced suppression was more impressive for CD4 compared to CD8 T cells (**Fig. 28 and 29**). Furthermore, PFKFB3 inhibition with PFK-158 resulted in reduced the suppressive activity of the M-MDSC subset (**Fig. 28 and 29**) while there was no change in the suppressive profile of PMN-MDSC subset (**Fig. 30 and 31**).

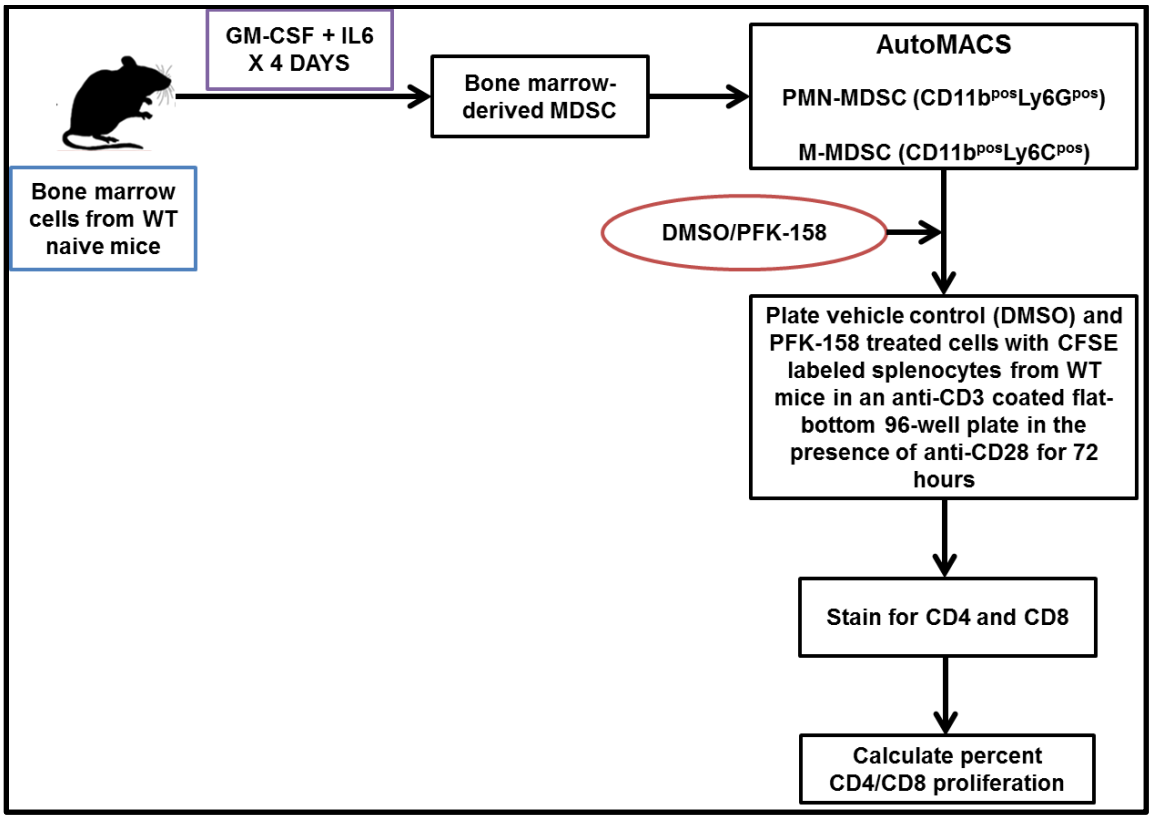

Figure 26. Schematic representation of the steps involved in the generation and sorting bone marrow-derived M-MDSCs and functional assay. Fresh bone marrow cells were cultured in the presence of GM-CSF (40 ng/mL) and IL6 (40 ng/mL) for four days (14). Following the manufacturer's protocol, monocytic and polymorphonuclear subsets were sorted using magnetic bead separation (Miltneyi Biotec). Sorted cells were cultured with vehicle control or PFK-158 (5 µM) for 16-18 hours. The following day, cells were washed and co-cultured with CFSE labeled splenocytes from WT mice in an anti-CD3 coated flat-bottom 96-well plate in the presence of anti-CD28 for 72 hours. Cells were then harvested and stained for CD4 and CD8. Flow cytometry was then performed to determine CD4 and CD8 T cell proliferation.

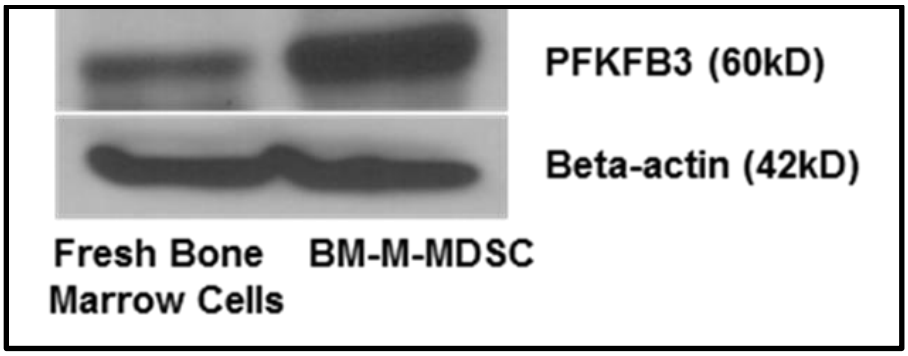

Figure 27. PFKFB3 is over-expressed in bone marrow-derived M-MDSCs. Representative western blot of PFKFB3 expression in bone marrow-derived M-MDSCs and fresh bone marrow cells.

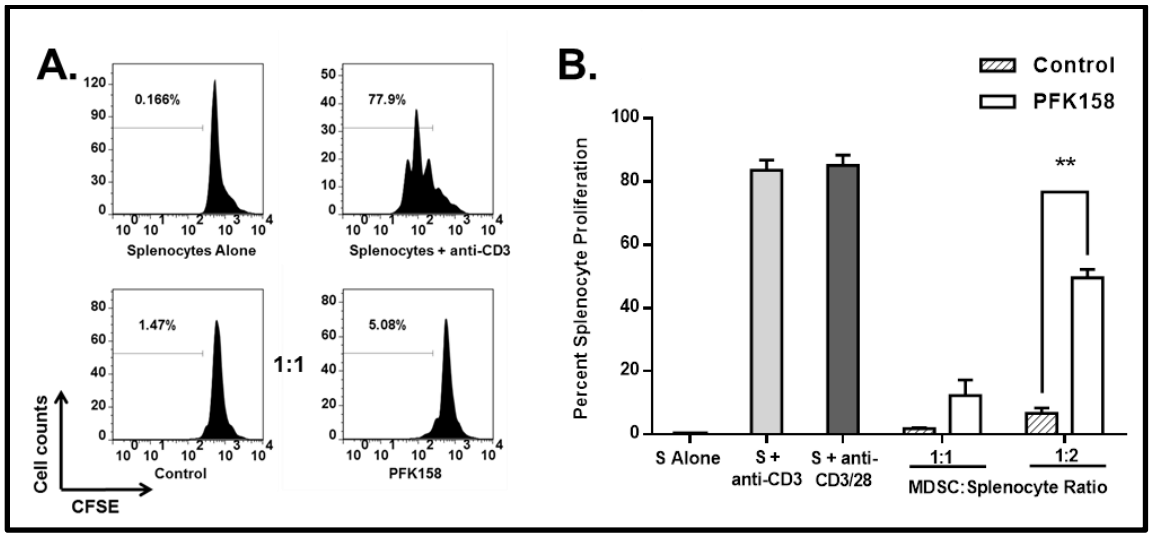

Figure 28. PFKFB3 inhibition with PFK-158 reverses bone marrow-derived M-MDSC suppression on CD4 T cell proliferation. Bone marrow-derived M-MDSCs were cultured with CFSE-labeled splenocytes in anti-CD3 coated 96-well flat bottom plate in the presence of anti-CD28 beads for three days. Splenocytes were then stained for CD4 and activation was determined. Representative (A) histograms and (B) bar graphs showing the percentage of proliferated splenocytes. Results are representative of three independent experiments. **p≤0.005.

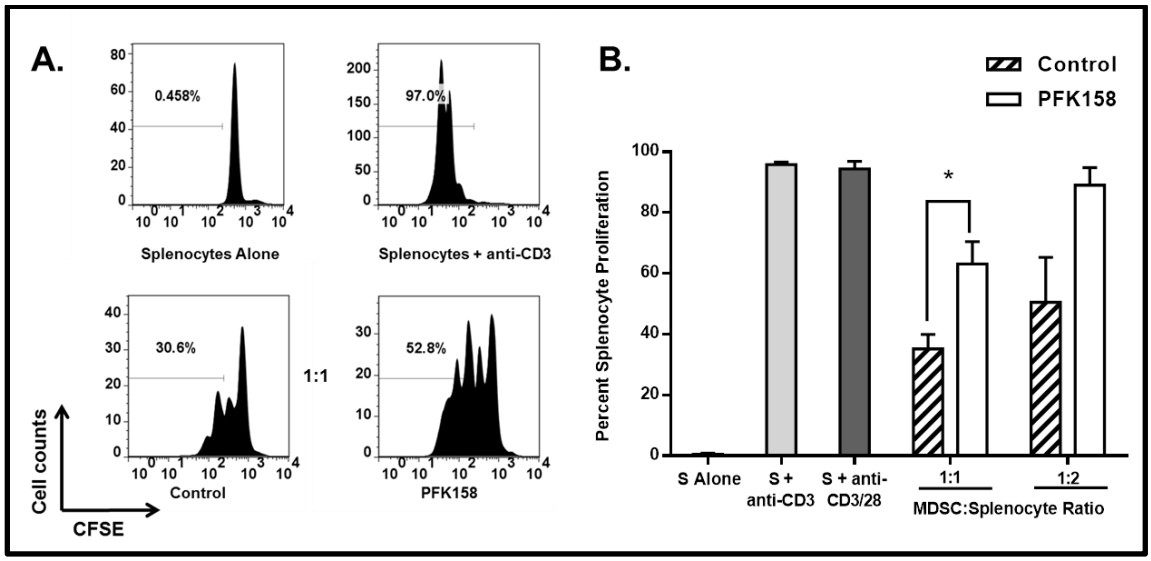

Figure 29. PFKFB3 inhibition with PFK-158 reverses bone marrow-derived M-MDSC suppression on CD8 T cell proliferation. (A and B) Bone marrow-derived M-MDSCs were cultured with CFSE-labeled splenocytes in anti-CD3 coated 96-well flat bottom plate in the presence of anti-CD28 beads for three days. Splenocytes were then stained for CD8 and activation was determined. Representative (A) histograms and (B) bar graphs showing the percentage of proliferated splenocytes. Results are representative of three independent experiments. *p≤0.05.

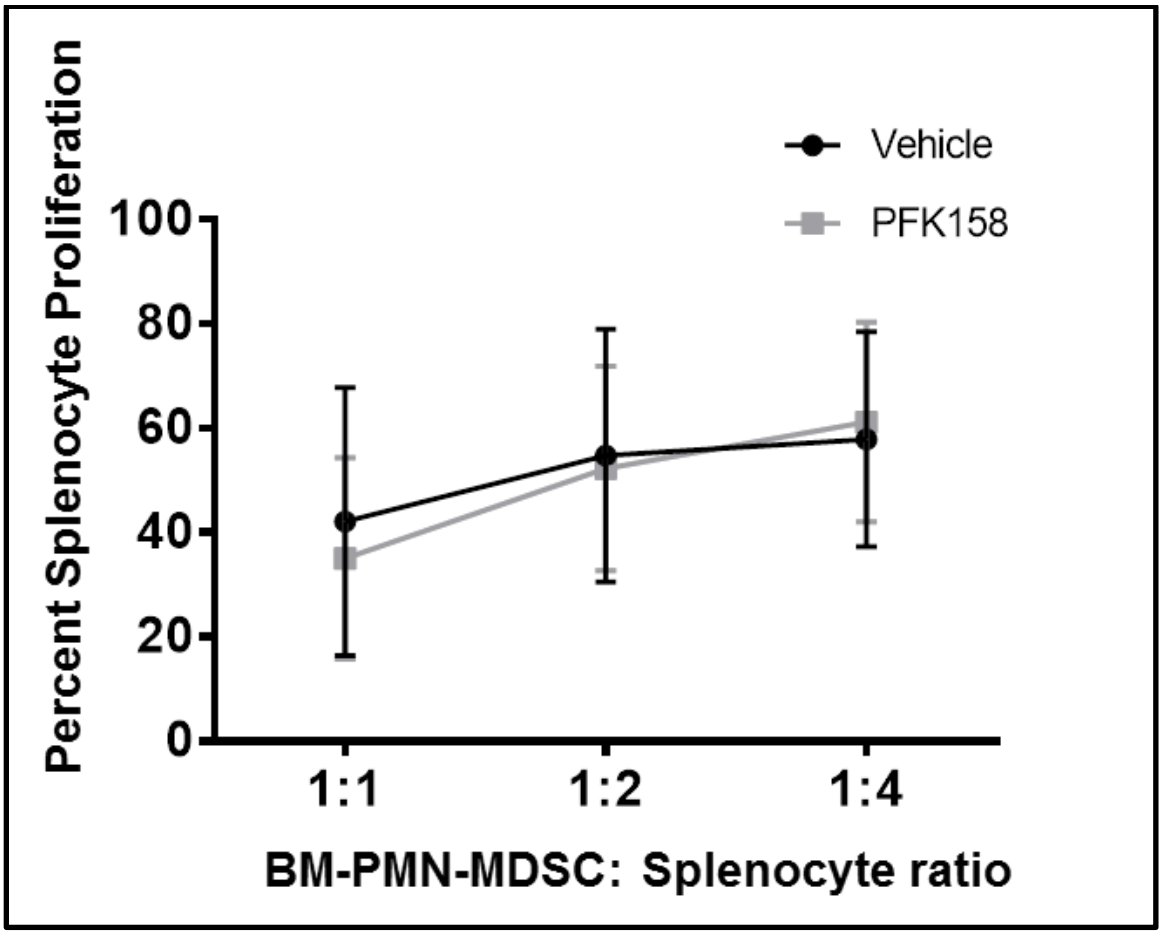

Figure 30. Bone marrow-derived PMN-MDSCs do not suppress CD4 T cell proliferation. Line graph for splenocytes showing the percentage of proliferated splenocytes. Results are representative of three independent experiments.

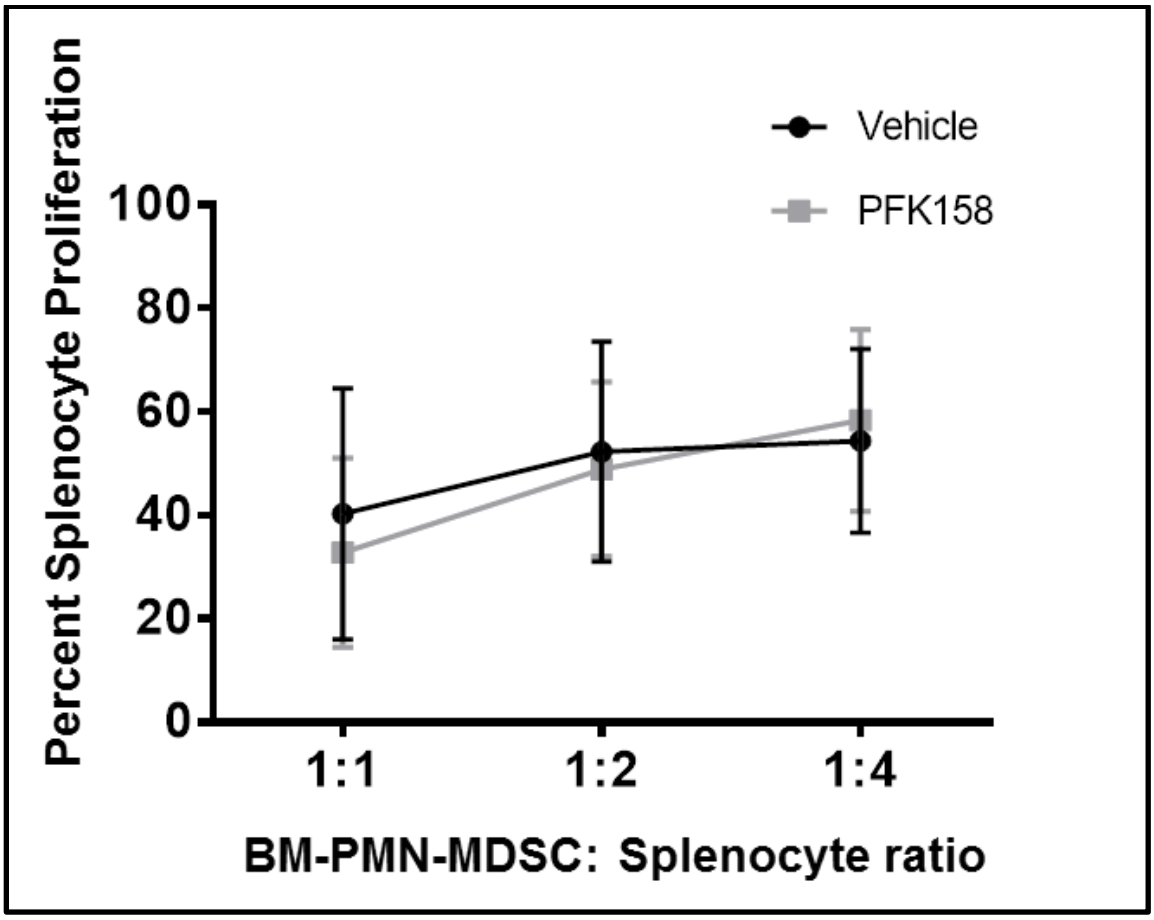

Figure 31. Bone marrow-derived PMN-MDSCs do not suppress CD8 T cell proliferation. Line graph for splenocytes showing the percentage of proliferated splenocytes. Results are representative of three independent experiments.

4.9 PFKFB3 inhibition reduces arginase 1 expression and activity in bone marrow-derived M-MDSCs

Tumor MDSCs result in antigen non-specific T cell suppression through dramatic upregulation of arginase 1 and iNOS. We showed that bone marrow-derived M-MDSCs suppress T cell function in an antigen independent manner. To study the mechanistic basis for reduced bone marrow-derived M-MDSC induced T cell suppression following PFKFB3 inhibition, we determined the change in arginase 1 activity. We found that following PFKFB3 inhibition with PFK-158, arginase 1 mRNA expression (**Fig. 32A**) and arginase activity decreased significantly compared with vehicle control (**Fig. 32 B**). Bone marrow-derived M-MDSCs did not produce NO even after LPS stimulation (**Fig. 32C**). These experiments provide evidence that bone marrow-derived M-MDSCs result in antigen non-specific T cell suppression primarily through upregulation of arginase expression and activity. And, PFKFB3 inhibition with PFK-158 reduces the arginase expression and activity.

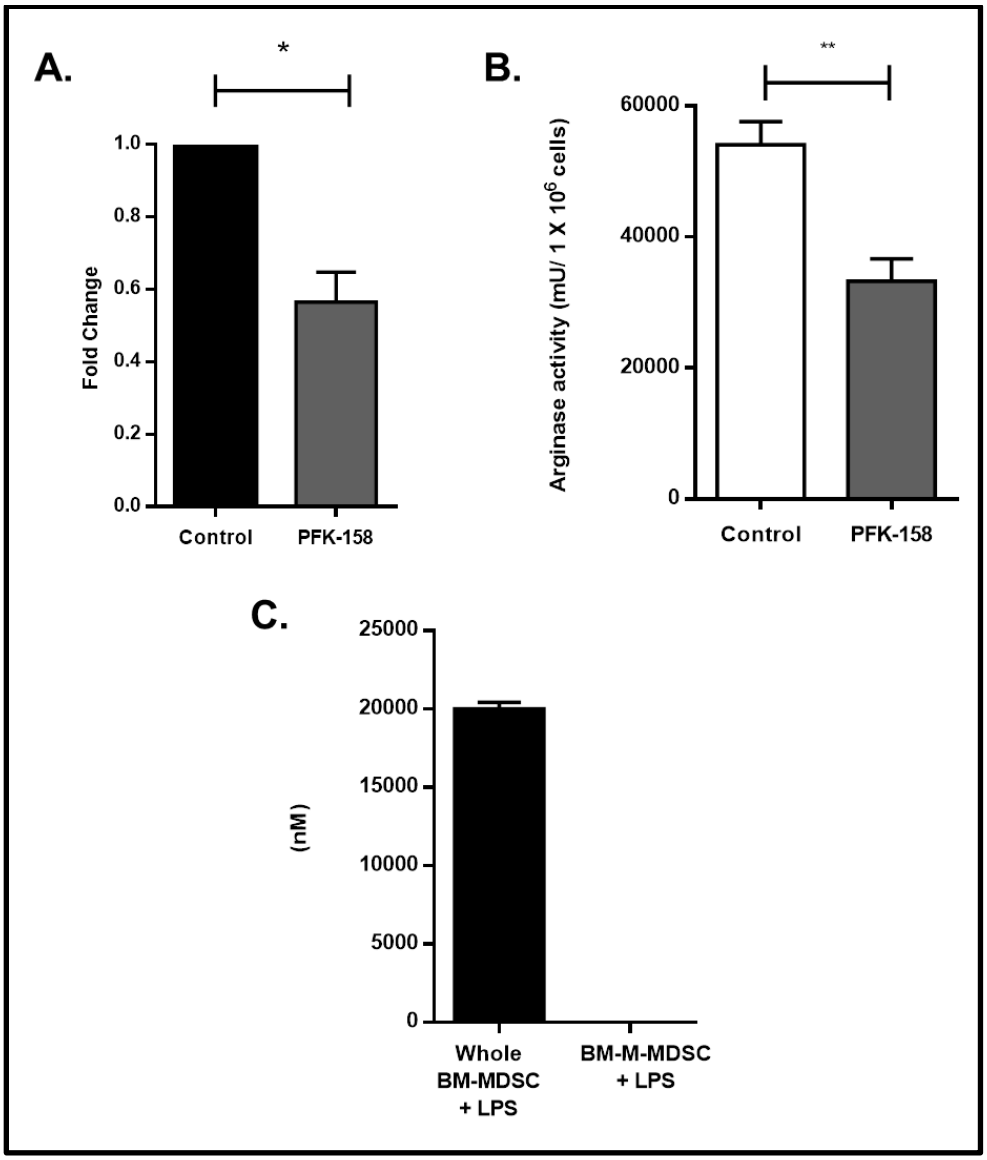

Figure 32. PFKFB3 maintains arginase 1 activity in bone marrow-derived M-MDSCs. (A) Bar graphs showing qRT-PCR analysis of arginase 1 mRNA expression, (B) Quantichrom™ arginase assay showing arginase activity in bone marrow-derived M-MDSCs following treatment with vehicle control and PFK-158, and (C) Griess assay showing NO production in whole BM-MDSCs and bone marrow-derived M-MDSCs following LPS stimulation. Results are representative of three independent experiments. *p≤0.05, **p≤0.005.

4.10 Bone marrow-derived MDSCs upregulate glycolysis

Next we sought to study the metabolic profile of MDSCs. To this end, we used the Seahorse® platform which analyzes the extracellular acidification rate (ECAR), an index for glycolysis and oxygen consumption rate (OCR) which provides a measure for mitochondrial activity or oxidative phosphorylation. Bone marrow-derived MDSCs were obtained following culture of bone marrow cells with GM-CSF and IL6 as described previously. In addition, fresh bone marrow cells were harvested from WT mice. Using the Seahorse® platform, we measured the ECAR and OCR for fresh bone marrow cells and bone marrow-derived MDSCs. We found that the bone marrow-derived MDSCs had higher ECAR and OCR compared with fresh bone marrow cells (**Fig. 33 A and B**).

Taking in to account PFKFB3 over-expression in bone marrow-derived M-MDSCs compared with fresh bone marrow cells (**Fig. 27**), we sought to determine the effect of PFKFB3 inhibition on ECAR and OCR in these cells. Bone marrow-derived M-MDSCs were sorted using magnetic bead separation as described previously and then treated with vehicle control and PFK-158 for 16-18 hours. Bioenergetic profile of these cells was then analyzed using the Seahorse®. Following PFKFB3 inhibition, both ECAR and OCR decreased significantly compared with vehicle control (**Fig. 33 C and D**). These data demonstrate that MDSCs upregulate glycolysis which is the result of higher expression of PFKFB3 in these cells.

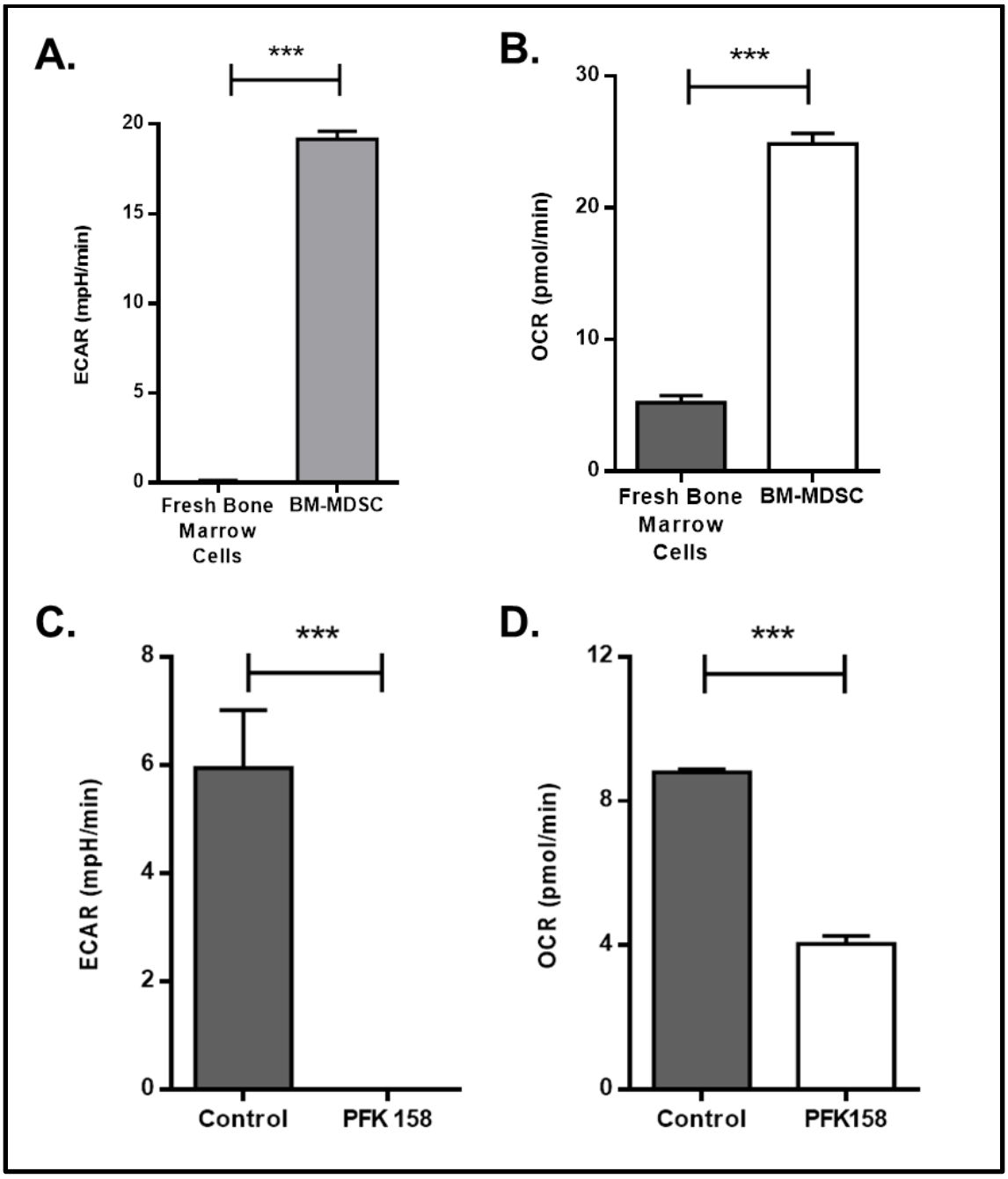

Figure 33. PFKFB3 maintains high rate of glycolysis in BM-MDSCs. Bar graphs of (A) ECAR and (B) OCR in fresh bone marrow cells and bone marrow-derived MDSCS, (C) ECAR and (D) OCR comparing bone marrow-derived M-MDSCs following treatment with vehicle control and PFK-158. Results are representative of three independent experiments. ***p≤0.0005.

4.11 HIF-1α expression correlates with the expression of PFKFB3 in M-MDSCs in hypoxic culture conditions

HIF-1α has been shown to play an important role in MDSC function and differentiation (11). We then sought to determine the relationship between the expression of HIF-1α and PFKFB3 in monocytic MDSCs. Splenic M-MDSCs from B16-F10 tumor-bearing mice were sorted as described previously using magnetic bead separation (Miltneyi Biotec). M-MDSCs were then cultured in 25% B16-F10 tumor cell conditioned media (TCCM) under hypoxic (1% O_2) and normoxic conditions for 24 and 48 hours (**Fig. 34**). Western blot analysis was then performed to evaluate the expression of HIF-1α and PFKFB3 under these conditions. HIF-1α expression was upregulated at 24 hours which correlated with a higher expression of PFKFB3 under hypoxia relative to the expression under normoxia (**Fig. 35**). At 48 hours, expression of HIF-1α and PFKFB3 was still high under hypoxia compared to normoxia (**Fig. 35**). These results clearly demonstrate that HIF-1α expression correlates with the expression of PFKFB3 in M-MDSCs under hypoxic conditions.

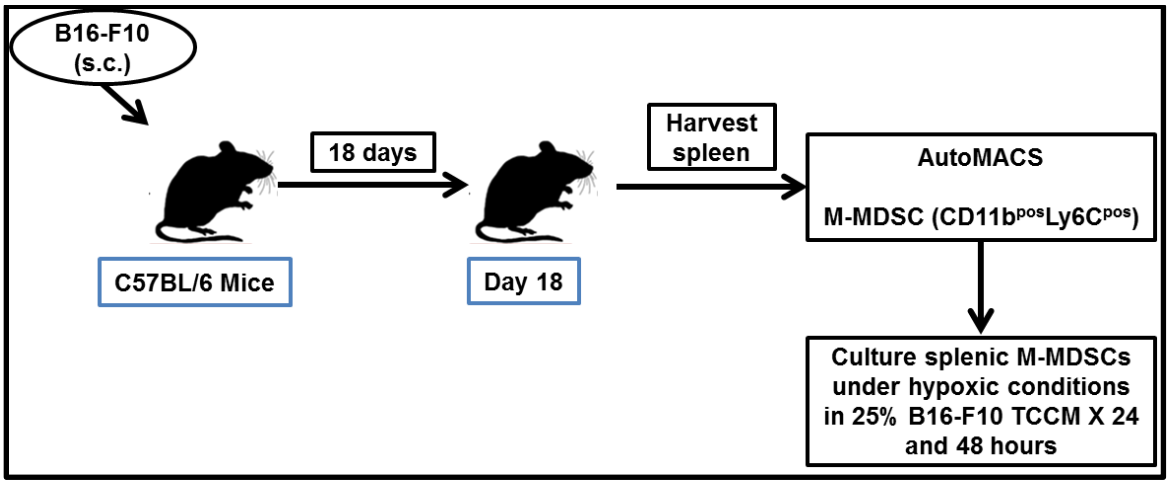

Figure 34. Schematic representation of the steps involved in the culture of splenic M-MDSCs under hypoxia. M-MDSC sorted from the spleens of B16-F10 tumor bearing mice were cultured in 25% B16-F10 tumor cell conditioned media (TCCM) under 1% oxygen for 24 and 48 hours.

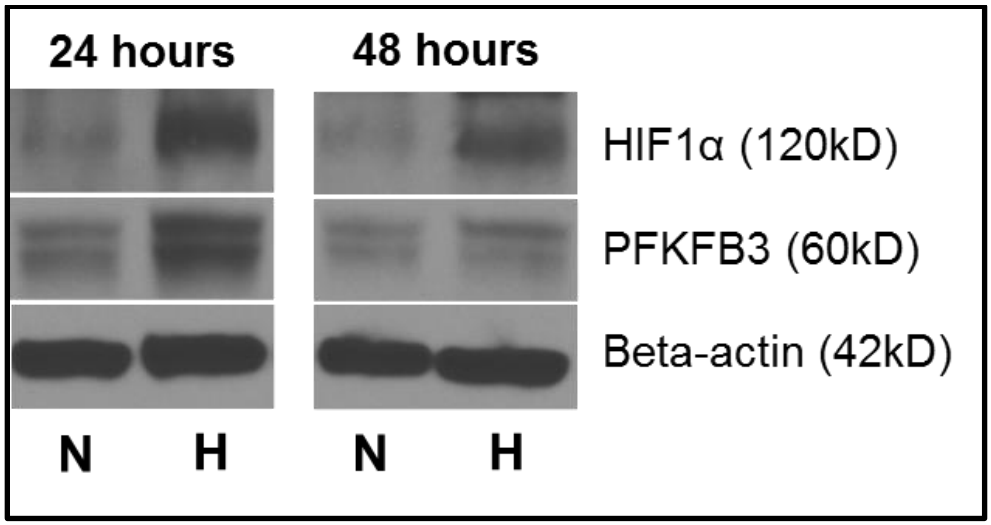

Figure 35. Hypoxia inducible factor 1α (HIF-1α) expression correlates with the expression of PFKFB3 under hypoxic conditions. Representative western blot of HIF-1α and PFKFB3 in splenic M-MDSCs cultured in 25% B16-F10 tumor cell conditioned media (TCCM) under normoxia and hypoxia (1% O_2) at 24 and 48 hours.

4.12 M-MDSCs under hypoxia result in antigen non-specific T cell suppression

In the hypoxic tumor microenvironment (TME), MDSCs have been shown to cause antigen non-specific T cell suppression (11). MDSCs isolated from HIF-1α knockout mice resulted in less antigen non-specific T cell suppression compared with HIF-1α WT mice (11). In order to study the differential functional characteristics of splenic M-MDSCs under hypoxia, cells were cultured in 25% B16-F10 TCCM under normoxia and hypoxia for 48 hours. M-MDSCs were then co-cultured with CFSE labeled splenocytes from WT mice in an anti-CD3 coated 96-well flat-bottom plate in the presence of anti-CD28 for 72 hours. Cells were then stained for CD4 and CD8, and T cell proliferation was measured using flow cytometry (**Fig. 36**). Our results show that MDSCs cultured under hypoxic conditions result in antigen non-specific suppression of CD4 and CD8 T cell proliferation (**Fig. 37 and 38**). However, MDSCs cultured under normoxia failed to cause substantial antigen non-specific T cell suppression (**Fig. 37 and 38**). These findings clearly demonstrate that M-MDSCs under hypoxia upregulate the expression of HIF-1α which then upregulates the expression of PFKFB3 and increases the rate of anaerobic glycolysis, and results in a functional phenotype of M-MDSCs which suppress T cell activity in an antigen non-specific manner. The experiment was not repeated as it was done to demonstrate the induction of antigen non-specific suppressive profile of splenic M-MDSCs cultured under hypoxic conditions.

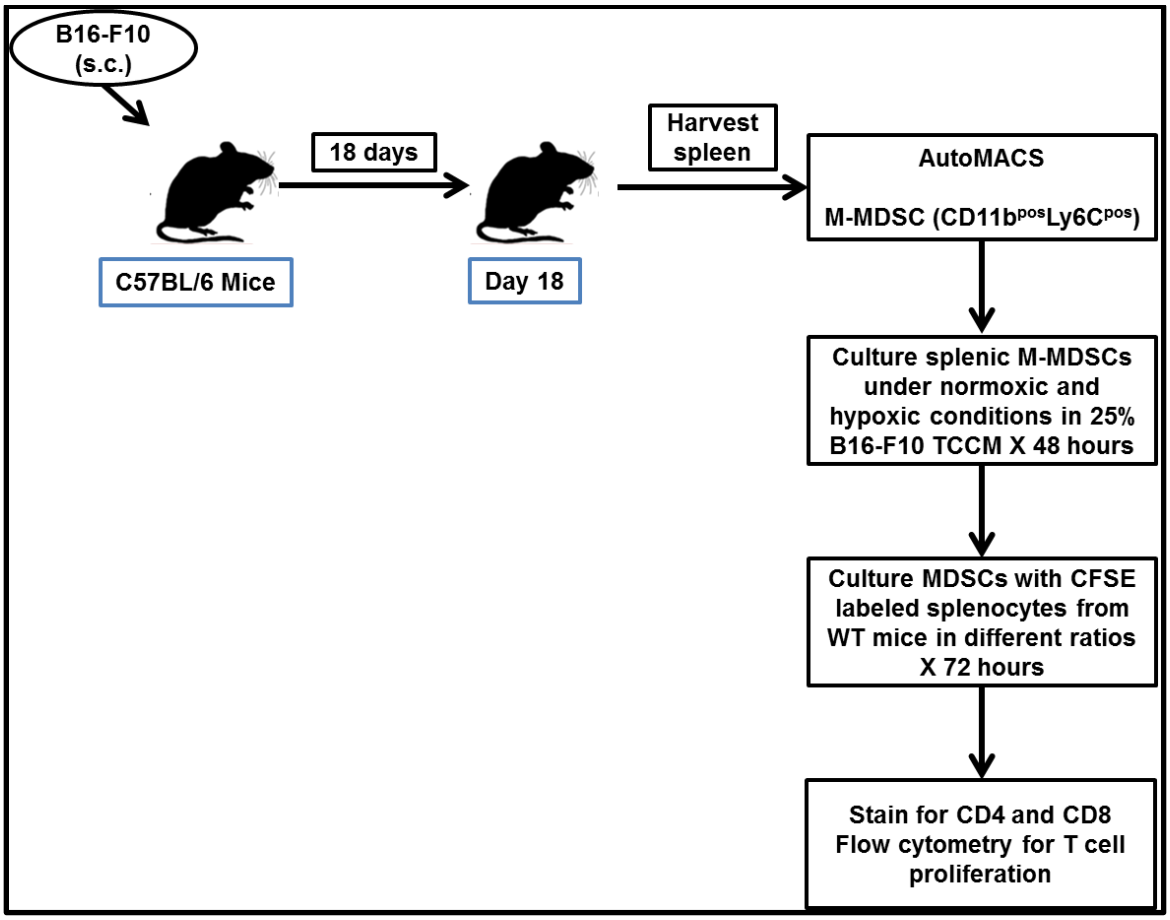

Figure 36. Schematic representation of the steps involved in set-up of functional assay for splenic M-MDSCs cultured under normoxia and hypoxia. M-MDSC sorted from the spleens of B16-F10 tumor bearing mice were cultured in 25% B16-F10 tumor cell conditioned media (TCCM) under normoxia or hypoxia for 48 hours. Cells were then co-cultured with CFSE labeled splenocytes from WT mice in anti-CD3 coated flat-bottom 96-well plate in the presence of anti-CD28 for 72 hours. Cells were then stained for CD4 and CD8 to determine differences in T cell proliferation under these two conditions.

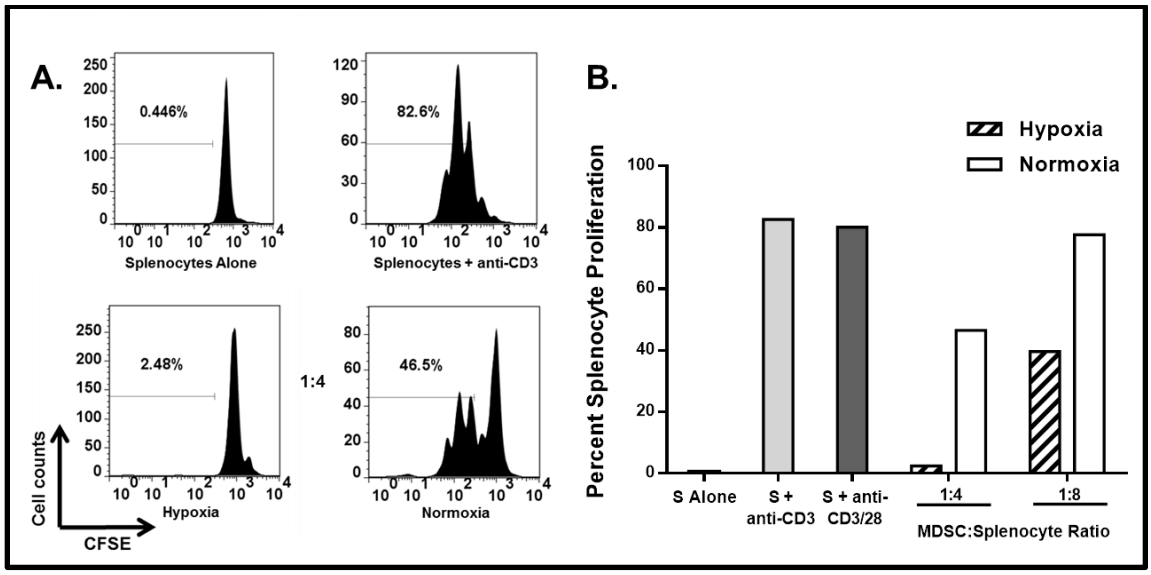

Figure 37. Splenic M-MDSCs cultured under hypoxic conditions result in antigen non-specific suppression of CD4 T cells. (A and B) Splenic M-MDSCs were cultured under normoxia and hypoxia as described above in the schematic representation. Subsequently, M-MDSCs were co-cultured with CFSE-labeled splenocytes in anti-CD3 coated 96-well flat-bottom plate in the presence of anti-CD28 beads for three days. Splenocytes were then stained for CD4 and activation was determined. Representative (A) histograms and (B) bar graphs showing the percentage of proliferated splenocytes.

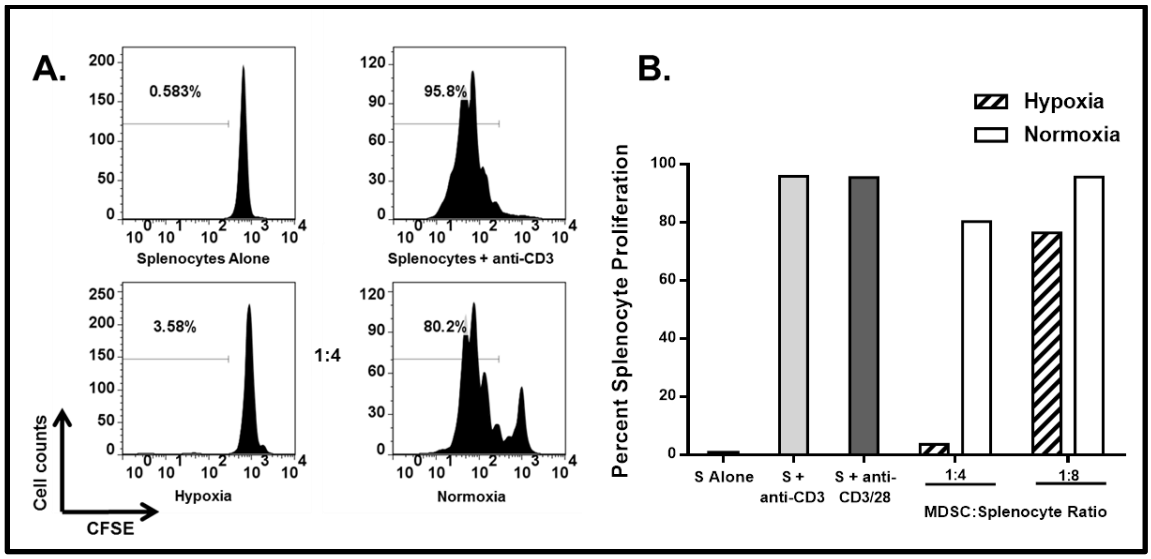

Figure 38. Splenic M-MDSCs cultured under hypoxic conditions result in antigen non-specific suppression of CD8 T cells. (A and B) Splenic M-MDSCs were cultured under normoxia and hypoxia as described above in the schematic representation. Subsequently, M-MDSCs were co-cultured with CFSE-labeled splenocytes in anti-CD3 coated 96-well flat-bottom plate in the presence of anti-CD28 beads for three days. Splenocytes were then stained for CD8 and activation was determined. Representative (A) histograms and (B) bar graphs showing the percentage of proliferated splenocytes.

4.13 PFKFB3 inhibition reduces M-MDSC-mediated antigen non-specific suppressive activity under hypoxic culture conditions

Next we wanted to determine if PFKFB3 inhibition resulted in reduced M-MDSC antigen non-specific suppressive activity under hypoxia. Splenic M-MDSCs from B16-F10 tumor-bearing mice were sorted as described previously using magnetic bead separation (Miltenyi Biotec). M-MDSCs were then cultured in 25% B16-F10 TCCM under 1% O_2 for 48 hours with vehicle control and PFK-158 (5 µM). At the end of 48 hours, cells were harvested, washed and co-cultured with CFSE labeled splenocytes from C57BL/6 WT mice in different ratios in an anti-CD3 coated 96-well plate in the presence of anti-CD28 for 72 hours. Cells were then harvested and stained for CD4 and CD8, and T cell proliferation was determined using flow cytometry (**Fig. 39**). PFKFB3 inhibition with PFK-158 resulted in reduced M-MDSC antigen non-specific CD4 and CD8 T cell suppression under hypoxia (Fig. 40 and 41). Again, M-MDSC suppression was more pronounced for CD4 compared to CD8 T cells (**Fig. 40 and 41**). These data provide further evidence that PFKFB3 inhibition can modulate M-MDSC suppression and improve T cell proliferation.

Similar to our previous experiments, we wanted to determine if hypoxic conditions and PFKFB3 inhibition resulted in the change of phenotype. At 48 hours, there was no difference in the frequency and phenotype of splenic M-MDSCs cultured under normoxia, hypoxia with vehicle control and hypoxia with PFK-158 (**Fig. 42**). The percentage of $GR1^{pos}$ population decreases when cells are cultured *ex vivo* due to spontaneous loss of antigenic expression.

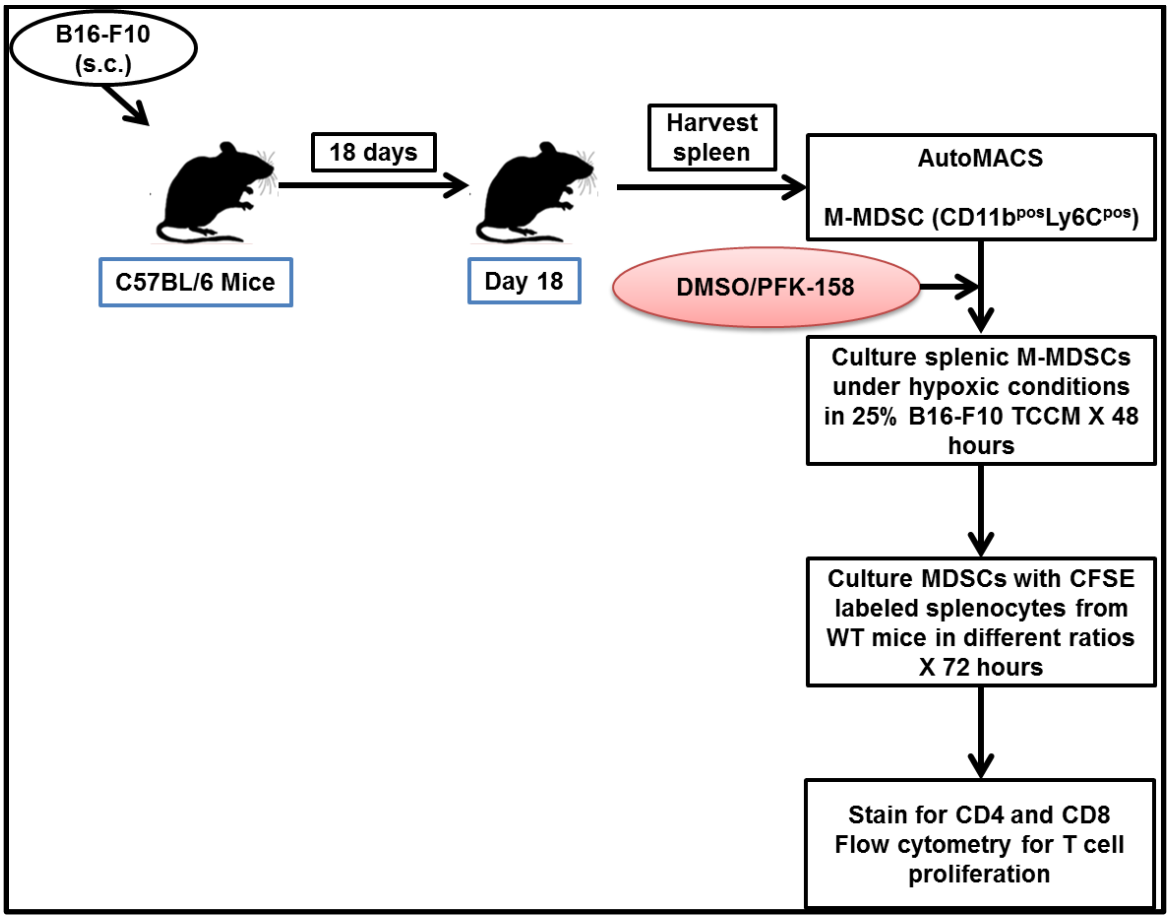

Figure 39. Schematic representation of the steps involved in set-up of functional assay with splenic M-MDSCs under hypoxia with or without PFK-158. M-MDSC sorted from the spleens of B16-F10 tumor bearing mice were cultured in 25% B16-F10 tumor cell conditioned media (TCCM) under hypoxia for 48 hours with vehicle control and PFK-158 (5 μM). Cells were harvested and washed after 48 hours, and then co-cultured with CFSE labeled splenocytes from WT mice in an anti-CD3 coated flat-bottom 96-well plate in the presence of anti-CD28 for 72 hours. Cells were then stained for CD4 and CD8 to determine differences in T cell proliferation under these two conditions.

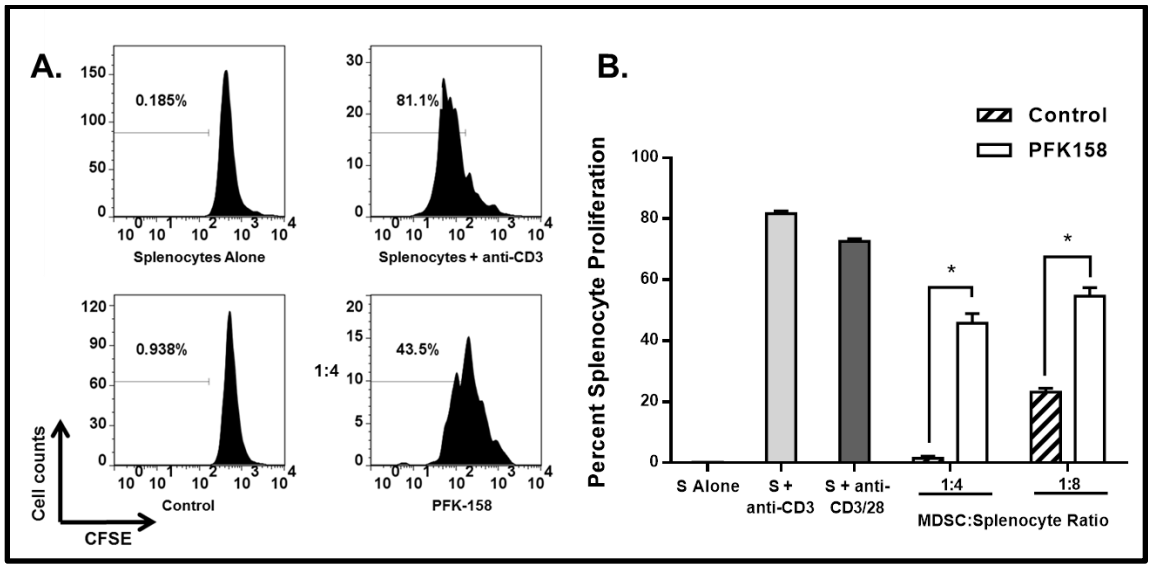

Figure 40. PFKFB3 inhibition reduces M-MDSC antigen non-specific suppressive activity for CD 4 T cells under hypoxic conditions. (A and B) Splenic M-MDSCs were cultured under hypoxia with vehicle control and PFK-158 as described above in the schematic representation. Subsequently, M-MDSCs were co-cultured with CFSE-labeled splenocytes in anti-CD3 coated 96-well flat-bottom plate in the presence of anti-CD28 beads for three days. Splenocytes were then stained for CD4 and activation was determined. Representative (A) histograms and (B) bar graphs showing the percentage of proliferated splenocytes. Results are representative of three independent experiments. *p≤0.05.

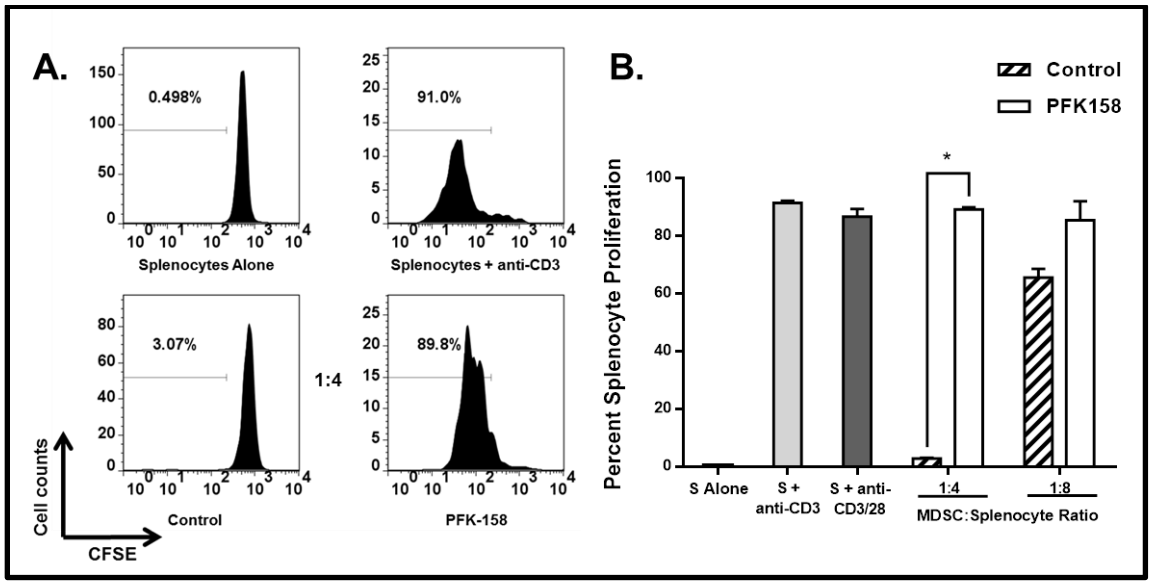

Figure 41. PFKFB3 inhibition reduces M-MDSC antigen non-specific suppressive activity for CD 8 T cells under hypoxic conditions. (A and B) Splenic M-MDSCs were cultured under hypoxia with or without PFK-158 as described above in the schematic representation. Subsequently, M-MDSCs were co-cultured with CFSE-labeled splenocytes in anti-CD3 coated 96-well flat-bottom plate in the presence of anti-CD28 beads for three days. Splenocytes were then stained for CD8 and activation was determined. Representative (A) histograms and (B) bar graphs showing the percentage of proliferated splenocytes. Results are representative of three independent experiments. *p≤0.05.

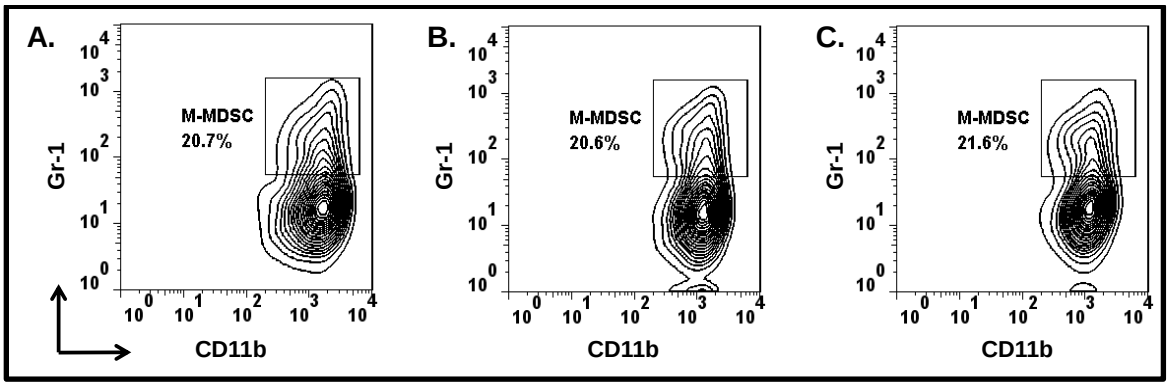

Figure 42. PFKFB3 inhibition does not change phenotype of splenic M-MDSCs under hypoxic conditions. Representative contour plot (A) splenic M-MDSC under normoxia, under hypoxia for 48 hours with (B) vehicle control, and (C) PFK-158.

4.14 PFK-158 reduces M-MDSC suppressive activity *in vivo*

In order to evaluate the efficacy of PFKFB3 inhibition on M-MDSC suppressive function, B16-F10 tumor bearing C57BL/6 WT mice were injected intra-peritoneally with PFK-158. Mice were randomized to vehicle control (DMSO) or PFK-158 groups. When the tumor volume reached approximately 100 mm^3, they were injected with DMSO and PFK-158 intraperitoneally on days 11, 13, 16 and 18. Tumor volumes were measured on the days of injections. On day 19, spleens from mice in the both groups were harvested. M-MDSCs were sorted as described previously using magnetic bead sorting (Miltneyi Biotec). Equal number of splenic M-MDSCs from both groups were co-cultured with CFSE labeled OT-II splenocytes in the presence of ovalbumin in flat-bottom 96-well plate for 72 hours. Cells were then stained for CD4 and T cell proliferation was measured using flow cytometry. PFKFB3 inhibition with PFK-158 was associated with decrease in tumor volumes compared to the control (**Fig. 43A**). Also, splenic M-MDSCs from PFK-158 treated mice were less suppressive to CD4 T cell function compared to the vehicle control treated mice (**Fig. 43B**).

Further, we sought to evaluate the effect of *in vivo* PFKFB3 inhibition on markers of suppression in splenic M-MDSCs. Using qRT-PCR, splenic M-MDSCs isolated from PFK-158 treated mice had lower expression of arginase 1 mRNA compared with vehicle control treated mice (**Fig. 44A**). Also, splenic M-MDSCs from tumor bearing mice treated with vehicle control had significantly higher arginase activity compared with naïve mice (**Fig. 44B**). This high arginase activity in tumor bearing mice decreased significantly following treatment with

PFK-158 (**Fig. 44B**). In addition, we analyzed the expression of iNOS by qRT-PCR in vehicle control and PFK-158 treated tumor-bearing mice. Treatment with PFK-158 resulted in reduced expression of iNOS mRNA compared to treatment with vehicle control (**Fig. 44C**).

Next, we wanted to assess phenotypic changes in different immune cell populations in tumor-bearing mice with and without treatment with PFK-158. Interestingly, following treatment with PFK-158 monocytic MDSC ($SSC^{low}CD11b^{pos}GR1^{low}$) population decreased compared with vehicle control treated mice (**Fig. 45**). However, PFKFB3 inhibition did not have any effect on the frequencies of PMN-MDSCs ($SSC^{high}CD11b^{pos}GR1^{high}$) between vehicle control and PFK-158 treated mice (**Fig. 45**). There was also no change in the frequencies of macrophages ($CD11b^{pos}F4/80^{pos}$) seen following treatment with PFK-158 (**Fig. 46A**); however, there was an increase in the population of DCs ($CD11b^{pos}CD11c^{pos}$) (**Fig. 46B**).

These data combined, provide substantial evidence that PFKFB3 inhibition *in vivo* not only reduces splenic M-MDSC suppressive activity through reduced expression of suppressive markers such as arginase 1 and iNOS but also reduces the frequency of this immune suppressive population.

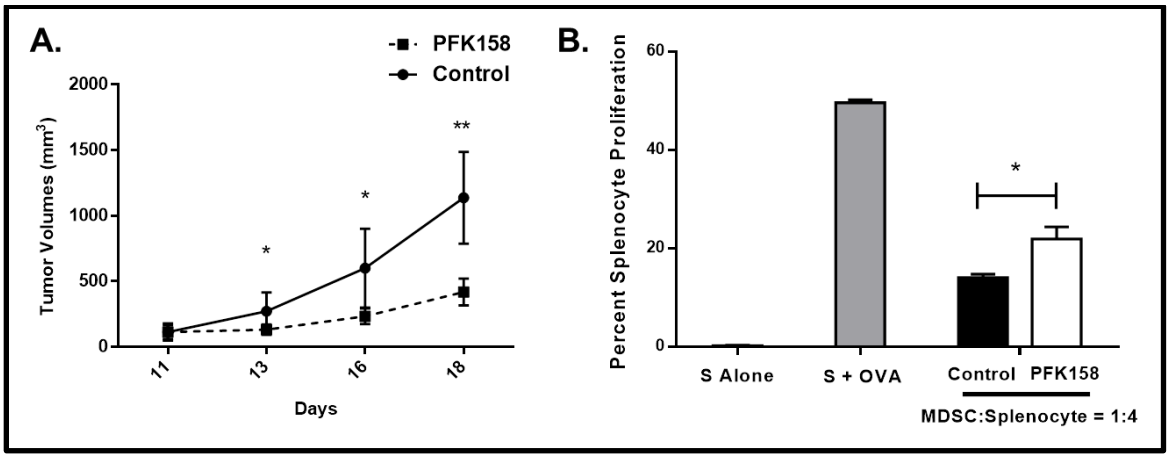

Figure 43. *In vivo* PFKFB3 inhibition reduces tumor volume and M-MDSC suppressive function. C57BL/6 WT mice were randomized to vehicle control and PFK-158 treatment (n = four per group). Mice were injected with vehicle control (DMSO) and PFK-158 when tumor volumes on average reached 100 mm^3. DMSO and PFK-158 were administered intra-peritoneally on days 11, 13, 16 and 18 for total of four injections. Tumor measurements were taken on the days of the injections using digital calipers and tumor volumes were calculated based on the formula=length × $width^2/2$. On day 19, spleens from each group were harvested and M-MDSCs were isolated using magnetic bead separation as described previously. M-MDSCs were co-cultured with CFSE labelled OT-II splenocytes in the presence of ovalbumin and percent splenocyte proliferation was determined using flow cytometry. (A) Line graph of tumor volumes and (B) bar graph showing the percentage of proliferated CD4 T cells following intra-peritoneal injections with DMSO and PFK-158. Results are representative of three independent experiments. *p≤0.05, **p≤0.005.

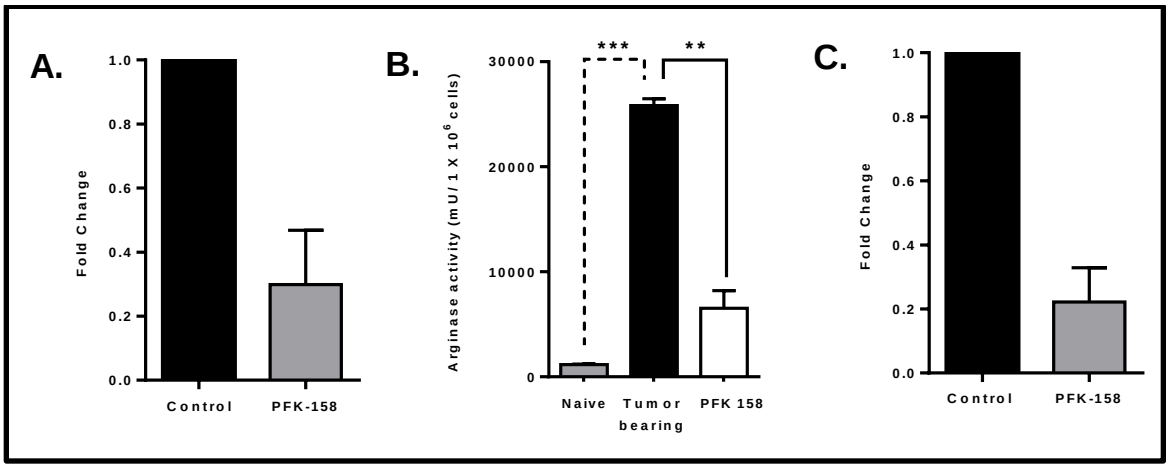

Figure 44. *In vivo* PFKFB3 inhibition reduces splenic M-MDSC suppressive markers. Representative bar graph showing results of (A) qRT-PCR for arginase 1 mRNA expression in splenic M-MDSCs isolated from the spleens of tumor bearing mice injected with DMSO and PFK-158, (B) Quantichrom^{TM} arginase activity assay in splenic M-MDSCs from naïve mice, tumor bearing mice injected with vehicle control and PFK-158, and (C) qRT-PCR for iNOS expression in splenic M-MDSCs isolated from the spleens of tumor bearing mice injected with DMSO and PFK-158. Results are representative of three independent experiments. *p≤0.005, ***p≤0.0005.

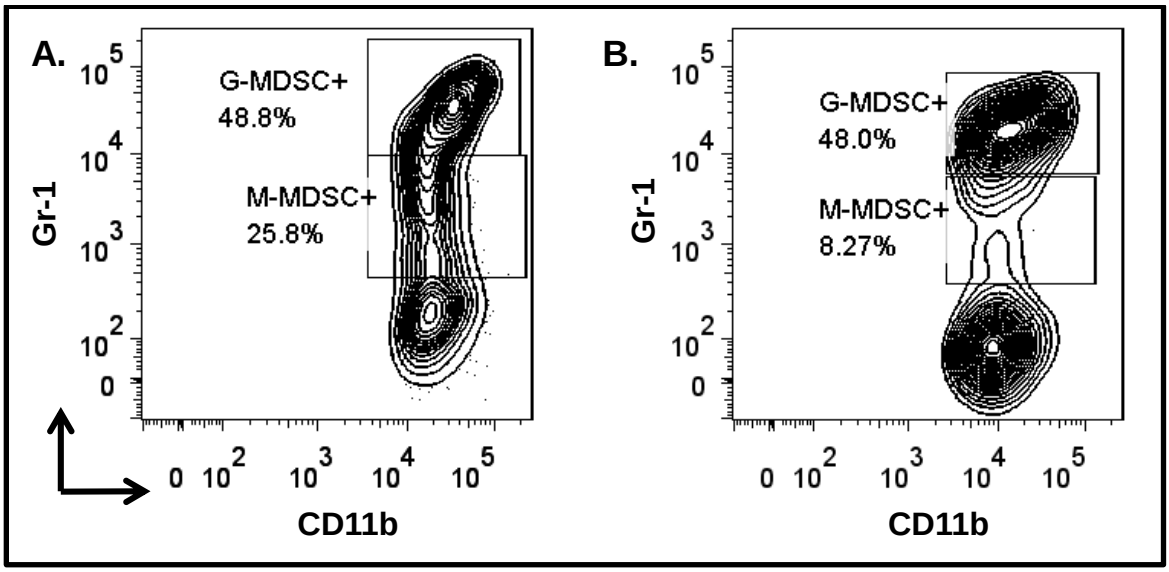

Figure 45. *In vivo* PFKFB3 inhibition reduces the frequencies of splenic M-MDSCs. Representative contour plots of splenic M-and PMN-MDSCs in (A) vehicle control and (B) PFK-158 treated mice.

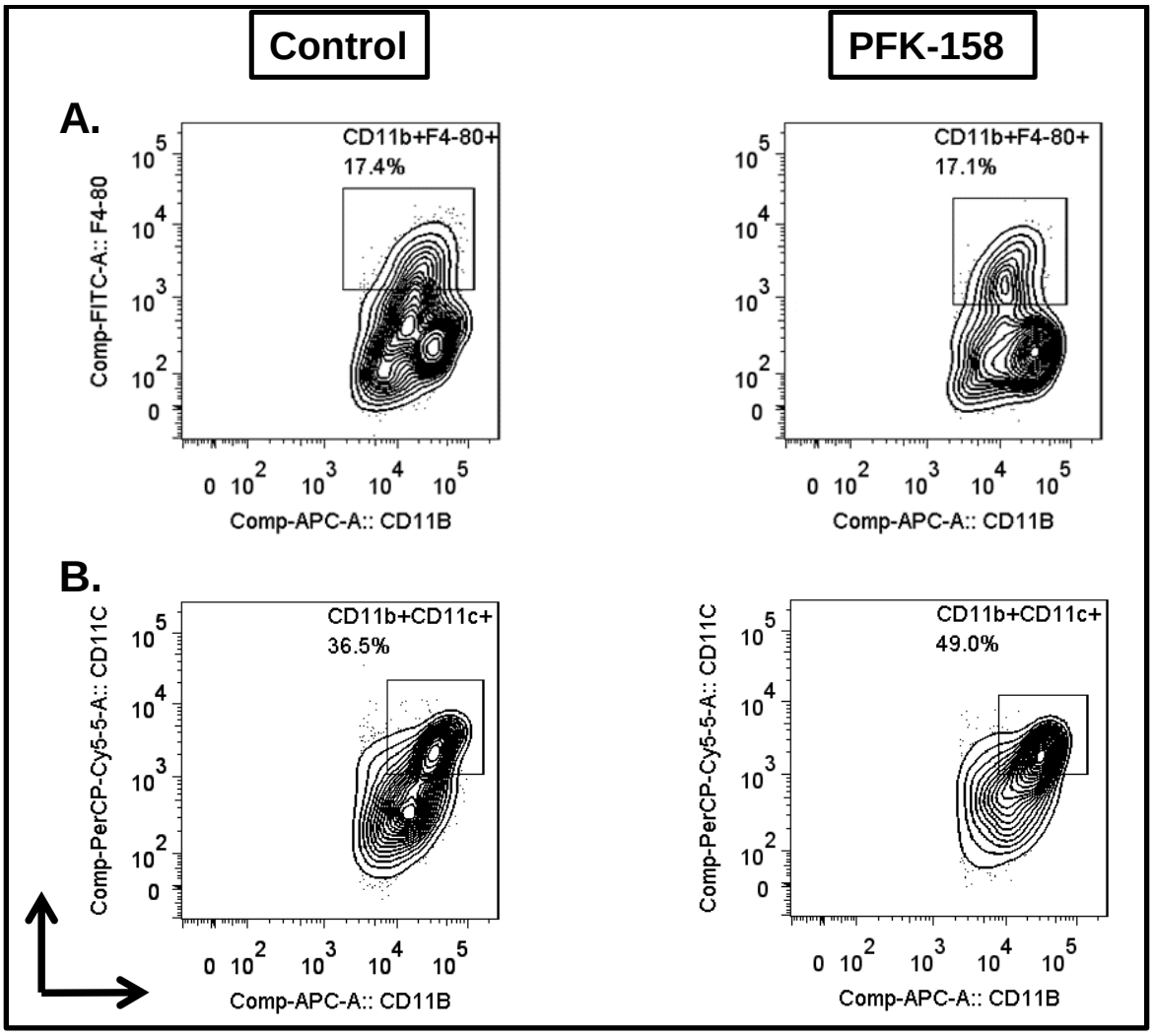

Figure 46. *In vivo* PFKFB3 inhibition increases the frequencies of DCs. (A) Representative contour plots of (A) macrophages and (B) DCs in vehicle control and PFK-158 treated mice.

4.15 PFKFB3 inhibition reduces lactic acid production in M-MDSCs

One of the consequences of increased glycolytic flux is the increased production of lactic acid (32). Changes in the amount of lactic acid produced following PFKFB3 inhibition with PFK-158 was performed using a colorimetric lactate assay. Supernatants from M-MDSCs cultured in equal numbers treated with vehicle control and PFK-158 were collected and amount of lactic acid was measured as per manufacturer's protocol. PFKFB3 inhibition resulted in significant decrease in lactic production in splenic M-MDSCs, whole BM-MDSCs and bone marrow-derived M-MDSCs compared to treatment with vehicle control (**Fig. 47A, B and C**). LDHA mRNA expression on qRT-PCR showed significant decrease in the mice treated PFK-158 compared to vehicle control (**Fig. 47D**).

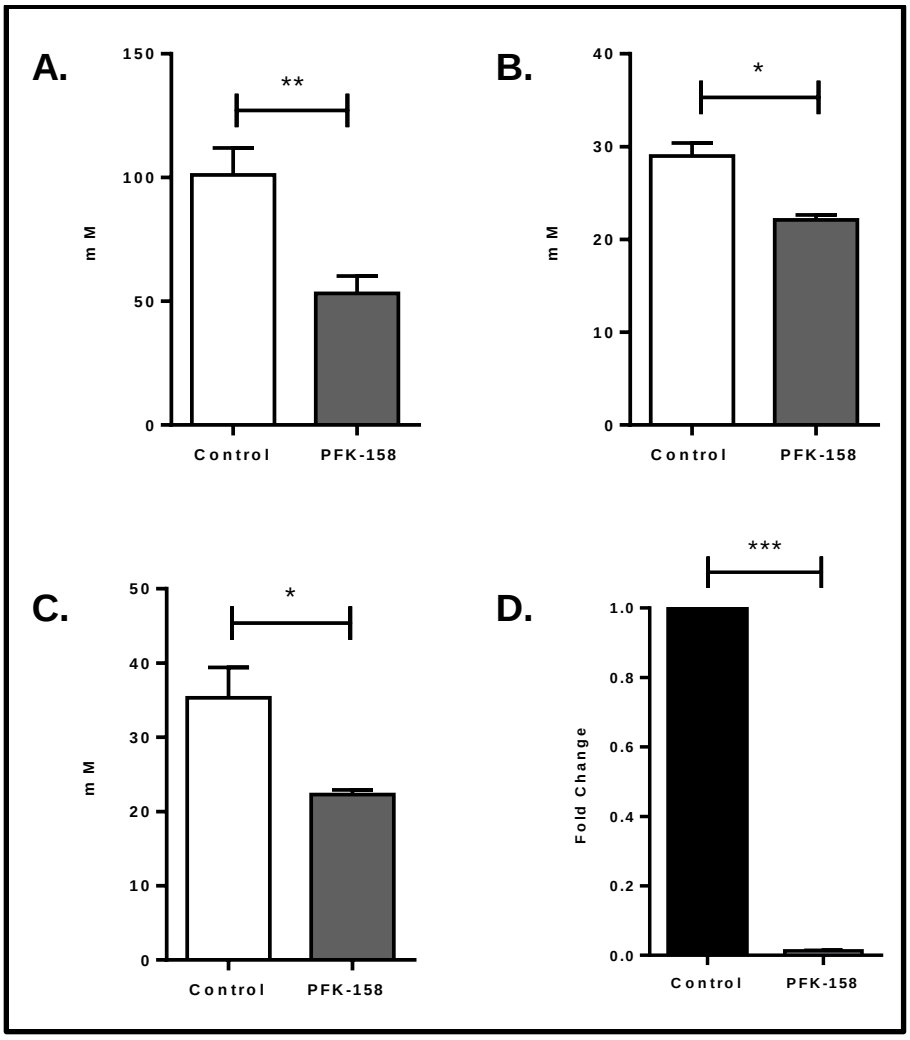

Figure 47. PFKFB3 maintains lactic acid production in M-MDSCs. Colorimetric lactate assay was performed to measure differences in lactic acid production between vehicle control and PFK-158 treated groups. Representative bar graphs for lactic acid production in (A) splenic M-MDSCs, (B) whole BM-MDSCs and (C) bone marrow-derived M-MDSCs with and without treatment with PFK-158, and (D) qRT-PCR for LDHA mRNA expression in the splenic M-MDSCs sorted from tumor-bearing mice injected with vehicle control or PFK-158. Results are representative of three independent experiments. *p≤0.05, **p≤0.005, ***p≤0.0005.

4.16 PFKFB3 inhibition reduces intracellular concentration of F-2,6-BP and glucose uptake

To evaluate the efficiency of PFK-158 at inhibiting PFKFB3, intracellular levels of F-2,6-BP were determined using a previously described protocol. PFK-158 at 5 μM dose significantly reduced intracellular levels of F-2,6-BP in the whole BM-MDSCs (**Fig. 48A**) and $GR1^{pos}$ BM-MDSCs (**Fig. 48B**). We also evaluated the efficiency of PFK-158 in reducing glucose uptake by MDSCs. In bone marrow-derived M-MDSCs, one hour treatment with PFK-158 resulted in reduced glucose uptake (**Fig. 49**). Together, these results provide evidence that PFK-158 inhibits PFKFB3 function and reduces glucose uptake by MDSCs.

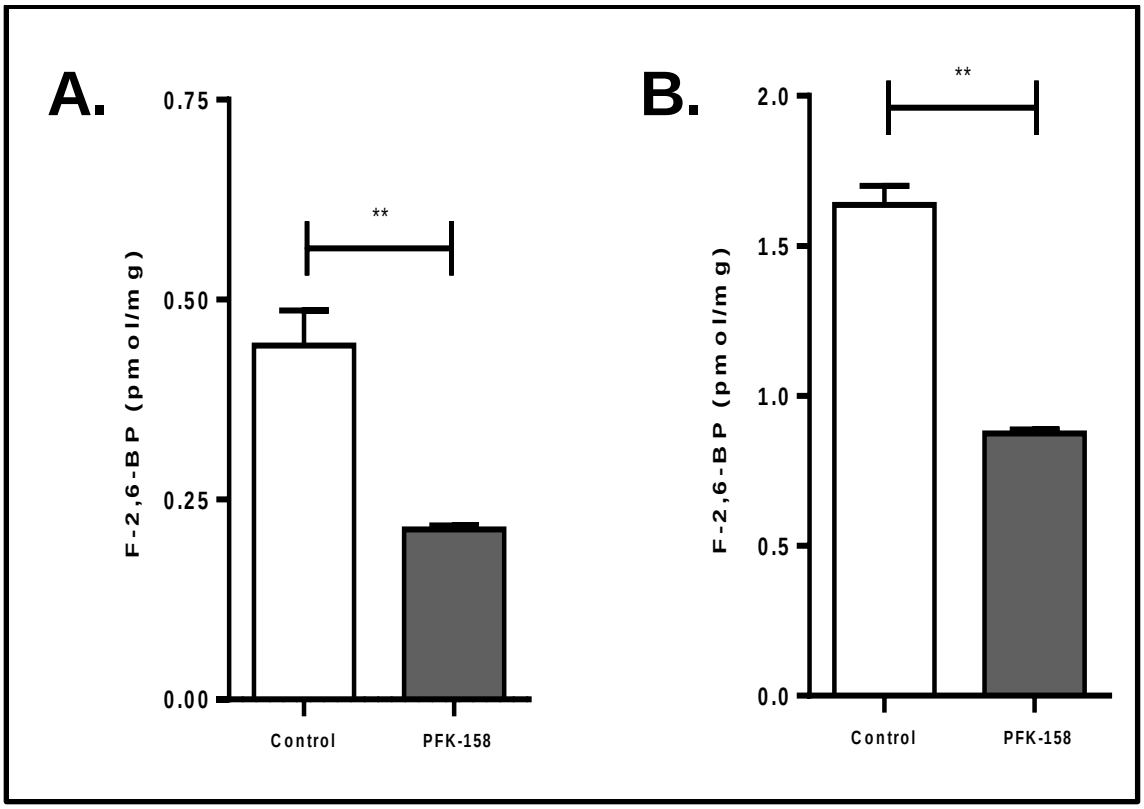

Figure 48. PFK-158 reduces intracellular concentration of F-2,6-BP. Intracellular concentration of F-2,6-BP was measured as per previously described protocol. Representative bar graphs for F-2,6-BP levels with and without treatment with PFK-158 in (A) whole BM-MDSCs and (B) $GR1^{pos}$ BM-MDSCs. Results are representative of three independent experiments. **p≤0.005.

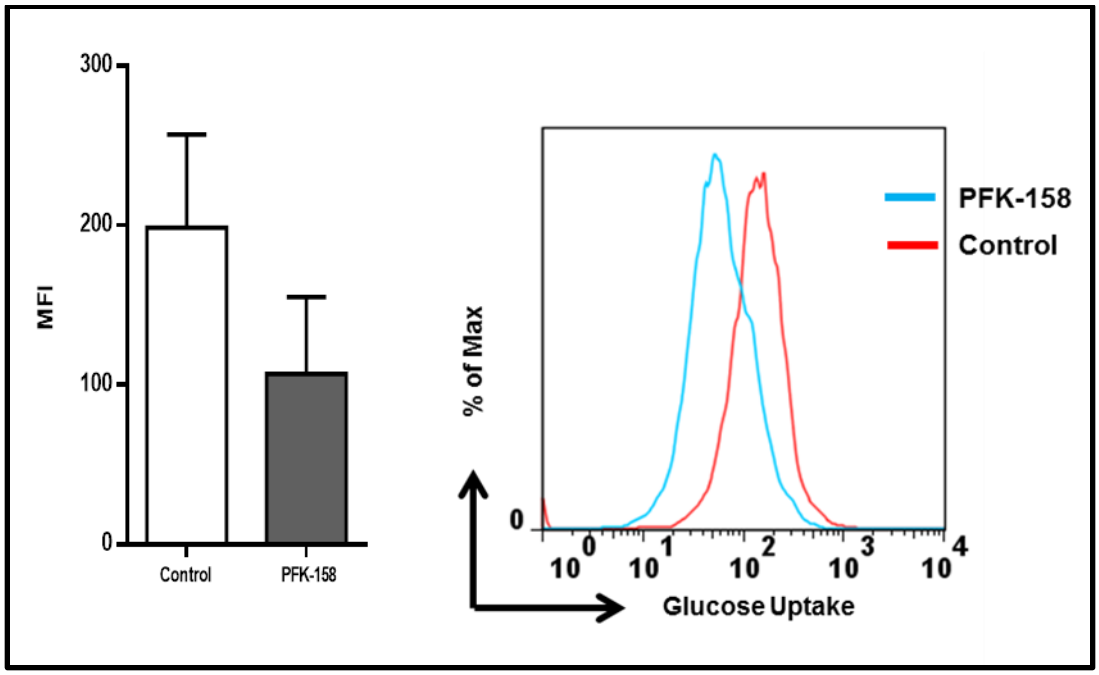

Figure 49. PFK-158 reduces glucose uptake in bone marrow-derived M-MDSCs. Glucose uptake by bone marrow-derived M-MDSCs was performed following one hour treatment with vehicle control and PFK-158. Cells were gated on FL1 channel. Representative bar graph and histogram for glucose uptake in bone marrow-derived M-MDSCs. Results are representative of three independent experiments.

5.0 RESULTS – HUMAN STUDIES

5.1 PFKFB3 inhibition reduces circulating M-MDSC suppressive activity from late-stage melanoma patients

We have now demonstrated that PFKFB3 inhibition reduces suppressive activity of M-MDSCs in mice. Next we wanted to determine if PFKFB3 inhibition resulted in reduced suppressive activity of circulating M-MDSCs from late-stage melanoma patients. Patients with late-stage melanoma presenting to the James Graham Brown Cancer Center at the University of Louisville who had been recently diagnosed and had not received any treatment in the prior six months were identified. Informed consent was obtained from the patients prior to the collection of peripheral blood as covered under University of Louisville IRB protocol number 08.0388. Peripheral blood from the patients was collected in CPT® tubes. Buffy coat was removed after centrifugation at 1600xg for 20 minutes. Cells were washed and $CD14^{pos}$ MDSCs were isolated using magnetic bead separation as per manufacturer's protocol (Miltneyi Biotec). M-MDSCs were then treated with vehicle control and PFK-158 for 16-18 hours. The following day,

cells were washed and co-cultured with CFSE labeled autologous T cells for four days. Flow cytometry was then performed to measure T cell proliferation (**Fig. 50**).

PFKFB3 inhibition with PFK-158 significantly reduced circulating M-MDSC suppression on T cell proliferation and increased IFN-γ secretion compared to vehicle control (**Fig. 51 A-C**). We also sought to determine the effect of PFKFB3 inhibition on M-MDSC markers of suppression. qRT-PCR showed that circulating M-MDSCs from late-stage melanoma patients had high expression of iNOS mRNA compared with normal donors (**Fig. 52A**). And following treatment with PFK-158, the expression of iNOS mRNA was reduced significantly (**Fig. 52B**). Similarly on arginase assay, PFKFB3 inhibition with PFK-158 resulted in significant reduction in activity compared to vehicle control (**Fig. 52C**). No difference in frequency or the phenotype was noted following treatment with vehicle control and PFK-158 (**Fig. 53 A and B**).

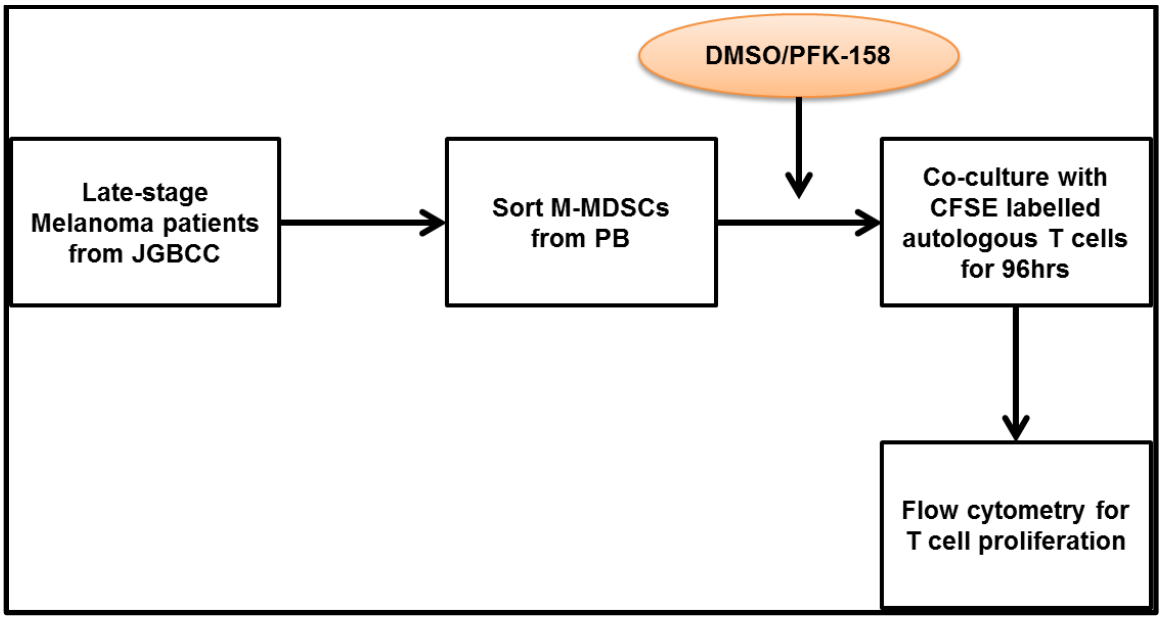

Figure 50. Schematic representation of the steps involved in isolating circulating M-MDSCs from late-stage melanoma patients. Patients with late-stage melanoma presenting to the James Graham Brown Cancer Center (JGBCC) at the University of Louisville were identified for the study. Peripheral blood was collected in CPT® tubes by the staff of the JGBCC Biorepository and covered under University of Louisville IRB protocol number 08.0388. Following centrifugation at 1600xg, buffy coat was collected and $CD14^{pos}$ M-MDSCs were sorted using magnetic bead separation as per manufacturer's protocol. M-MDSCs were then treated with vehicle control and PFK-158 for 16-18 hours. Cells were washed and then co-cultured with CFSE labelled autologous T cells for 96 hours. Flow cytometry was then performed to determine T cell proliferation.

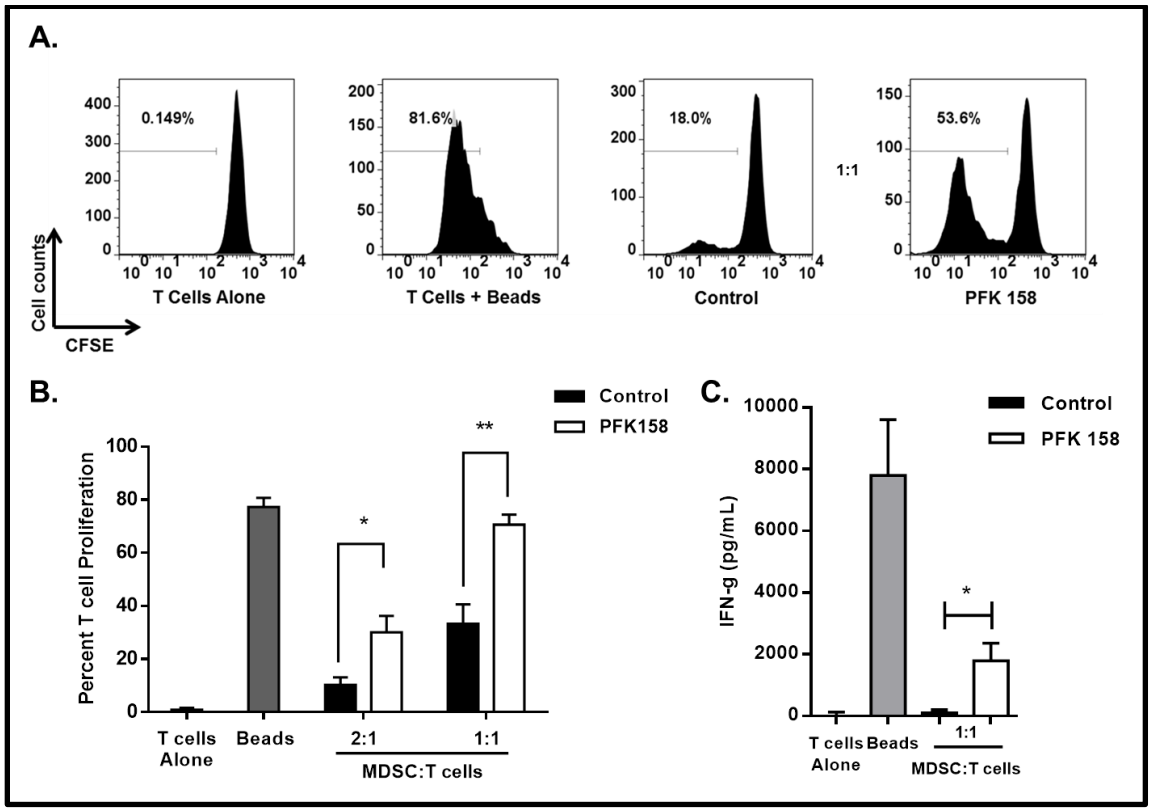

Figure 51. PFKFB3 inhibition reverses suppressive activity of circulating M-MDSCs from late-stage melanoma patients. Melanoma patient-derived $CD14^{pos}$ MDSCs (n=7) were pretreated with vehicle control and PFK-158 (5 μM). M-MDSCs were then co-cultured with CFSE-labeled autologous T cells in the presence of anti-CD3/anti-CD28 beads for four days and T-cell activation was determined. Representative (A) histograms and (B) bar graphs showing the percentage of proliferated T cells and (C) IFN-γ production. *p≤0.05, **p≤0.005.

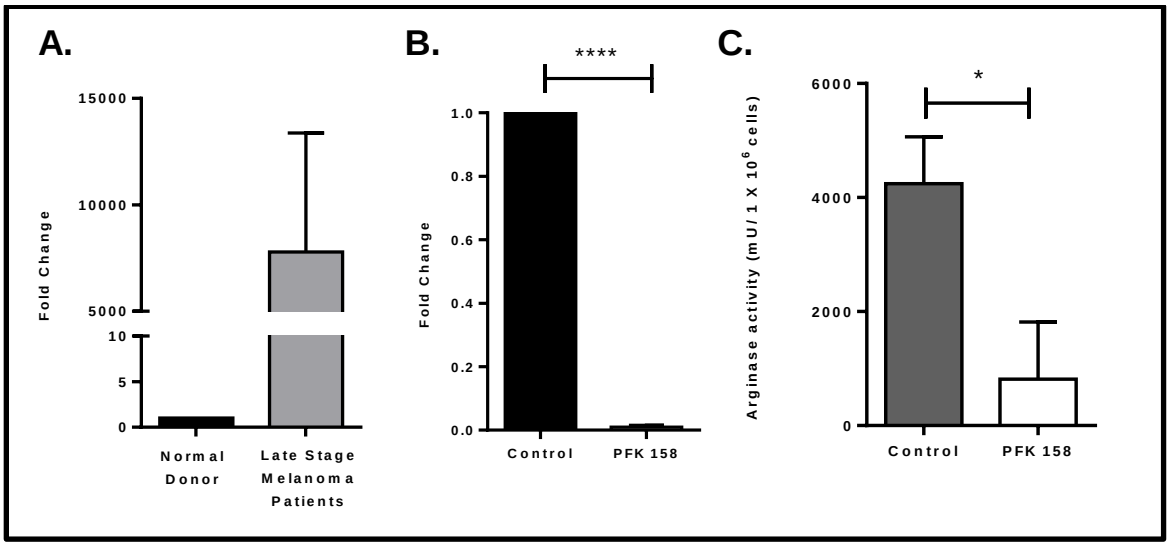

Figure 52. PFKFB3 inhibition decreases markers of suppression in circulating M-MDSCs from late-stage melanoma patients. Representative bar graphs showing results of (A) qRT-PCR analysis of iNOS mRNA expression in circulating $CD14^{pos}$ cells from normal donors (n=5) and late-stage melanoma patients (n=5), (B) iNOS mRNA expression (n=5) and (C) Quantichrom™ arginase assay (n=2) showing arginase activity in circulating M-MDSCs following treatment with vehicle control and PFK-158. *p≤0.05, ***p≤0.0005.

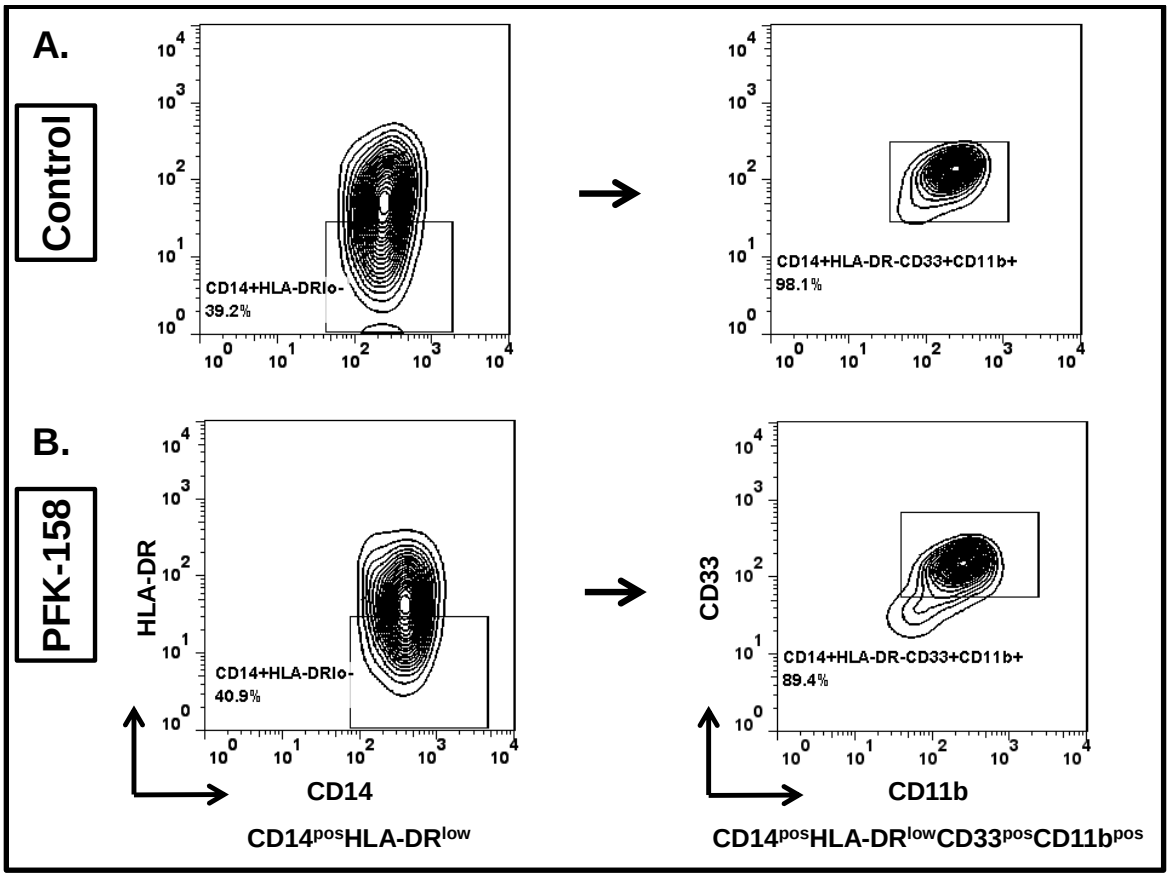

Figure 53. PFKFB3 inhibition does not change frequency and phenotype of circulating M-MDSCs from late-stage melanoma patients. Representative contour plots of circulating M-MDSCs from late-stage melanoma patients ($CD14^{pos}HLA\text{-}DR^{low}CD33^{pos}CD11b^{pos}$) cultured with (A) vehicle control (DMSO) and (B) PFK-158.

5.2 PFKFB3 inhibition reduces A375-MDSC suppressive activity

We next sought to recapitulate the findings of PFKFB3 inhibition in circulating M-MDSCs from late-stage melanoma patients using MDSCs derived from the A375:monocyte co-culture model. We tested two independent models for different timing of PFKFB3 inhibition by PFK-158. In the first model, we cultured A375 melanoma cells with $CD14^{pos}$ monocytes from normal donors in the presence of PFK-158 during the induction phase, followed by co-culturing purified A375-MDSCs ($CD14^{pos}CD11b^{pos}$) with CFSE labeled autologous T cells for an additional 96 hours (**Fig. 54**). In the second model, A375:monocyte co-culture was allowed to differentiate for 72 hours, followed by purification of A375-MDSCs which were then treated with PFK-158 and vehicle control for 16-18 hours and then co-cultured with CFSE labeled autologous T cells for four days (**Fig. 55**). At the end of the 96-hour MDSC:T cell co-culture, T cell proliferation was measured by flow cytometry. In both the models, PFKFB3 inhibition resulted in reduced A375-MDSC suppressive activity as determined by increased T cell proliferation and IFN-γ production in PFK-158 treated A375-MDSC:T cell co-cultures (**Fig. 56 and 57**). In the first model, PFK-158 was added during the $CD14^{pos}$ monocyte and A375 co-culture. This may have inadvertently resulted in reduced TDSFs from the decrease in melanoma cell line proliferation. In order to overcome this limitation, second model was employed where PFK-158 was added following $CD11b^{pos}$ cell sorting. On western blot analysis, A375-MDSCs expressed high PFKFB3 compared to cultured monocytes and fresh monocytes from normal donors (**Fig. 58**).

Next step was to determine the mechanisms for A375-MDSC suppressive activity. qRT-PCR showed that A375-MDSCs had high expression of both arginase 1 and iNOS mRNA compared with cultured monocytes (**Fig. 59A and 60A**). PFKFB3 inhibition with PFK-158 resulted in significant decrease in mRNA expression of both these markers (**Fig. 59B and 60B**). Arginase assay showed that A375-MDSCs had significantly higher activity compared with fresh and cultured monocytes (**Fig. 59C**). The arginase activity decreased significantly following PFKFB3 inhibition (**Fig. 59C**). Furthermore, there was no difference in DCF-detectable ROS in A375-MDSC following PFKFB3 inhibition. These data validate our murine studies, where PFKFB3 inhibition was associated with reduced M-MDSC suppressive activity which correlated with significant reductions in arginase and iNOS expression.

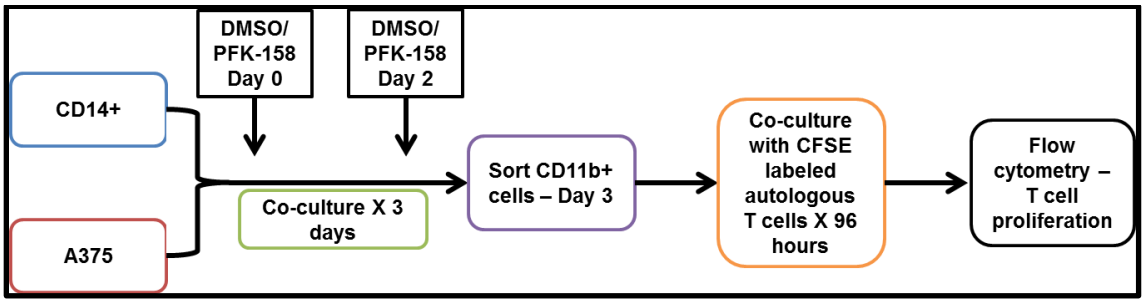

Figure 54. Schematic representation of the steps involved in generation of A375-MDSCs and PFKFB3 inhibition during the differentiation process.

$CD14^{pos}$ monocytes sorted from the peripheral blood of normal donor were cultured with A375 melanoma cells for four days. PFK-158 (5 µM) or vehicle control (DMSO) was added on day zero and day two. On day three, using magnetic bead separation $CD11b^{pos}$ cells were isolated as per manufacturer's protocol. A375-MDSCs ($CD14^{pos}CD11b^{pos}$) cells were then co-cultured with CFSE labelled autologous T cells for 96 hours and flow cytometry was performed to determine T cell proliferation.

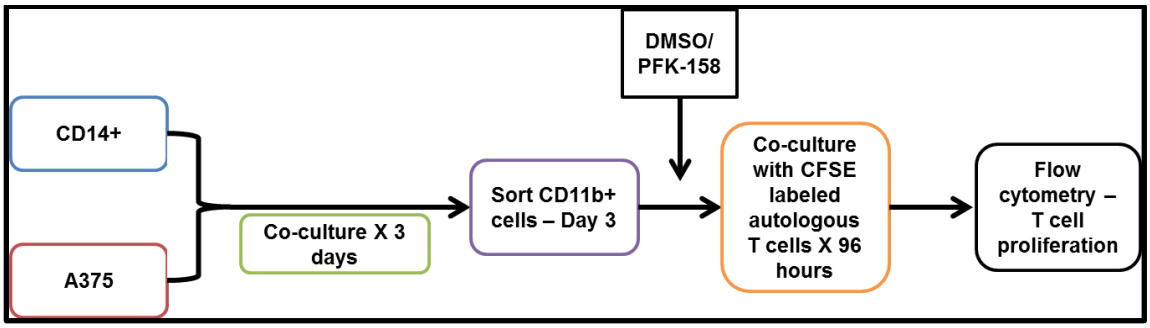

Figure 55. Schematic representation of the steps involved in generation of A375-MDSCs and PFKFB3 inhibition post-differentiation process. $CD14^{pos}$ monocytes sorted from the peripheral blood of normal donor were cultured with A375 melanoma cells for three days. On day three, using magnetic bead separation $CD11b^{pos}$ cells were isolated as per manufacturer's protocol. A375-MDSCs ($CD14^{pos}CD11b^{pos}$) were then treated with vehicle control and PFK-158 (2.5 µM or 5 µM) for 16-18 hours. The following day, cells were washed and co-cultured with CFSE labelled autologous T cells for 96 hours. Flow cytometry was then performed to determine T cell proliferation.

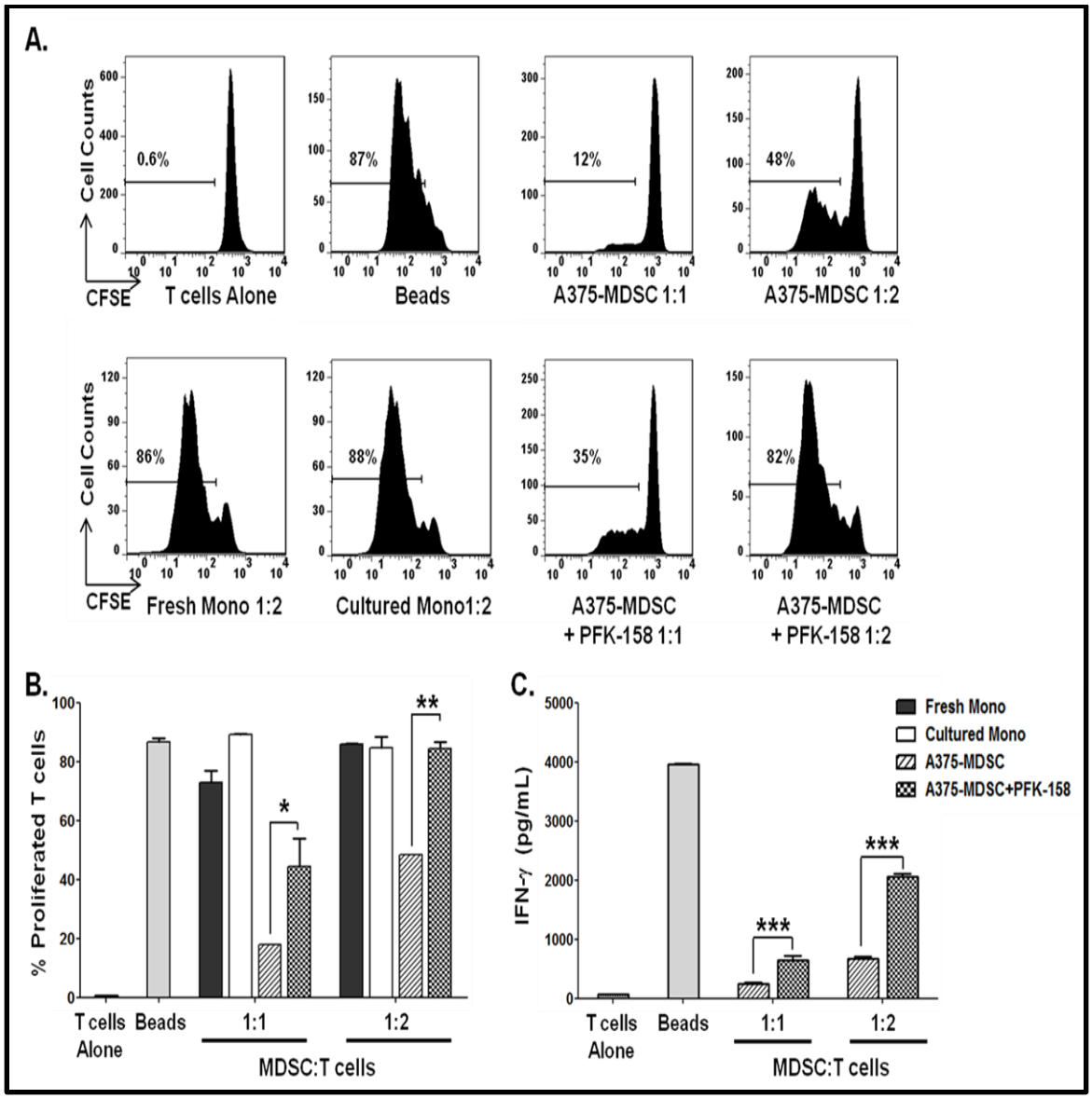

Figure 56. PFKFB3 inhibition during the A375-MDSC differentiation process reduces their suppressive activity. Autologous CFSE-labeled T cells were cultured in the presence of fresh healthy donor monocytes (fresh mono), with monocytes cultured for 72 hours in the absence of melanoma cells (cultured mono), or with monocytes co-cultured with A375 cells in the absence (A375-MDSC), or presence of PFK-158 (A375-MDSC + PFK-158 (5 µM), day zero and day two). T cells were activated with anti-CD3/anti-CD28 beads in the absence or

presence of the indicated monocytes/MDSCs for four days. (A) Representative histograms and (B) bar graphs showing the percentage of proliferated CFSE-labeled T cells and (C) IFN-γ production. Results are representative of three independent experiments. *p≤0.05, **p≤0.005, ***p≤0.0005.

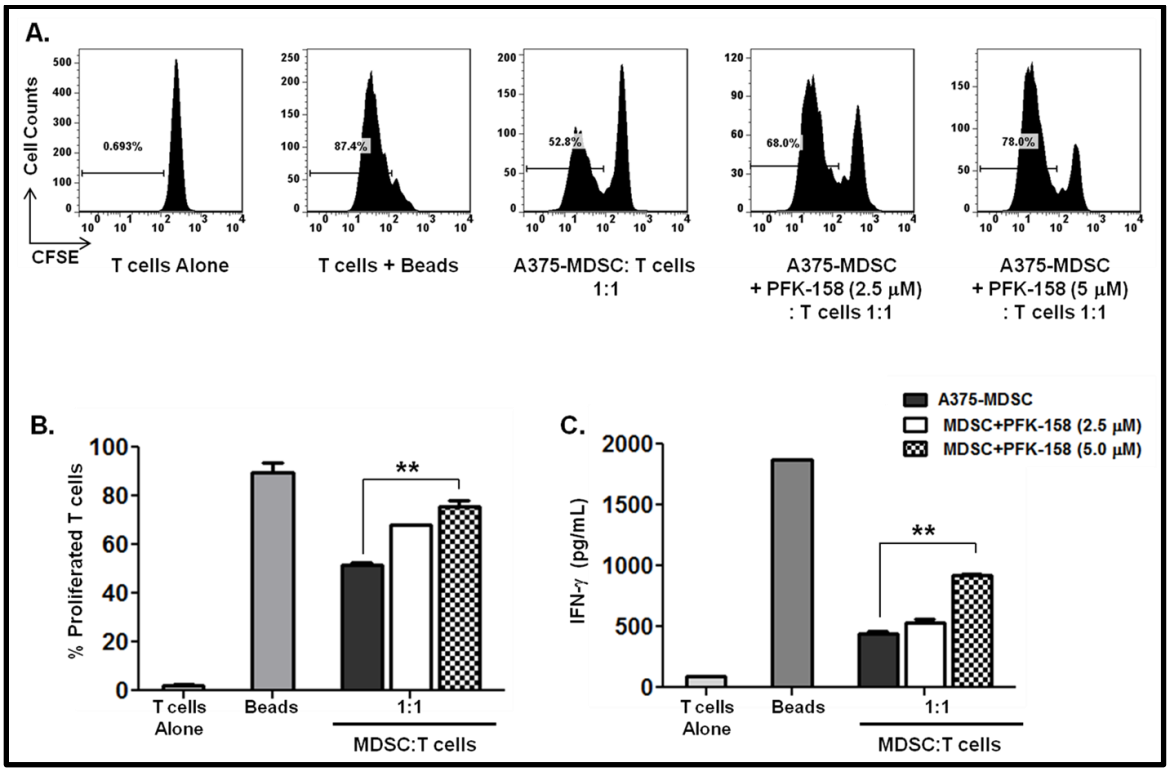

Figure 57. PFKFB3 inhibition in A375-MDSCs after differentiation reduces their suppressive activity. Autologous CFSE-labeled T cells were cultured in the presence of A375-MDSC treated with vehicle control and PFK-158 (2.5 µM or 5 µM). T cells were activated with anti-CD3/anti-CD28 beads in the absence or presence of the indicated MDSCs for four days. Representative (A) histograms and (B) bar graphs showing the percentage of proliferated CFSE-labeled T cells and (C) IFN-γ production. Results are representative of three independent experiments. **p≤0.005.

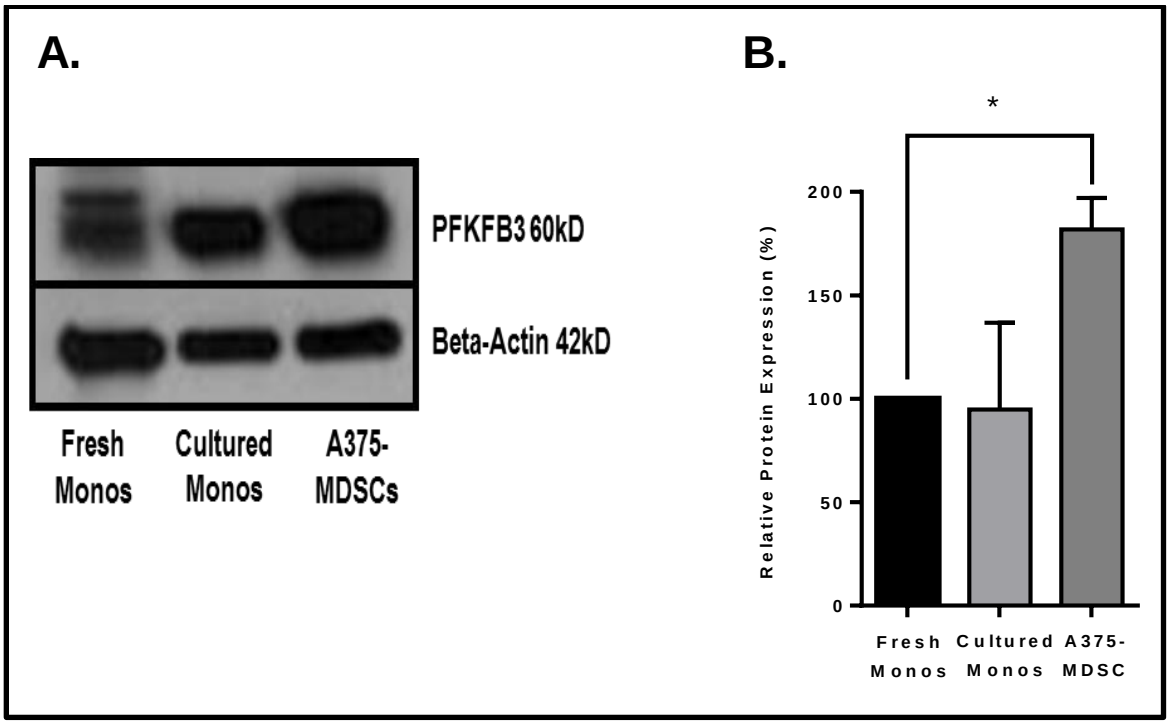

Figure 58. PFKFB3 is over-expressed in A375-MDSCs. Western blot analysis of PFKFB3 expression in A375-MDSCs compared with fresh and cultured monocytes. (A) Western blot film and (B) bar graphs showing relative PFKFB3 expression in fresh monocytes, cultured monocytes and A375-MDSCs. Results are representative of three independent experiments. *p≤0.05.

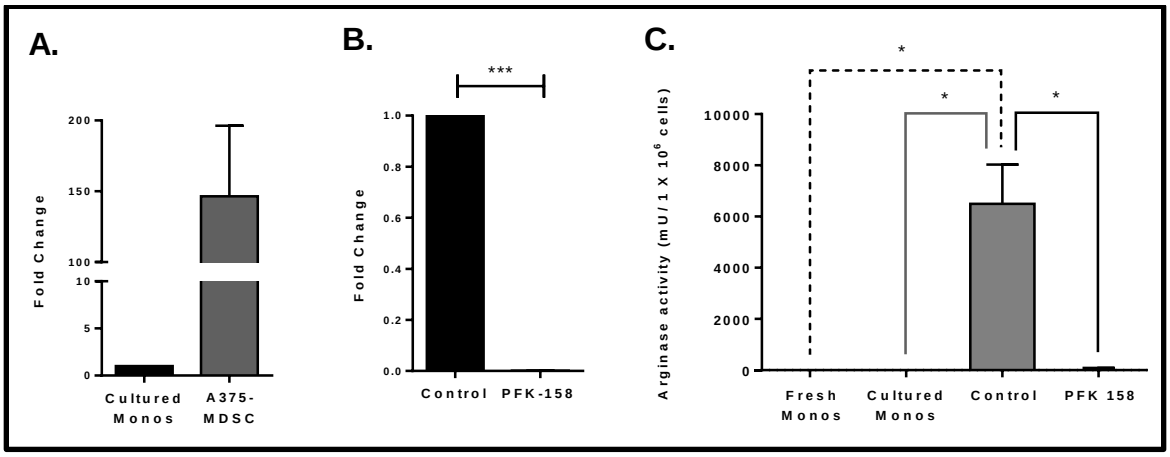

Figure 59. PFKFB3 maintains arginase expression in A375-MDSCs. Bar graphs showing results of (A) qRT-PCR of arginase 1 mRNA expression in healthy donor monocytes (n=5) cultured for 72 hours in the absence (cultured monocytes) or presence of A375 cells, (B) qRT-PCR of arginase 1 mRNA expression in A375-MDSCs treated with vehicle control and PFK-158 and (C) Quantichrom^{TM} arginase assay showing arginase activity in cell lysates from fresh monocytes, cultured monocytes, A375-MDSC treated with vehicle control and PFK-158. Results are representative of three independent experiments. *p≤0.05, ***p≤0.0005.

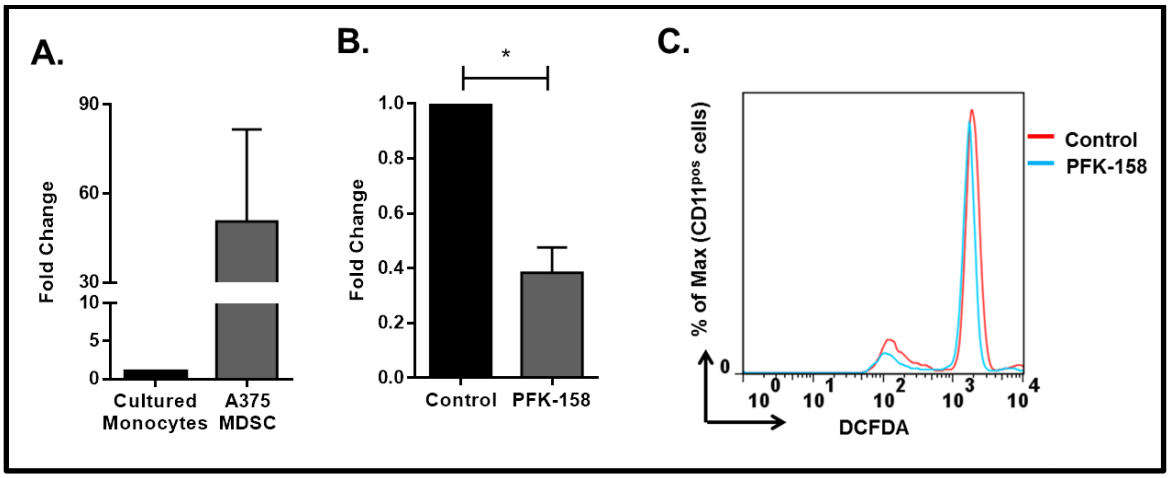

Figure 60. PFKFB3 maintains iNOS mRNA expression in A375-MDSCs. Bar graphs showing results of (A) qRT-PCR of iNOS mRNA expression in healthy donor monocytes (n=5) cultured for 72 hours in the absence (cultured monocytes) or presence of A375 cells, (B) qRT-PCR of iNOS mRNA expression in A375-MDSCs treated with vehicle control and PFK-158, and (C) histogram of mean fluorescent intensities (MFI) of DCF-detectable ROS in A375-MDSC treated with vehicle control and PFK-158. Results are representative of three independent experiments. *p≤0.05.

5.3 A375-MDSCs upregulate glycolysis and lactic acid production

We have shown that A375-MDSCs over express PFKFB3 which is associated with high rate of glycolysis. We used the Seahorse® platform to study the bioenergetic profile of A375-MDSCs. Using the Seahorse® platform, ECAR and OCR for fresh monocytes from healthy donor, cultured monocytes (monocytes cultured for 72 hours in the absence of A375 cells) and A375-MDSCs was measured. A375-MDSCs had significantly higher ECAR compared with fresh and cultured monocytes indicating high rate of glycolysis in these cells (**Fig. 61A**). A375-MDSCs also had higher OCR compared to the fresh and cultured monocytes (**Fig. 61B**). Next, we sought to determine is PFKFB3 inhibition resulted in decrease in the rate of glycolysis. A375-MDSCs were treated with vehicle control and PFK-158 (5 µM) for 16-18 hours. The following day, cells were washed and plated in the Seahorse® XFe96 plate. ECAR and OCR were measured. PFKFB3 inhibition with PFK-158 resulted in significant decrease in both ECAR and OCR compared to treatment with vehicle control (**Fig. 61C and D**).

Increased rate of glycolysis as a consequence of over-expression of PFKFB3 is associated with increased production of lactic acid. Increased lactic acid in addition to the upregulation of arginase and iNOS likely provides MDSCs with an additional mechanism for suppression of T cell activity. Lactate assay showed that A375-MDSCs produced increased amount of lactic acid compared to cultured monocytes which decreased following PFKFB3 inhibition with PFK-158 (**Fig. 62A**). In addition, we also assessed change in lactic acid production by

circulating M-MDSCs from late-stage melanoma patients following PFKFB3 inhibition. Similar results were obtained where lactic acid production decreased significantly following overnight treatment with PFK-158 (5 μM) (**Fig. 62B**). In line with its mechanism of action, treatment with PFK-158 decreased the intracellular concentration of F-2,6-BP in A375-MDScs (**Fig. 62C**).

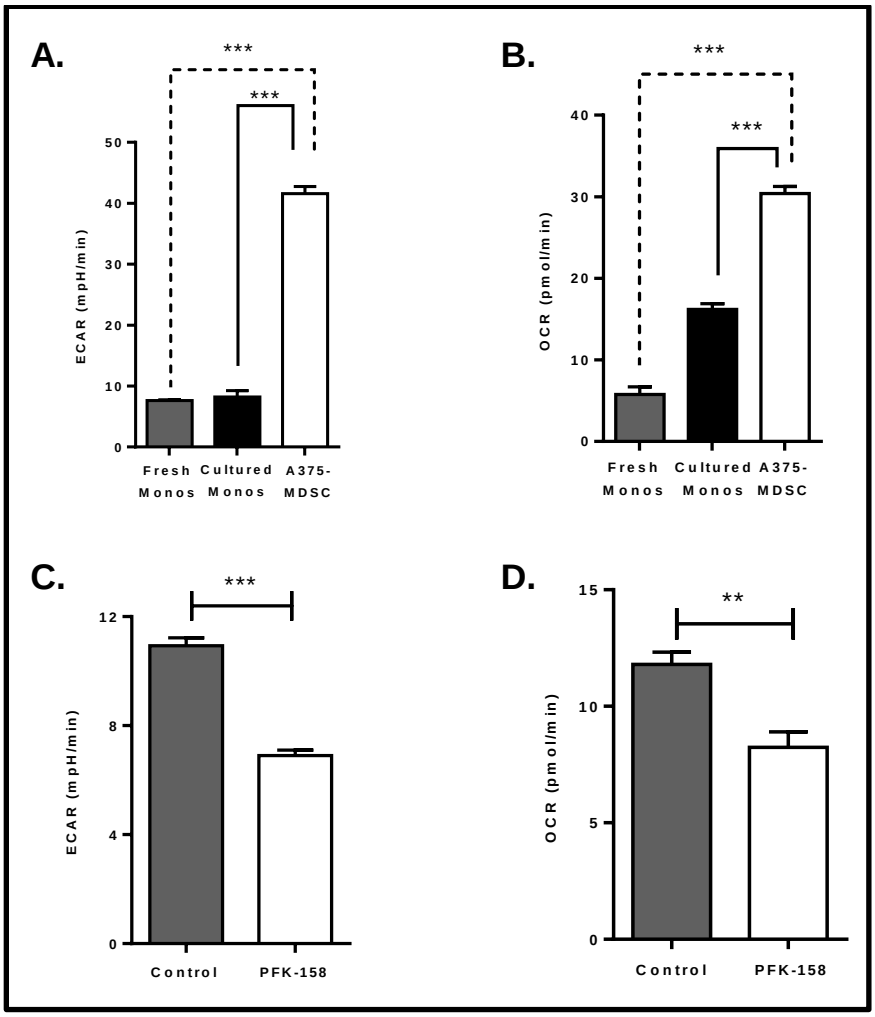

Figure 61. PFKFB3 over-expression maintains high rate of glycolysis in A375-MDSCs. Bioenergetic analysis was performed using the Seahorse® platform to determine extracellular acidification rate (ECAR) and oxygen consumption rate (OCR) in fresh monocytes, cultured monocytes and A375-MDSCs and A375-MDSC + PFK-158. Representative bar graphs showing results of (A) ECAR and (B) OCR of fresh monocytes, cultured monocytes and A375-MDSCs. Representative bar graphs showing results of (C) ECAR and (D) OCR of A375-MDSCs treated with vehicle control and PFK-158. Results are representative of three independent experiments. **p≤0.005, ***p≤0.0005.

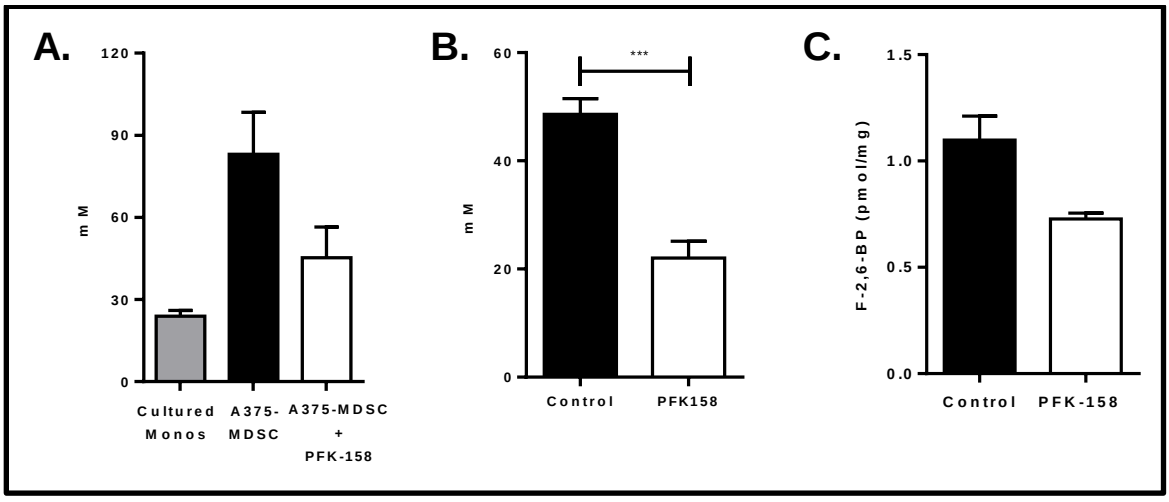

Figure 62. PFKFB3 inhibition reduces lactic acid production and intracellular concentration of F-2,6-BP. Lactate assay was performed using the supernatants from cultured monocytes, A375-MDSCs + vehicle control and A375-MDSCs + PFK-158 (5 µM). Peripheral blood M-MDSCs from late-stage melanoma patients were cultured with vehicle control or PFK-158 (5 µM) for 16-18 hours and supernatant was collected for lactic acid production. Representative bar graphs showing results of lactic acid measurements for (A) cultured monocytes, A375-MDSCs + vehicle control and A375-MDSCs + PFK-158, and (B) circulating M-MDSCs treated with vehicle control and PFK-158. (C) A375-MDSCs were treated with vehicle control or PFK-158 post-differentiation for 16-18 hours and intracellular concentration of F-2,6-BP was determined based on previously described protocol (88). Results are representative of three independent experiments. ***p≤0.0005.

5.4 Treatment of cancer patients with PFK-158 reduced the frequency of circulating M-MDSCs and increased activated T cells

To study the effects of PFKFB3 inhibition on the immune cell populations in human patients, we analyzed the peripheral blood from a patient with metastatic breast cancer who had responded to treatment on a Phase 1 clinical trial with PFK-158. At cycle one day one (C1D1), patient had high circulating M-MDSCs ($Lin^{neg}CD14^{pos}Cd11b^{pos}HLA\text{-}DR^{low}$) (**Fig. 63A**). However, at C1D22 of PFK-158 administration the percentage of the circulating M-MDSCs decreased by over six fold (**Fig. 63B**). The decrease in the frequency of M-MDSCs was associated with not only a decrease in the frequency of other immune suppressive populations but also an increase in the percentage of activated CD8 T cells (**Fig. 64 A-C**). Imaging studies showed that the same patient had stabilization of vertebral bony mets and necrosis of liver lesions following four cycles of PFK-158 (**Fig. 65**).

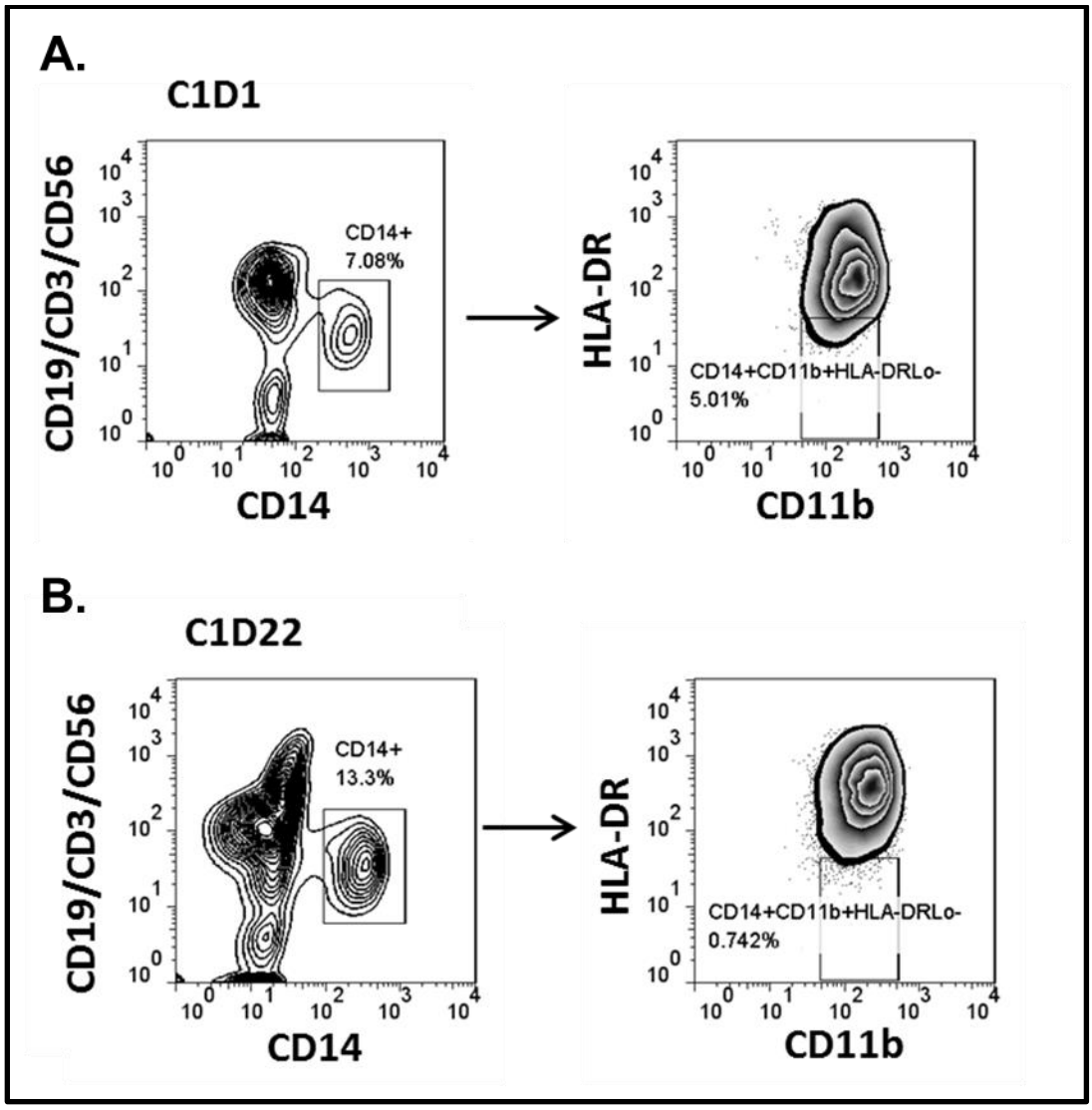

Figure 63. PFK-158 treatment was associated with a decrease in the circulating M-MDSCs in a patient with metastatic breast cancer. Flow cytometry analysis of peripheral blood in a patient with metastatic breast cancer who had responded to the treatment on Phase 1 clinical trial with PFK-158. Representative contour plots at (A) cycle one day one (C1D1) and (B) C1D22 of PFK-158 treatment showing percentage of $Lin^{neg}CD14^{pos}CD11b^{pos}HLA\text{-}DR^{low}$ M-MDSC population.

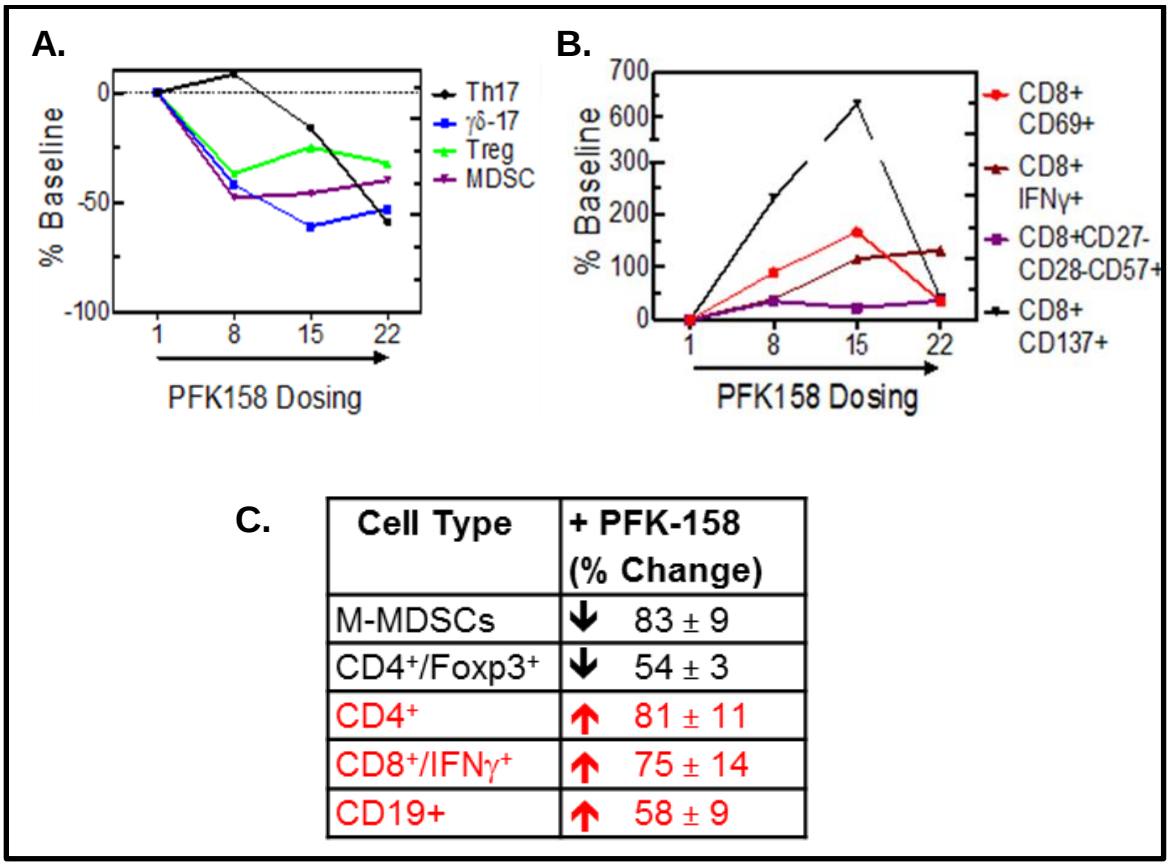

C.

Cell Type	+ PFK-158 (% Change)
M-MDSCs	↓ 83 ± 9
$CD4^+/Foxp3^+$	↓ 54 ± 3
$CD4^+$	↑ 81 ± 11
$CD8^+/IFN\gamma^+$	↑ 75 ± 14
CD19+	↑ 58 ± 9

Figure 64. PFK-158 treatment was associated with a decrease in the percentage of immune suppressive and an increase in the activated CD8 T cell populations. Representative line graph showing the trend of (A) immune suppressive and (B) activated T cell populations following each cycle of PFK-158, cycles one through 22 in a patient with metastatic breast cancer. (C) Percentage change (expressed as mean ± SD) in the immune cellular population following treatment with PFK-158.

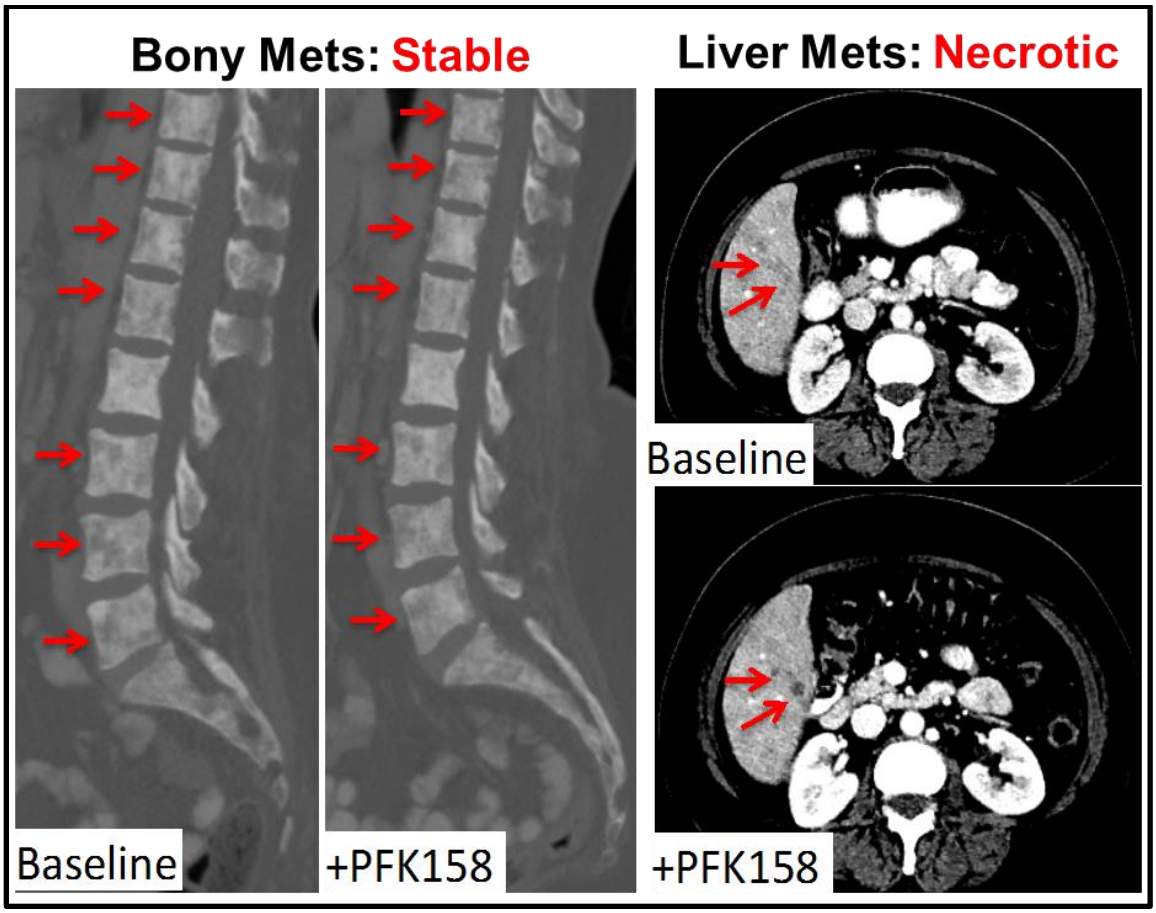

Figure 65. Patient with metastatic breast cancer who received PFK-158 as part of Phase study had stabilization of vertebral bony mets and necrosis of liver mets at cycle four.

6.0 DISCUSSION, CONCLUSION AND FUTURE DIRECTIONS

6.1 Discussion and Conclusion:

Complex interactions between the tumors and the immune system have recently received tremendous attention. The concept of “cancer immune surveillance” or recently rephrased as “cancer immunoediting” was first described more than a century ago (89, 90). This concept is divided in to three phases – elimination, equilibrium and escape (89, 90). In the elimination phase, the immune system is able to recognize and eliminate the cancer cells. Partial elimination of the cancer cells can result in a state of equilibrium during which cancer cells continue to evolve and mount increasing pressure on the immune system, ultimately leading to the escape phase. During the escape phase, tumors not only evolve to express epitopes that are not recognized by the immune system but also secrete factors or ligands that attract immune suppressive populations and downregulate effective anti-tumor responses by the immune effector cells.

In 2011, recognizing the importance of immune system in cancer development and progression, Hanahan and Weinberg published an update to their original publication “The Hallmarks of Cancer” (91). This update included an emerging hallmark “avoiding immune destruction” and an enabling characteristic “tumor-promoting inflammation” (92). Experimental animal models have shown that deficiencies in the development or function of CD8 CTLs, CD4 Th1 or NK cells increase their susceptibility to tumor development (90, 93). Combined deficiencies in both T and NK cells further enhances the susceptibility to tumor development indicating the importance of both the innate and the adaptive immune system in immune surveillance and tumor eradication (90, 93). Similarly in transplantation models, cancer cells from immunodeficient mice are not capable of initiating tumors in syngeneic immunocompetent hosts; however, cancers cells from immunocompetent mice are able to initiate tumors in both immunodeficient and immunocompetent hosts (90). These models highlight the concept of highly immunogenic tumors which induce effective anti-tumor responses as opposed to weakly immunogenic tumors. Some highly immunogenic tumors include RCC, melanoma and merkel cell carcinoma where spontaneous regressions are not uncommonly seen. In addition, the induction of inflammatory response in the tumors and recruitment of immune suppressive inflammatory cells to the TME promote tumor growth and suppress anti-tumor immune responses.

Better understanding of these complex interactions between the tumors and the immune system has helped us make significant advances in the field of

cancer immunotherapy. New therapies such as immune checkpoint blockade mAbs and adoptive cell therapies (ACT) have translated in to better response rates (RR) and OS in cancer patients. Presence of lymphocytic infiltrates within the tumor has been shown to correlate highly with improved outcomes across various tumor subtypes (94-97). These tumor infiltrating CD4 and CD8 T cells recognize TAAs and are tumoricidal as proven by the anti-tumor activity of adoptively transferred ex vivo expanded tumor-infiltrating lymphocytes (TILs). Further, the response to treatment strongly correlates with the absolute numbers of CD8 T cells infused. In phase III clinical trials, anti-CTLA4 monoclonal antibody ipilimumab showed a four month increase in median OS in patients with metastatic melanoma which has translated into long-term survival in 20–25% (98-100). More striking results were seen with anti-PD1/anti-PD-L1 blocking therapies with ORR ranging from 18 to 52% across different cancer types and well selected patients (101-103). In addition, these therapies are associated with durable complete remissions (CR) even after the discontinuation of the therapy. Despite these advances, many patients still fail to achieve any meaningful response.

Resistance to immune checkpoint blockade therapies has been described at two levels – intrinsic and naturally acquired resistance (104). Patients who are non-responders, lack anti-tumor immune response and fail to elicit an effective T cell response upon immunotherapy are described to have intrinsic resistance (104). This could be the result of local or systemic factors that contribute to ineffective anti-tumor response. Systemic factors could be related to a weak

immune system especially in the elderly and immunodeficient patients or expression of few neoantigens by certain tumors. Local factors are associated with lack of TILs or tolerogenic TME. T cell function in the TME is inhibited by the infiltration of suppressive myeloid and lymphoid cells, expression of inhibitory receptors/ligands and secretion of inhibitory cytokines by the tumors and immune suppressive cells (**Table. 4**) (104). Naturally acquired resistance occurs when patients may have an ongoing anti-tumor immune response but fail to derive any benefit from immune modulatory therapies (104). This may result from loss/downregulation of MHC class I by tumor cells or from expression of other T cell inhibitory receptors (**Table. 4**).

Numerous therapeutic strategies are currently under or in late-phase development which are designed to target the immune suppressive components of the TME. These include modalities to strengthen T cell responses by ex vivo enrichment of antigen-specific T cells, chimeric antigen receptor T cells and combination of immune checkpoint blockade agents such as ipilimumab and nivolumab. Inhibitors of immune suppressive molecules such as IDO (ClinicalTrials.gov Identifier: NCT02752074) are currently being studied in combination with immune checkpoint blockade antibodies. Combination therapeutic strategies with chemotherapy agents, radiotherapy and small molecule inhibitors with immune checkpoint blocking agents are being studied as they have been shown to modulate the TME by reducing immune suppressive cell populations, and release and upregulate neoantigens.

Table 4. List of immune suppressive cells and negative regulators of T cell function (104, 105).

Immune suppressive cells	T cell inhibitory receptors	Immune suppressive molecules
Regulatory T cells (Tregs)	Programmed cell death protein 1 (PD1)	Transforming growth factor-β
T helper 17 cells (Th17)	Cytotoxic T-lymphocyte-associated protein 4 (CTLA4)	Interleukin-1 (IL-1), IL-6, IL-10, IL-12, IL-17, IL-18
Tumor associated macrophages (TAMs)	T-cell immunoglobulin and mucin-domain containing-3 (TIM-3)	Indoleamine 2,3 dioxygenase (IDO), arginase, nitric oxide (NO), peroxynitrite (PNT), reactive oxygen and nitrogen species (ROS/RNS)
Tumor associated neutrophils (TANs)	Glucocorticoid-induced TNFR-related protein (GITR)	Tumor necrosis factor-α (TNF-α)
Tumor-associated fibroblast and other stromal cells	Lymphocyte activation gene 3 protein (LAG3)	
Tolerogenic dendritic cells (DC)	Inducible T cell co-stimulator (ICOS)	
Type 2 natural killer T cells (NKT cells)	B and T lymphocyte attenuator (BTLA)	
Myeloid derived suppressor cells (MDSCs)	CD28	
Regulatory B cells		
Regulatory γδ T cells		

MDSC targeting therapies are divided in to four major categories – deactivation of MDSCs, inducing differentiation of MDSCs to mature myeloid cells, inhibition of myeloid cell development in to MDSCs and depletion of MDSCs (30). Deactivation of MDSCs has been studied in the context of blocking the suppressive markers such as arginase 1, ROS and iNOS. COX-2 inhibitors have been shown to reduce the expression of arginase 1 (30). Agents like ATRA have been shown to induce the differentiation of MDSCs to mature myeloid cells

(30). Bisphosphonates block the differentiation of myeloid cells to MDSCs and chemotherapy agents such as 5-FU and gemcitabine, and recently, ibrutininb has been shown to deplete MDSCs (30). However, randomized controlled studies to study the effect of these therapeutic strategies on MDSC populations are lacking.

Our studies demonstrate for the first time a correlation between upregulated glycolysis and immune suppressive phenotype of monocytic MDSCs. We show that the enzyme PFKFB3, an important regulator of glycolysis is over-expressed in M-MDSCs and is required for their functional differentiation. We had demonstrated previously that circulating M-MDSCs in late-stage melanoma patients are differentially expanded and result in T cell suppression (50). We now provide further evidence that in B16-F10 melanoma and BM-MDSC model, monocytic and not polymorphonuclear MDSCs are suppressive to T cell function. In an attempt to evaluate the role of PFKFB3 in modulating the immune suppressive phenotype of M-MDSCs, we isolated $CD14^{pos}$ circulating M-MDSCs from late-stage melanoma patients. *Ex vivo* inhibition of PFKFB3 with the first-in-class small molecule inhibitor, PFK-158 improved T cell activity and IFN-γ production. Similar results were seen in A375-MDSCs, an ex vivo model of human MDSCs. PFKFB3 inhibition in murine splenic M-MDSCs reduced antigen specific T cell suppression. In splenic M-MDSCs cultured under hypoxic conditions and bone marrow-derived M-MDSCs, PFKFB3 inhibition reduced the antigen non-specific T cell function. Interestingly, *in vivo* PFKFB3 inhibition both in mice and in patients enrolled under Phase 1 study resulted in substantial

decline in M-MDSC population. In mice, splenic M-MDSC suppressive activity was also reduced following treatment with PFK-158.

High rate of glycolysis and increased glucose catabolism has been well described in tumors (58, 59). Glycolysis alone is insufficient to meet the energy needs of the cell. However in addition to ATP, tumors also need biosynthetic precursors from glycolytic intermediates in order to proliferate and invade (32). Furthermore, high glycolytic flux to pyruvate/lactate decreases intracellular and extracellular pH causing apoptosis in the neighboring normal cells (18, 32, 58-60). Tumors are able to upregulate glycolysis through over-expression of several key regulators of glycolysis including PFKFB3. This enzyme produces F-2,6-BP that allosterically activates PFK-1, an irreversible and committed step that dictates the pace of glycolysis.

A previous study showed that mTORC1-dependent aerobic glycolysis was necessary for lineage differentiation of M-MDSCs but not PMN-MDSCs (72). And, exposure to GM-CSF and IL6 has been shown to upregulate L-glutamine and glucose metabolism by anaerobic glycolysis resulting in the accumulation of TCA or Kreb cycle intermediates, lactic acid, and upregulated production of energy-rich nucleotides, arginase and iNOS (69). Fumarate and succinate both TCA cycle intermediates and lactic acid have been shown to stabilize the expression of HIF-1α through inhibition of HIF hydroxylases resulting in upregulated PFKFB3 expression and glycolysis in M-MDSCs (24, 63, 85). In our study, we showed that HIF-1α maintains the expression of PFKFB3 in M-MDSCs especially under hypoxia. Yet, another study showed that monocytes exposed to

hypoxia rapidly stimulate glycolysis by activating PFKFB3 through phosphorylation of serine (58). However, PMN-MDSCs have been shown to upregulate FAO along with an increase in mitochondrial mass and oxygen consumption rate (53). These differences in metabolic profiles of PMN- and M-MDSCs may explain functional differences in these two subsets. Despite, the well-established role of PFKFB3 in carcinogenesis, its role as an immunomodulator has never been explored. Similar to the tumors, our studies show that M-MDSCs over-express PFKFB3, upregulate glycolysis and produce lactic acid. And, PFKFB3 inhibition was associated with decrease in glycolysis and lactic acid production. These data suggest that increased rate of glycolysis through upregulation of PFKFB3 may be necessary to maintain the suppressive phenotype of M-MDSCs.

M-MDSCs mount their suppression on T cell activity primarily through the increased expression of arginase 1 and iNOS (**Fig. 66**) (4, 12, 19, 34, 36, 42). L-arginine is very important for T cell function and its depletion by arginase 1 and iNOS results in translational blockade of CD3ζ chain and prevents T cells from responding to various stimuli (10, 26, 38). In addition, iNOS catabolizes L-arginine producing NO as a by-product that causes nitrosylation of the TCR (36, 52). In our study, we confirmed that M-MDSCs express high levels of arginase 1 and iNOS, and PFKFB3 inhibition with PFK-158 reduced the expression or activity of both these markers. However, we did not see any change in the expression of NOX2 or NOX 4 enzymes nor did we see a change in DCF-detectable ROS. These findings fall in line with the functional and metabolic

changes reported in activated macrophages and DCs where inflammatory signals or hypoxia stimulate the upregulation of glycolysis, lactic acid production and flux through PPP, and decreased oxygen consumption (63, 65, 66). This is accompanied by increased expression of inflammatory genes such as iNOS and Arg1 (63, 67, 68). Furthermore, in macrophages it has been shown that lactic acid can stabilize HIF-1α even under normoxic conditions and stimulate the expression of Arg1 and VEGF (85). Hypoxia in macrophages can also induce iNOS-HRE which can activate iNOS promoter and mRNA expression (86). Similarly in BM-MDSCs, GM-CSF and IL6 result in increased L-glutamine and glucose metabolism by anaerobic metabolism, accumulation of lactic acid and increased expression of Arg1 and iNOS (69). In our present study, we do not provide any evidence for the mechanistic link between upregulated glycolysis in M-MDSCs and increased expression of Arg1 and iNOS. We speculate that similar mechanisms linking hypoxia and production of lactic acid with increased expression of Arg1 and iNOS may exist in M-MDSCs as have been described in activated macrophages. However, neutrophils also have been shown to upregulate glycolysis but have significant increase in oxygen consumption which is used primarily to produce ROS (62). Likely a similar mechanism is in play in PMN-MDSCs where increase in oxygen consumption and mitochondrial mass generates NAPDH required for production of ROS by NOX enzymes (**Fig. 67**). The ability to upregulate HIF-1α, PFKFB3 and anaerobic glycolysis provides M-MDSCs with the ability to survive in the hypoxic TME and differentiate in to TAMs. PMN-MDSCs on the other hand increase the mitochondrial mass and

oxidative phosphorylation and produce ROS; but are unable to survive in hypoxic TME.

Several observational studies have demonstrated the role of increased number of MDSCs – both polymorphonuclear and monocytic in downregulating T cell responses in cancer patients. This increase is also correlated with poor prognosis and OS (2, 10, 12, 13, 15, 17, 21, 50, 52). Our studies involving PFKFB3 inhibition in both murine and human M-MDSCs provide strong evidence for the role of PFKFB3 in maintaining M-MDSC induced T cell suppression. PFK-158 is a first-in-class small molecule inhibitor of PFKFB3 developed in the lab of Jason Chesney at the University of Louisville. A phase 1 clinical trial was conducted at four major institutions in the United States. Patients with solid tumors who had failed at least one previous regimen were enrolled. Drug was dosed at 24 mg/m^2 to 650 mg/m^2 delivered intravenously every other day for three weeks followed by one week rest. Cycle was repeated every four weeks until disease progression or unacceptable toxicity. Out of 27 patients enrolled under the study, 18 patients completed two cycles. Six of the 18 patients experienced clinical benefit in terms of stable disease (SD) and no drug-related serious adverse effects (SAEs) were reported. In addition to the decrease in M-MDSC population, patients with clinical benefit showed a decrease in Th17 and γδ regulatory T cells and an increase in CD4^{pos} and CD8^{pos} effector T cells. Following treatment, PD1 expression on CD8^{pos} T cells decreased. Results from the Phase 1 study of PFK-158 proved its role as safe and effective immunomodulatory drug.

Based on the data presented in this study, there is strong evidence that PFKFB3 inhibition or downregulation of glycolysis modulates M-MDSC suppressive function while it has no impact on PMN-MDSC frequency or function (**Fig. 66 and 67**). We believe that PFKFB3 inhibition improves anti-tumor immune responses *in vivo* through reduction in the frequency and suppressive function of M-MDSCs (**Fig. 66**). Further, immunomodulatory effects of PFK-158 were seen primarily in the low-dose cohorts in the Phase 1 clinical trial which indicates that anti-tumor responses were primarily driven through the decrease in the frequency and downregulation of M-MDSC suppressive function, and increase in the activity of $CD8^{pos}$ T cells as opposed to entirely the anti-tumor activity of the drug. Although it would be reasonable to suspect that there was some anti-tumor activity which may have contributed to reduced tumor volumes and decrease in secretion of TDSFs resulting in decrease in the number of circulating M-MDSCs. However, anti-tumor effect of PFK-158 would not be as dramatic as seen in the clinical trial especially at low doses resulting from its cytotoxic activity alone.

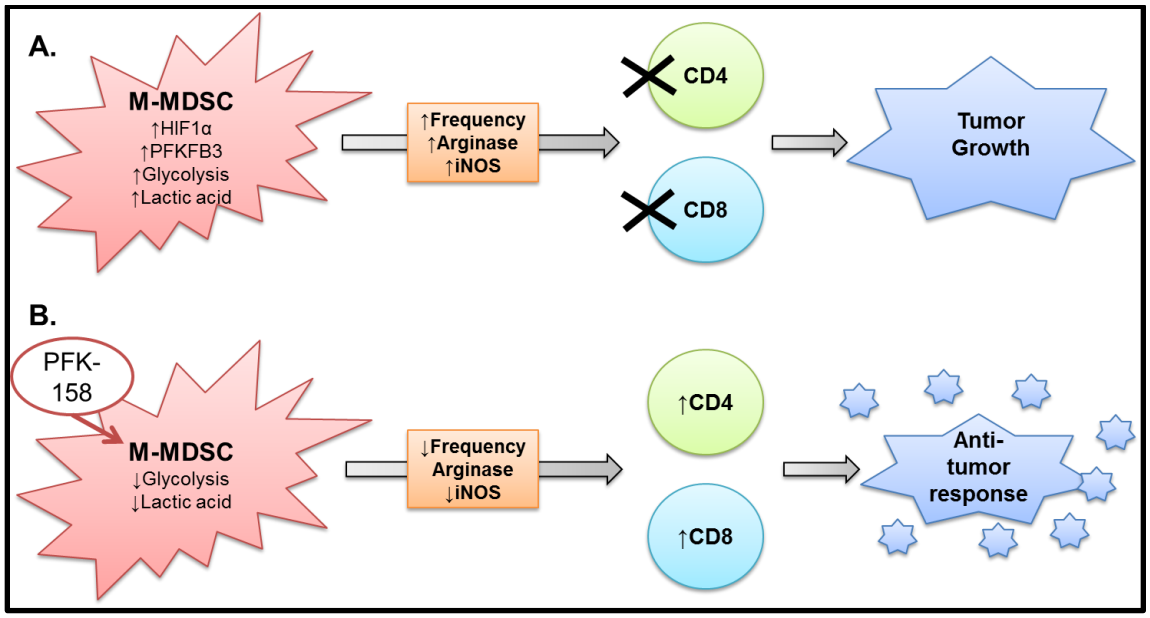

Figure 66. Model for M-MDSC induced T cell suppression and reversal of suppression with PFK-158.

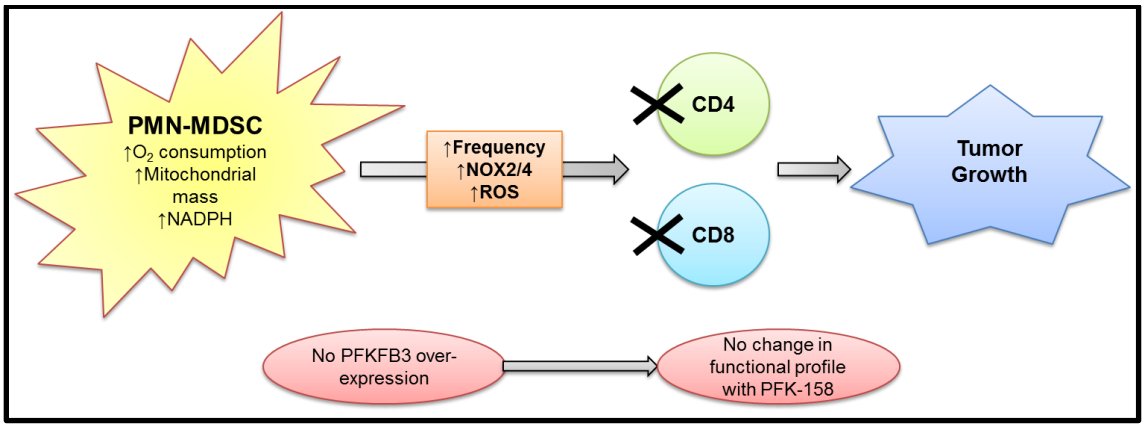

Figure 67. Model for PMN-MDSC induced T cell suppression with no reversal seen with PFK-158.

We present here some very exciting results from our studies but we also realize few limitations and/or pitfalls. We used B16-F10 transplantation model to study the functional and metabolic characteristics of MDSCs. Subcutaneous/transplantation tumor models do not recapitulate natural history or progression of tumors in animals or humans. This in turn may not provide true

insights into patterns of accumulation of immune suppressive populations let alone their functional characteristics at primary site versus metastatic lesions versus in circulation. In order to overcome this limitation, use of the MT/ret transgenic mouse may prove to be a better model to study various immune suppressive populations including MDSCs. These mice express the human ret transgene in melanocytes which is controlled by the mouse metallothionein I promoter-enhancer and develop spontaneous malignant cutaneous melanoma which metastasizes to lymph nodes, lungs, brain, kidney, and spleen (106, 107). This model shows similarity to human melanoma with respect to histopathology and clinical development and provides ability to study natural interactions of tumors with the host immune system over a period of time (106, 107). Also for future *in vivo* tumor experiments, we may use a tumor cell line with knock-down expression of PFKFB3 so that the tumor growth and the secretion of TDSFs is not significantly different between the PFK-158 and vehicle-treated mice.

MDSCs are characterized by their morphological, phenotypic and functional heterogeneity. This exhibits their incredible plasticity and how different conditions – different cancers and infections can modulate this immune suppressive myeloid population (24). The heterogeneity of MDSCs is also exhibited in the fact that in some tumor models PMN-MDSCs and in others M-MDSCs are suppressive (35). Many previous studies reported in the literature were limited by the ambiguous morphological and functional markers of PMN- and M-MDSCs, and hence, the results of these studies did not reflect upon the true characteristics of these cells. Furthermore, MDSCs in humans lack a true

homologue of GR1 as in mice or unique surface marker, thus impairing the ability to specifically target them with mAb. In order to overcome the ambiguity and confusion related characterization of MDSC subsets, consensus standards have been published (35). In our studies, we preferentially followed phenotypic and functional characteristics defined recently as per consensus standards. Despite adhering to current standards, we suspect that as our knowledge of this highly heterogeneous myeloid cellular population grows the results of our current study may need to be refined based on prevailing phenotypic and functional definitions.

In our study, we report that in mice *in vivo* experiments and in patients on Phase 1 clinical trial, a marked reduction in the circulating M-MDSC population was seen. However, in the *in vitro* experiments we report no change in cell viability. Justification for these disparate results lies in the fact that different doses of PFK-158 were used for *in vitro* and *in vivo* experiments. For the *in vitro* experiments, we used non-lethal dose of PFK-158 to demonstrate the immunomodulatory effects resulting from PFKFB3 inhibition and not from elimination of M-MDSCs. Also, M-MDSCs were normalized to number for these functional studies. For the *in vivo* mice experiments, previously studied dose of PFK-158 was used and for patients on Phase 1 clinical trial, maximal tolerated dose (MTD) for human subjects was being determined. The decrease in the M-MDSC population in mice following subcutaneous injection and in human patients following parenteral injection is thought to be secondary to the higher dose and likely from decrease in the Th17 cells which regulate MDSCs. In order to overcome these limitations and to determine the direct effect of PFKFB3

inhibition on M-MDSC mediated T cell suppression, we plan to conduct tumor inoculation studies and *ex vivo* M-MDSC functional analysis in PFKFB3 conditional knockout (*KO*) mice. We will compare tumor growth and *ex-vivo* function of splenic M-MDSCs from PFKFB3 *KO* mice with WT mice. A cross between PFKFB3$^{flox/flox}$ and lysM-Cre mice will help us determine the requirement of the PFKFB3 expression for suppressive function of the myeloid compartment when compared with tumor-bearing WT mice.

We also concede that other metabolic inhibitors that target glycolysis and glycolytic enzymes may have similar immunomodulatory effects on M-MDSCs as PFK-158. Furthermore in our current study, we do not show changes in the expression of HIF-1α if any following PFKFB3 inhibition as HIF-1α is thought to be the likely promoter of expression of inflammatory genes such as Arg1 and iNOS.

In conclusion, we show that in the melanoma model, M- and not PMN-MDSCs suppress T cell activity. M-MDSCs express high PFKFB3 resulting in high rate of glycolysis and lactic acid production. Increased PFKFB3 expression in M-MDSCs under hypoxic conditions is dependent on expression of HIF-1α and is required to maintain their suppressive phenotype, and expression of inflammatory genes such as Arg1 and iNOS. PFKFB3 inhibition was associated with reduced M-MDSC suppression and improved T cell activity and function *in vitro*. PFKFB3 inhibition *in vivo* was associated with reduced M-MDSC frequency and tumor volumes, and reduced suppressive activity. Metabolic targeting of this highly suppressive population with PFK-158 provides an opportunity to further

improve anti-tumor T cell responses especially in combination with immune checkpoint blockade.

6.2 Future directions

These are exciting times in oncology, especially in cancer immunotherapy. Prior to the FDA approval of anti-CTLA4 antibody ipilimumab (Yervoy®) in March 2011, immunotherapy in solid malignancies was mostly discredited. High-dose IL-2 in advanced melanoma and RCC was associated with significant toxicities and poor response rates. At present, numerous clinical trials with anti-PD1 alone or in combination with anti-CTLA4 or anti-TIM3 or anti-LAG3 mAbs are ongoing in different cancer types. Immunotherapies are also being studied in combination with contemporary cancer treatments such as chemo and radiotherapies. Despite ORR upwards of 20% across different cancer subtypes, intrinsic and naturally acquired resistance to anti-PD1 therapies are being recognized in non-responders. Agents that target other immune checkpoint receptors or immune suppressive populations are now being studied to overcome this resistance. In our study and Phase 1 clinical trial with PFK-158, we provide substantial evidence for PFKFB3 inhibition as a novel immunomodulatory therapeutic agent. PFKFB3 inhibition decreases immune suppressive M-MDSC population and its suppressive activity and can be effectively combined with immune checkpoint blockade therapies for improved anti-tumor T cell responses. We next intend to study PFKFB3 inhibition in combination with anti-PD1/anti-CTLA4 therapy in the

context of a Phase 1 clinical trial and hopefully, bring this novel treatment strategy to the clinic and to the patients.

Further, our study has laid the foundation to study the metabolic profile of TAMs as they differentiate from M-MDSCs in the TME. We suspect that PFKFB3 is over-expressed in TAMs and PFKFB3 inhibition with PFK-158 will modulate their immune suppressive profile, thus providing another mechanistic link to immunomodulatory effects of PFK-158. We have provided evidence that increase in the rate of glycolysis in M-MDSCs results in the upregulation of Arg1 and iNOS; however, exact mechanistic link between the two is still not clear. Future project can attempt to identify the link between upregulated glycolysis and expression of inflammatory genes whether it is a transcriptional factor or a metabolic by-product.

This work was supported by the following grants to Jason Chesney, M.D., Ph.D.;
NIH: U01-HL127518
R01-CA149438
P30-GM106396

REFERENCES

1. Goedegebuure P, Mitchem JB, Porembka MR, Tan MC, Belt BA, Wang-Gillam A, Gillanders WE, Hawkins WG, Linehan DC. Myeloid-derived suppressor cells: general characteristics and relevance to clinical management of pancreatic cancer. Curr Cancer Drug Targets. 2011;11(6):734-51. PubMed PMID: 21599634; PMCID: PMC3670669.

2. Weide B, Martens A, Zelba H, Stutz C, Derhovanessian E, Di Giacomo AM, Maio M, Sucker A, Schilling B, Schadendorf D, Buttner P, Garbe C, Pawelec G. Myeloid-derived suppressor cells predict survival of patients with advanced melanoma: comparison with regulatory T cells and NY-ESO-1- or melan-A-specific T cells. Clinical cancer research : an official journal of the American Association for Cancer Research. 2014;20(6):1601-9. doi: 10.1158/1078-0432.CCR-13-2508. PubMed PMID: 24323899.

3. Solito S, Falisi E, Diaz-Montero CM, Doni A, Pinton L, Rosato A, Francescato S, Basso G, Zanovello P, Onicescu G, Garrett-Mayer E, Montero AJ, Bronte V, Mandruzzato S. A human promyelocytic-like population is responsible for the immune suppression mediated by myeloid-derived suppressor cells. Blood. 2011;118(8):2254-65. doi: 10.1182/blood-2010-12-325753. PubMed PMID: 21734236; PMCID: PMC3709641.

4. Gabitass RF, Annels NE, Stocken DD, Pandha HA, Middleton GW. Elevated myeloid-derived suppressor cells in pancreatic, esophageal and gastric cancer are an independent prognostic factor and are associated with significant elevation of the Th2 cytokine interleukin-13. Cancer Immunol Immunother. 2011;60(10):1419-30. doi: 10.1007/s00262-011-1028-0. PubMed PMID: 21644036; PMCID: PMC3176406.

5. Talmadge JE, Gabrilovich DI. History of myeloid-derived suppressor cells. Nat Rev Cancer. 2013;13(10):739-52. doi: 10.1038/nrc3581. PubMed PMID: 24060865; PMCID: PMC4358792.

6. De Sanctis F, Bronte V, Ugel S. Tumor-Induced Myeloid-Derived Suppressor Cells. Microbiol Spectr. 2016;4(3). doi: 10.1128/microbiolspec.MCHD-0016-2015. PubMed PMID: 27337449.

7. Damuzzo V, Pinton L, Desantis G, Solito S, Marigo I, Bronte V, Mandruzzato S. Complexity and challenges in defining myeloid-derived suppressor cells. Cytometry B Clin Cytom. 2015;88(2):77-91. doi: 10.1002/cyto.b.21206. PubMed PMID: 25504825; PMCID: PMC4405078.

8. Marvel D, Gabrilovich DI. Myeloid-derived suppressor cells in the tumor microenvironment: expect the unexpected. J Clin Invest. 2015;125(9):3356-64. doi: 10.1172/JCI80005. PubMed PMID: 26168215; PMCID: PMC4588239.

9. Corzo CA, Cotter MJ, Cheng P, Cheng F, Kusmartsev S, Sotomayor E, Padhya T, McCaffrey TV, McCaffrey JC, Gabrilovich DI. Mechanism regulating reactive oxygen species in tumor-induced myeloid-derived suppressor cells. Journal of immunology. 2009;182(9):5693-701. doi: 10.4049/jimmunol.0900092. PubMed PMID: 19380816; PMCID: 2833019.

10. Gros A, Turcotte S, Wunderlich JR, Ahmadzadeh M, Dudley ME, Rosenberg SA. Myeloid cells obtained from the blood but not from the tumor can suppress T-cell proliferation in patients with melanoma. Clinical cancer research : an official journal of the American Association for Cancer Research. 2012;18(19):5212-23. doi: 10.1158/1078-0432.CCR-12-1108. PubMed PMID: 22837179.

11. Corzo CA, Condamine T, Lu L, Cotter MJ, Youn JI, Cheng P, Cho HI, Celis E, Quiceno DG, Padhya T, McCaffrey TV, McCaffrey JC, Gabrilovich DI. HIF-1alpha regulates function and differentiation of myeloid-derived suppressor cells in the tumor microenvironment. The Journal of experimental medicine. 2010;207(11):2439-53. doi: 10.1084/jem.20100587. PubMed PMID: 20876310; PMCID: 2964584.

12. Poschke I, Kiessling R. On the armament and appearances of human myeloid-derived suppressor cells. Clinical immunology. 2012;144(3):250-68. doi: 10.1016/j.clim.2012.06.003. PubMed PMID: 22858650.

13. Youn JI, Nagaraj S, Collazo M, Gabrilovich DI. Subsets of myeloid-derived suppressor cells in tumor-bearing mice. Journal of immunology. 2008;181(8):5791-802. PubMed PMID: 18832739; PMCID: PMC2575748.

14. Marigo I, Bosio E, Solito S, Mesa C, Fernandez A, Dolcetti L, Ugel S, Sonda N, Bicciato S, Falisi E, Calabrese F, Basso G, Zanovello P, Cozzi E, Mandruzzato S, Bronte V. Tumor-induced tolerance and immune suppression depend on the C/EBPbeta transcription factor. Immunity. 2010;32(6):790-802. doi: 10.1016/j.immuni.2010.05.010. PubMed PMID: 20605485.

15. Poschke I, Mougiakakos D, Hansson J, Masucci GV, Kiessling R. Immature immunosuppressive CD14+HLA-DR-/low cells in melanoma patients are Stat3hi and overexpress CD80, CD83, and DC-sign. Cancer Res. 2010;70(11):4335-45. doi: 10.1158/0008-5472.CAN-09-3767. PubMed PMID: 20484028.

16. Albeituni SH, Ding C, Liu M, Hu X, Luo F, Kloecker G, Bousamra M, 2nd, Zhang HG, Yan J. Yeast-Derived Particulate beta-Glucan Treatment Subverts the Suppression of Myeloid-Derived Suppressor Cells (MDSC) by Inducing Polymorphonuclear MDSC Apoptosis and Monocytic MDSC Differentiation to APC in Cancer. Journal of immunology. 2016. doi: 10.4049/jimmunol.1501853. PubMed PMID: 26810222.

17. Mitchell RA, Yaddanapudi K. Stromal-dependent tumor promotion by MIF family members. Cellular signalling. 2014;26(12):2969-78. doi: 10.1016/j.cellsig.2014.09.012. PubMed PMID: 25277536; PMCID: PMC4293307.

18. Husain Z, Huang Y, Seth P, Sukhatme VP. Tumor-derived lactate modifies antitumor immune response: effect on myeloid-derived suppressor cells and NK cells. Journal of immunology. 2013;191(3):1486-95. doi: 10.4049/jimmunol.1202702. PubMed PMID: 23817426.

19. Greten TF, Manns MP, Korangy F. Myeloid derived suppressor cells in human diseases. Int Immunopharmacol. 2011;11(7):802-7. doi: 10.1016/j.intimp.2011.01.003. PubMed PMID: 21237299; PMCID: PMC3478130.

20. Peranzoni E, Zilio S, Marigo I, Dolcetti L, Zanovello P, Mandruzzato S, Bronte V. Myeloid-derived suppressor cell heterogeneity and subset definition. Curr Opin Immunol. 2010;22(2):238-44. doi: 10.1016/j.coi.2010.01.021. PubMed PMID: 20171075.

21. Solito S, Marigo I, Pinton L, Damuzzo V, Mandruzzato S, Bronte V. Myeloid-derived suppressor cell heterogeneity in human cancers. Ann N Y Acad Sci. 2014;1319:47-65. doi: 10.1111/nyas.12469. PubMed PMID: 24965257.

22. Zhang B, Wang Z, Wu L, Zhang M, Li W, Ding J, Zhu J, Wei H, Zhao K. Circulating and tumor-infiltrating myeloid-derived suppressor cells in patients with colorectal carcinoma. PLoS One. 2013;8(2):e57114. doi: 10.1371/journal.pone.0057114. PubMed PMID: 23437326; PMCID: PMC3577767.

23. Yang WC, Ma G, Chen SH, Pan PY. Polarization and reprogramming of myeloid-derived suppressor cells. J Mol Cell Biol. 2013;5(3):207-9. doi: 10.1093/jmcb/mjt009. PubMed PMID: 23532593; PMCID: PMC3695657.

24. Youn JI, Gabrilovich DI. The biology of myeloid-derived suppressor cells: the blessing and the curse of morphological and functional heterogeneity. Eur J Immunol. 2010;40(11):2969-75. doi: 10.1002/eji.201040895. PubMed PMID: 21061430; PMCID: PMC3277452.

25. Gabrilovich DI, Nagaraj S. Myeloid-derived suppressor cells as regulators of the immune system. Nat Rev Immunol. 2009;9(3):162-74. doi: 10.1038/nri2506. PubMed PMID: 19197294; PMCID: PMC2828349.

26. Mao Y, Poschke I, Wennerberg E, Pico de Coana Y, Egyhazi Brage S, Schultz I, Hansson J, Masucci G, Lundqvist A, Kiessling R. Melanoma-educated CD14+ cells acquire a myeloid-derived suppressor cell phenotype through COX-2-dependent mechanisms. Cancer Res. 2013;73(13):3877-87. doi: 10.1158/0008-5472.CAN-12-4115. PubMed PMID: 23633486.

27. Drujont L, Carretero-Iglesia L, Bouchet-Delbos L, Beriou G, Merieau E, Hill M, Delneste Y, Cuturi MC, Louvet C. Evaluation of the therapeutic potential of bone marrow-derived myeloid suppressor cell (MDSC) adoptive transfer in mouse models of autoimmunity and allograft rejection. PLoS One. 2014;9(6):e100013. doi: 10.1371/journal.pone.0100013. PubMed PMID: 24927018; PMCID: PMC4057339.

28. Najjar YG, Finke JH. Clinical perspectives on targeting of myeloid derived suppressor cells in the treatment of cancer. Front Oncol. 2013;3:49. doi: 10.3389/fonc.2013.00049. PubMed PMID: 23508517; PMCID: PMC3597982.

29. Maeda A, Kawamura T, Ueno T, Usui N, Miyagawa S. Monocytic suppressor cells derived from human peripheral blood suppress xenogenic immune reactions. Xenotransplantation. 2014;21(1):46-56. doi: 10.1111/xen.12067. PubMed PMID: 24372857.

30. Wesolowski R, Markowitz J, Carson WE, 3rd. Myeloid derived suppressor cells - a new therapeutic target in the treatment of cancer. J Immunother Cancer. 2013;1:10. doi: 10.1186/2051-1426-1-10. PubMed PMID: 24829747; PMCID: PMC4019895.

31. Stiff A, Trikha P, Wesolowski R, Kendra K, Hsu V, Uppati S, McMichael E, Duggan M, Campbell A, Keller K, Landi I, Zhong Y, Dubovsky J, Howard JH, Yu L, Harrington B, Old M, Reiff S, Mace T, Tridandapani S, Muthusamy N, Caligiuri MA, Byrd JC, Carson WE, 3rd. Myeloid-Derived Suppressor Cells Express Bruton's Tyrosine Kinase and Can Be Depleted in Tumor-Bearing Hosts by Ibrutinib Treatment. Cancer Res. 2016;76(8):2125-36. doi: 10.1158/0008-5472.CAN-15-1490. PubMed PMID: 26880800; PMCID: PMC4873459.

32. Husain Z, Seth P, Sukhatme VP. Tumor-derived lactate and myeloid-derived suppressor cells: Linking metabolism to cancer immunology. Oncoimmunology. 2013;2(11):e26383. doi: 10.4161/onci.26383. PubMed PMID: 24404426; PMCID: PMC3881600.

33. Ugel S, De Sanctis F, Mandruzzato S, Bronte V. Tumor-induced myeloid deviation: when myeloid-derived suppressor cells meet tumor-associated macrophages. J Clin Invest. 2015;125(9):3365-76. doi: 10.1172/JCI80006. PubMed PMID: 26325033; PMCID: PMC4588310.

34. Schouppe E, Van Overmeire E, Laoui D, Keirsse J, Van Ginderachter JA. Modulation of CD8(+) T-cell activation events by monocytic and granulocytic myeloid-derived suppressor cells. Immunobiology. 2013;218(11):1385-91. doi: 10.1016/j.imbio.2013.07.003. PubMed PMID: 23932436.

35. Bronte V, Brandau S, Chen SH, Colombo MP, Frey AB, Greten TF, Mandruzzato S, Murray PJ, Ochoa A, Ostrand-Rosenberg S, Rodriguez PC, Sica A, Umansky V, Vonderheide RH, Gabrilovich DI. Recommendations for myeloid-derived suppressor cell nomenclature and characterization standards. Nat Commun. 2016;7:12150. doi: 10.1038/ncomms12150. PubMed PMID: 27381735; PMCID: PMC4935811.

36. Nagaraj S, Gabrilovich DI. Regulation of suppressive function of myeloid-derived suppressor cells by CD4+ T cells. Semin Cancer Biol. 2012;22(4):282-8. doi: 10.1016/j.semcancer.2012.01.010. PubMed PMID: 22313876; PMCID: PMC3349790.

37. Kumar V, Gabrilovich DI. Hypoxia-inducible factors in regulation of immune responses in tumour microenvironment. Immunology. 2014;143(4):512-9. doi: 10.1111/imm.12380. PubMed PMID: 25196648; PMCID: PMC4253499.

38. Baniyash M, Sade-Feldman M, Kanterman J. Chronic inflammation and cancer: suppressing the suppressors. Cancer Immunol Immunother. 2014;63(1):11-20. doi: 10.1007/s00262-013-1468-9. PubMed PMID: 23990173.

39. Filipazzi P, Valenti R, Huber V, Pilla L, Canese P, Iero M, Castelli C, Mariani L, Parmiani G, Rivoltini L. Identification of a new subset of myeloid suppressor cells in peripheral blood of melanoma patients with modulation by a granulocyte-macrophage colony-stimulation factor-based antitumor vaccine. Journal of clinical oncology : official

journal of the American Society of Clinical Oncology. 2007;25(18):2546-53. doi: 10.1200/JCO.2006.08.5829. PubMed PMID: 17577033.

40. Kim YS, Kim YJ, Lee JM, Kim EK, Park YJ, Choe SK, Ko HJ, Kang CY. Functional changes in myeloid-derived suppressor cells (MDSCs) during tumor growth: FKBP51 contributes to the regulation of the immunosuppressive function of MDSCs. Journal of immunology. 2012;188(9):4226-34. doi: 10.4049/jimmunol.1103040. PubMed PMID: 22474024.

41. Albeituni SH, Ding C, Liu M, Hu X, Luo F, Kloecker G, Bousamra M, 2nd, Zhang HG, Yan J. Yeast-Derived Particulate beta-Glucan Treatment Subverts the Suppression of Myeloid-Derived Suppressor Cells (MDSC) by Inducing Polymorphonuclear MDSC Apoptosis and Monocytic MDSC Differentiation to APC in Cancer. Journal of immunology. 2016;196(5):2167-80. doi: 10.4049/jimmunol.1501853. PubMed PMID: 26810222; PMCID: PMC4761495.

42. Schlecker E, Stojanovic A, Eisen C, Quack C, Falk CS, Umansky V, Cerwenka A. Tumor-infiltrating monocytic myeloid-derived suppressor cells mediate CCR5-dependent recruitment of regulatory T cells favoring tumor growth. Journal of immunology. 2012;189(12):5602-11. doi: 10.4049/jimmunol.1201018. PubMed PMID: 23152559.

43. Ortiz ML, Lu L, Ramachandran I, Gabrilovich DI. Myeloid-derived suppressor cells in the development of lung cancer. Cancer Immunol Res. 2014;2(1):50-8. doi: 10.1158/2326-6066.CIR-13-0129. PubMed PMID: 24778162; PMCID: PMC4007346.

44. Ost M, Singh A, Peschel A, Mehling R, Rieber N, Hartl D. Myeloid-Derived Suppressor Cells in Bacterial Infections. Front Cell Infect Microbiol. 2016;6:37. doi: 10.3389/fcimb.2016.00037. PubMed PMID: 27066459; PMCID: PMC4814452.

45. Gorgun GT, Whitehill G, Anderson JL, Hideshima T, Maguire C, Laubach J, Raje N, Munshi NC, Richardson PG, Anderson KC. Tumor-promoting immune-suppressive myeloid-derived suppressor cells in the multiple myeloma microenvironment in humans. Blood. 2013;121(15):2975-87. doi: 10.1182/blood-2012-08-448548. PubMed PMID: 23321256; PMCID: PMC3624943.

46. Sica A, Bronte V. Altered macrophage differentiation and immune dysfunction in tumor development. J Clin Invest. 2007;117(5):1155-66. doi: 10.1172/JCI31422. PubMed PMID: 17476345; PMCID: PMC1857267.

47. Dolcetti L, Peranzoni E, Ugel S, Marigo I, Fernandez Gomez A, Mesa C, Geilich M, Winkels G, Traggiai E, Casati A, Grassi F, Bronte V. Hierarchy of immunosuppressive strength among myeloid-derived suppressor cell subsets is determined by GM-CSF. Eur J Immunol. 2010;40(1):22-35. doi: 10.1002/eji.200939903. PubMed PMID: 19941314.

48. Zhao F, Obermann S, von Wasielewski R, Haile L, Manns MP, Korangy F, Greten TF. Increase in frequency of myeloid-derived suppressor cells in mice with spontaneous pancreatic carcinoma. Immunology. 2009;128(1):141-9. doi: 10.1111/j.1365-2567.2009.03105.x. PubMed PMID: 19689743; PMCID: PMC2747147.

49. Nagaraj S, Youn JI, Gabrilovich DI. Reciprocal relationship between myeloid-derived suppressor cells and T cells. Journal of immunology. 2013;191(1):17-23. doi: 10.4049/jimmunol.1300654. PubMed PMID: 23794702; PMCID: PMC3694485.

50. Yaddanapudi K, Rendon BE, Lamont G, Kim EJ, Al Rayyan N, Richie J, Albeituni S, Waigel S, Wise A, Mitchell RA. MIF Is Necessary for Late-Stage Melanoma Patient MDSC Immune Suppression and Differentiation. Cancer Immunol Res. 2016;4(2):101-12. doi: 10.1158/2326-6066.CIR-15-0070-T. PubMed PMID: 26603621; PMCID: PMC4740231.

51. Kumar V, Patel S, Tcyganov E, Gabrilovich DI. The Nature of Myeloid-Derived Suppressor Cells in the Tumor Microenvironment. Trends Immunol. 2016;37(3):208-20. doi: 10.1016/j.it.2016.01.004. PubMed PMID: 26858199; PMCID: PMC4775398.

52. Idorn M, Kollgaard T, Kongsted P, Sengelov L, Thor Straten P. Correlation between frequencies of blood monocytic myeloid-derived suppressor cells, regulatory T cells and negative prognostic markers in patients with castration-resistant metastatic prostate cancer. Cancer Immunol Immunother. 2014;63(11):1177-87. doi: 10.1007/s00262-014-1591-2. PubMed PMID: 25085000.

53. Hossain F, Al-Khami AA, Wyczechowska D, Hernandez C, Zheng L, Reiss K, Valle LD, Trillo-Tinoco J, Maj T, Zou W, Rodriguez PC, Ochoa AC. Inhibition of Fatty Acid Oxidation Modulates Immunosuppressive Functions of Myeloid-Derived Suppressor Cells and Enhances Cancer Therapies. Cancer Immunol Res. 2015;3(11):1236-47. doi: 10.1158/2326-6066.CIR-15-0036. PubMed PMID: 26025381; PMCID: PMC4636942.

54. Bronte V. Tumor cells hijack macrophages via lactic acid. Immunol Cell Biol. 2014;92(8):647-9. doi: 10.1038/icb.2014.67. PubMed PMID: 25091608.

55. Lu T, Ramakrishnan R, Altiok S, Youn JI, Cheng P, Celis E, Pisarev V, Sherman S, Sporn MB, Gabrilovich D. Tumor-infiltrating myeloid cells induce tumor cell resistance to cytotoxic T cells in mice. J Clin Invest. 2011;121(10):4015-29. doi: 10.1172/JCI45862. PubMed PMID: 21911941; PMCID: PMC3195459.

56. Martens A, Wistuba-Hamprecht K, Geukes Foppen M, Yuan J, Postow MA, Wong P, Romano E, Khammari A, Dreno B, Capone M, Ascierto PA, Di Giacomo AM, Maio M, Schilling B, Sucker A, Schadendorf D, Hassel JC, Eigentler TK, Martus P, Wolchok JD, Blank C, Pawelec G, Garbe C, Weide B. Baseline Peripheral Blood Biomarkers Associated with Clinical Outcome of Advanced Melanoma Patients Treated with Ipilimumab. Clinical cancer research : an official journal of the American Association for Cancer Research. 2016;22(12):2908-18. doi: 10.1158/1078-0432.CCR-15-2412. PubMed PMID: 26787752.

57. Kodumudi KN, Weber A, Sarnaik AA, Pilon-Thomas S. Blockade of myeloid-derived suppressor cells after induction of lymphopenia improves adoptive T cell therapy in a murine model of melanoma. Journal of immunology. 2012;189(11):5147-54. doi: 10.4049/jimmunol.1200274. PubMed PMID: 23100512; PMCID: PMC3505990.

58. Chesney J. 6-phosphofructo-2-kinase/fructose-2,6-bisphosphatase and tumor cell glycolysis. Curr Opin Clin Nutr Metab Care. 2006;9(5):535-9. doi: 10.1097/01.mco.0000241661.15514.fb. PubMed PMID: 16912547.

59. Clem BF, O'Neal J, Tapolsky G, Clem AL, Imbert-Fernandez Y, Kerr DA, 2nd, Klarer AC, Redman R, Miller DM, Trent JO, Telang S, Chesney J. Targeting 6-phosphofructo-2-kinase (PFKFB3) as a therapeutic strategy against cancer. Mol Cancer Ther. 2013;12(8):1461-70. doi: 10.1158/1535-7163.MCT-13-0097. PubMed PMID: 23674815; PMCID: PMC3742633.

60. Yalcin A, Telang S, Clem B, Chesney J. Regulation of glucose metabolism by 6-phosphofructo-2-kinase/fructose-2,6-bisphosphatases in cancer. Exp Mol Pathol. 2009;86(3):174-9. doi: 10.1016/j.yexmp.2009.01.003. PubMed PMID: 19454274.

61. Bartrons R, Caro J. Hypoxia, glucose metabolism and the Warburg's effect. J Bioenerg Biomembr. 2007;39(3):223-9. doi: 10.1007/s10863-007-9080-3. PubMed PMID: 17661163.

62. Sbarra AJ, Karnovsky ML. The biochemical basis of phagocytosis. I. Metabolic changes during the ingestion of particles by polymorphonuclear leukocytes. J Biol Chem. 1959;234(6):1355-62. PubMed PMID: 13654378.

63. Kelly B, O'Neill LA. Metabolic reprogramming in macrophages and dendritic cells in innate immunity. Cell Res. 2015;25(7):771-84. doi: 10.1038/cr.2015.68. PubMed PMID: 26045163; PMCID: PMC4493277.

64. Guthrie LA, McPhail LC, Henson PM, Johnston RB, Jr. Priming of neutrophils for enhanced release of oxygen metabolites by bacterial lipopolysaccharide. Evidence for increased activity of the superoxide-producing enzyme. The Journal of experimental medicine. 1984;160(6):1656-71. PubMed PMID: 6096475; PMCID: PMC2187529.

65. Hard GC. Some biochemical aspects of the immune macrophage. Br J Exp Pathol. 1970;51(1):97-105. PubMed PMID: 5434449; PMCID: PMC2072214.

66. Newsholme P, Gordon S, Newsholme EA. Rates of utilization and fates of glucose, glutamine, pyruvate, fatty acids and ketone bodies by mouse macrophages. Biochem J. 1987;242(3):631-6. PubMed PMID: 3593269; PMCID: PMC1147758.

67. Lorsbach RB, Murphy WJ, Lowenstein CJ, Snyder SH, Russell SW. Expression of the nitric oxide synthase gene in mouse macrophages activated for tumor cell killing. Molecular basis for the synergy between interferon-gamma and lipopolysaccharide. J Biol Chem. 1993;268(3):1908-13. PubMed PMID: 7678412.

68. Lu L, Bonham CA, Chambers FG, Watkins SC, Hoffman RA, Simmons RL, Thomson AW. Induction of nitric oxide synthase in mouse dendritic cells by IFN-gamma, endotoxin, and interaction with allogeneic T cells: nitric oxide production is associated with dendritic cell apoptosis. Journal of immunology. 1996;157(8):3577-86. PubMed PMID: 8871658.

69. Hammami I, Chen J, Murschel F, Bronte V, De Crescenzo G, Jolicoeur M. Immunosuppressive activity enhances central carbon metabolism and bioenergetics in myeloid-derived suppressor cells *in vitro* models. BMC Cell Biol. 2012;13:18. doi: 10.1186/1471-2121-13-18. PubMed PMID: 22762146; PMCID: PMC3433355.

70. Ando M, Uehara I, Kogure K, Asano Y, Nakajima W, Abe Y, Kawauchi K, Tanaka N. Interleukin 6 enhances glycolysis through expression of the glycolytic enzymes hexokinase 2 and 6-phosphofructo-2-kinase/fructose-2,6-bisphosphatase-3. J Nippon Med Sch. 2010;77(2):97-105. PubMed PMID: 20453422.

71. Dhar-Mascareno M, Chen J, Zhang RH, Carcamo JM, Golde DW. Granulocyte-macrophage colony-stimulating factor signals for increased glucose transport via phosphatidylinositol 3-kinase- and hydrogen peroxide-dependent mechanisms. J Biol Chem. 2003;278(13):11107-14. doi: 10.1074/jbc.M212541200. PubMed PMID: 12538575.

72. Wu T, Zhao Y, Wang H, Li Y, Shao L, Wang R, Lu J, Yang Z, Wang J, Zhao Y. mTOR masters monocytic myeloid-derived suppressor cells in mice with allografts or tumors. Sci Rep. 2016;6:20250. doi: 10.1038/srep20250. PubMed PMID: 26833095; PMCID: PMC4735296.

73. Romero-Garcia S, Moreno-Altamirano MM, Prado-Garcia H, Sanchez-Garcia FJ. Lactate Contribution to the Tumor Microenvironment: Mechanisms, Effects on Immune Cells and Therapeutic Relevance. Front Immunol. 2016;7:52. doi: 10.3389/fimmu.2016.00052. PubMed PMID: 26909082; PMCID: PMC4754406.

74. DeBerardinis RJ, Mancuso A, Daikhin E, Nissim I, Yudkoff M, Wehrli S, Thompson CB. Beyond aerobic glycolysis: transformed cells can engage in glutamine metabolism that exceeds the requirement for protein and nucleotide synthesis. Proc Natl Acad Sci U S A. 2007;104(49):19345-50. doi: 10.1073/pnas.0709747104. PubMed PMID: 18032601; PMCID: PMC2148292.

75. Feron O. Pyruvate into lactate and back: from the Warburg effect to symbiotic energy fuel exchange in cancer cells. Radiother Oncol. 2009;92(3):329-33. doi: 10.1016/j.radonc.2009.06.025. PubMed PMID: 19604589.

76. Pearce EJ, Everts B. Dendritic cell metabolism. Nat Rev Immunol. 2015;15(1):18-29. doi: 10.1038/nri3771. PubMed PMID: 25534620; PMCID: PMC4495583.

77. Latham T, Mackay L, Sproul D, Karim M, Culley J, Harrison DJ, Hayward L, Langridge-Smith P, Gilbert N, Ramsahoye BH. Lactate, a product of glycolytic metabolism, inhibits histone deacetylase activity and promotes changes in gene expression. Nucleic Acids Res. 2012;40(11):4794-803. doi: 10.1093/nar/gks066. PubMed PMID: 22323521; PMCID: PMC3367171

78. Byles V, Covarrubias AJ, Ben-Sahra I, Lamming DW, Sabatini DM, Manning BD, Horng T. The TSC-mTOR pathway regulates macrophage polarization. Nat Commun. 2013;4:2834. doi: 10.1038/ncomms3834. PubMed PMID: 24280772; PMCID: PMC3876736.

79. Huo Y, Iadevaia V, Yao Z, Kelly I, Cosulich S, Guichard S, Foster LJ, Proud CG. Stable isotope-labelling analysis of the impact of inhibition of the mammalian target of rapamycin on protein synthesis. Biochem J. 2012;444(1):141-51. doi: 10.1042/BJ20112107. PubMed PMID: 22428559.

80. Denko NC. Hypoxia, HIF1 and glucose metabolism in the solid tumour. Nat Rev Cancer. 2008;8(9):705-13. doi: 10.1038/nrc2468. PubMed PMID: 19143055.

81. Semenza GL, Nejfelt MK, Chi SM, Antonarakis SE. Hypoxia-inducible nuclear factors bind to an enhancer element located 3' to the human erythropoietin gene. Proc Natl Acad Sci U S A. 1991;88(13):5680-4. PubMed PMID: 2062846; PMCID: PMC51941.

82. Mole DR, Blancher C, Copley RR, Pollard PJ, Gleadle JM, Ragoussis J, Ratcliffe PJ. Genome-wide association of hypoxia-inducible factor (HIF)-1alpha and HIF-2alpha DNA binding with expression profiling of hypoxia-inducible transcripts. J Biol Chem. 2009;284(25):16767-75. doi: 10.1074/jbc.M901790200. PubMed PMID: 19386601; PMCID: PMC2719312.

83. Chen C, Pore N, Behrooz A, Ismail-Beigi F, Maity A. Regulation of glut1 mRNA by hypoxia-inducible factor-1. Interaction between H-ras and hypoxia. J Biol Chem. 2001;276(12):9519-25. doi: 10.1074/jbc.M010144200. PubMed PMID: 11120745.

84. Semenza GL, Jiang BH, Leung SW, Passantino R, Concordet JP, Maire P, Giallongo A. Hypoxia response elements in the aldolase A, enolase 1, and lactate dehydrogenase A gene promoters contain essential binding sites for hypoxia-inducible factor 1. J Biol Chem. 1996;271(51):32529-37. PubMed PMID: 8955077.

85. Colegio OR, Chu NQ, Szabo AL, Chu T, Rhebergen AM, Jairam V, Cyrus N, Brokowski CE, Eisenbarth SC, Phillips GM, Cline GW, Phillips AJ, Medzhitov R. Functional polarization of tumour-associated macrophages by tumour-derived lactic acid. Nature. 2014;513(7519):559-63. doi: 10.1038/nature13490. PubMed PMID: 25043024; PMCID: PMC4301845.

86. Melillo G, Musso T, Sica A, Taylor LS, Cox GW, Varesio L. A hypoxia-responsive element mediates a novel pathway of activation of the inducible nitric oxide synthase promoter. The Journal of experimental medicine. 1995;182(6):1683-93. PubMed PMID: 7500013; PMCID: PMC2192245.

87. Highfill SL, Rodriguez PC, Zhou Q, Goetz CA, Koehn BH, Veenstra R, Taylor PA, Panoskaltsis-Mortari A, Serody JS, Munn DH, Tolar J, Ochoa AC, Blazar BR. Bone marrow myeloid-derived suppressor cells (MDSCs) inhibit graft-versus-host disease (GVHD) via an arginase-1-dependent mechanism that is up-regulated by interleukin-13. Blood. 2010;116(25):5738-47. doi: 10.1182/blood-2010-06-287839. PubMed PMID: 20807889; PMCID: PMC3031417.

88. Van Schaftingen E, Lederer B, Bartrons R, Hers HG. A kinetic study of pyrophosphate: fructose-6-phosphate phosphotransferase from potato tubers. Application to a microassay of fructose 2,6-bisphosphate. Eur J Biochem. 1982;129(1):191-5. PubMed PMID: 6297885.

89. Swann JB, Smyth MJ. Immune surveillance of tumors. J Clin Invest. 2007;117(5):1137-46. doi: 10.1172/JCI31405. PubMed PMID: 17476343; PMCID: PMC1857231.

90. Kim R, Emi M, Tanabe K. Cancer immunoediting from immune surveillance to immune escape. Immunology. 2007;121(1):1-14. doi: 10.1111/j.1365-2567.2007.02587.x. PubMed PMID: 17386080; PMCID: PMC2265921.

91. Hanahan D, Weinberg RA. The hallmarks of cancer. Cell. 2000;100(1):57-70. PubMed PMID: 10647931.

92. Hanahan D, Weinberg RA. Hallmarks of cancer: the next generation. Cell. 2011;144(5):646-74. doi: 10.1016/j.cell.2011.02.013. PubMed PMID: 21376230.

93. Teng MW, Swann JB, Koebel CM, Schreiber RD, Smyth MJ. Immune-mediated dormancy: an equilibrium with cancer. J Leukoc Biol. 2008;84(4):988-93. doi: 10.1189/jlb.1107774. PubMed PMID: 18515327.

94. Alexe G, Dalgin GS, Scanfeld D, Tamayo P, Mesirov JP, DeLisi C, Harris L, Barnard N, Martel M, Levine AJ, Ganesan S, Bhanot G. High expression of lymphocyte-associated genes in node-negative HER2+ breast cancers correlates with lower recurrence rates. Cancer Res. 2007;67(22):10669-76. doi: 10.1158/0008-5472.CAN-07-0539. PubMed PMID: 18006808.

95. Erdag G, Schaefer JT, Smolkin ME, Deacon DH, Shea SM, Dengel LT, Patterson JW, Slingluff CL, Jr. Immunotype and immunohistologic characteristics of tumor-infiltrating immune cells are associated with clinical outcome in metastatic melanoma. Cancer Res. 2012;72(5):1070-80. doi: 10.1158/0008-5472.CAN-11-3218. PubMed PMID: 22266112; PMCID: PMC3306813.

96. Hwang WT, Adams SF, Tahirovic E, Hagemann IS, Coukos G. Prognostic significance of tumor-infiltrating T cells in ovarian cancer: a meta-analysis. Gynecol Oncol. 2012;124(2):192-8. doi: 10.1016/j.ygyno.2011.09.039. PubMed PMID: 22040834; PMCID: PMC3298445.

97. Nakano O, Sato M, Naito Y, Suzuki K, Orikasa S, Aizawa M, Suzuki Y, Shintaku I, Nagura H, Ohtani H. Proliferative activity of intratumoral CD8(+) T-lymphocytes as a prognostic factor in human renal cell carcinoma: clinicopathologic demonstration of antitumor immunity. Cancer Res. 2001;61(13):5132-6. PubMed PMID: 11431351.

98. Hodi FS, O'Day SJ, McDermott DF, Weber RW, Sosman JA, Haanen JB, Gonzalez R, Robert C, Schadendorf D, Hassel JC, Akerley W, van den Eertwegh AJ, Lutzky J, Lorigan P, Vaubel JM, Linette GP, Hogg D, Ottensmeier CH, Lebbe C, Peschel C, Quirt I, Clark JI, Wolchok JD, Weber JS, Tian J, Yellin MJ, Nichol GM, Hoos A, Urba WJ. Improved survival with ipilimumab in patients with metastatic melanoma. N Engl J Med. 2010;363(8):711-23. doi: 10.1056/NEJMoa1003466. PubMed PMID: 20525992; PMCID: PMC3549297.

99. Robert C, Thomas L, Bondarenko I, O'Day S, Weber J, Garbe C, Lebbe C, Baurain JF, Testori A, Grob JJ, Davidson N, Richards J, Maio M, Hauschild A, Miller WH, Jr., Gascon P, Lotem M, Harmankaya K, Ibrahim R, Francis S, Chen TT, Humphrey R, Hoos A, Wolchok JD. Ipilimumab plus dacarbazine for previously untreated metastatic melanoma. N Engl J Med. 2011;364(26):2517-26. doi: 10.1056/NEJMoa1104621. PubMed PMID: 21639810.

100. Prieto PA, Yang JC, Sherry RM, Hughes MS, Kammula US, White DE, Levy CL, Rosenberg SA, Phan GQ. CTLA-4 blockade with ipilimumab: long-term follow-up of 177 patients with metastatic melanoma. Clinical cancer research : an official journal of the American Association for Cancer Research. 2012;18(7):2039-47. doi: 10.1158/1078-0432.CCR-11-1823. PubMed PMID: 22271879; PMCID: PMC3319861.

101. Topalian SL, Hodi FS, Brahmer JR, Gettinger SN, Smith DC, McDermott DF, Powderly JD, Carvajal RD, Sosman JA, Atkins MB, Leming PD, Spigel DR, Antonia SJ, Horn L, Drake CG, Pardoll DM, Chen L, Sharfman WH, Anders RA, Taube JM, McMiller TL, Xu H, Korman AJ, Jure-Kunkel M, Agrawal S, McDonald D, Kollia GD, Gupta A, Wigginton JM, Sznol M. Safety, activity, and immune correlates of anti-PD-1 antibody in cancer. N Engl J Med. 2012;366(26):2443-54. doi: 10.1056/NEJMoa1200690. PubMed PMID: 22658127; PMCID: PMC3544539.

102. Brahmer JR, Tykodi SS, Chow LQ, Hwu WJ, Topalian SL, Hwu P, Drake CG, Camacho LH, Kauh J, Odunsi K, Pitot HC, Hamid O, Bhatia S, Martins R, Eaton K, Chen S, Salay TM, Alaparthy S, Grosso JF, Korman AJ, Parker SM, Agrawal S, Goldberg SM, Pardoll DM, Gupta A, Wigginton JM. Safety and activity of anti-PD-L1 antibody in patients with advanced cancer. N Engl J Med. 2012;366(26):2455-65. doi: 10.1056/NEJMoa1200694. PubMed PMID: 22658128; PMCID: PMC3563263.

103. Hamid O, Robert C, Daud A, Hodi FS, Hwu WJ, Kefford R, Wolchok JD, Hersey P, Joseph RW, Weber JS, Dronca R, Gangadhar TC, Patnaik A, Zarour H, Joshua AM, Gergich K, Elassaiss-Schaap J, Algazi A, Mateus C, Boasberg P, Tumeh PC, Chmielowski B, Ebbinghaus SW, Li XN, Kang SP, Ribas A. Safety and tumor responses with lambrolizumab (anti-PD-1) in melanoma. N Engl J Med. 2013;369(2):134-44. doi: 10.1056/NEJMoa1305133. PubMed PMID: 23724846; PMCID: PMC4126516.

104. Kelderman S, Schumacher TN, Haanen JB. Acquired and intrinsic resistance in cancer immunotherapy. Mol Oncol. 2014;8(6):1132-9. doi: 10.1016/j.molonc.2014.07.011. PubMed PMID: 25106088.

105. Pardoll DM. The blockade of immune checkpoints in cancer immunotherapy. Nat Rev Cancer. 2012;12(4):252-64. doi: 10.1038/nrc3239. PubMed PMID: 22437870; PMCID: PMC4856023.

106. Kato M, Takahashi M, Akhand AA, Liu W, Dai Y, Shimizu S, Iwamoto T, Suzuki H, Nakashima I. Transgenic mouse model for skin malignant melanoma. Oncogene. 1998;17(14):1885-8. doi: 10.1038/sj.onc.1202077. PubMed PMID: 9778055.

107. Umansky V, Abschuetz O, Osen W, Ramacher M, Zhao F, Kato M, Schadendorf D. Melanoma-specific memory T cells are functionally active in Ret transgenic mice without macroscopic tumors. Cancer Res. 2008;68(22):9451-8. doi: 10.1158/0008-5472.CAN-08-1464. PubMed PMID: 19010920.

COPYRIGHT PERMISSIONS

1. Figure 1. Copyright permission granted. License number 4093671453921.
2. Figure 2. Copyright permission granted. License number 4093680416520.
3. Figure 3. Copyright permission granted. License number 4093671453921.
4. Figure 4. Copyright permission granted. License number 4093681414380.
5. Figure 5. Copyright permission granted. License number 4093690601093.
6. Figure 5. Open access article distributed under the terms of the Creative Commons Attribution Noncommercial License.

7. Figure 5. Permission granted via email.

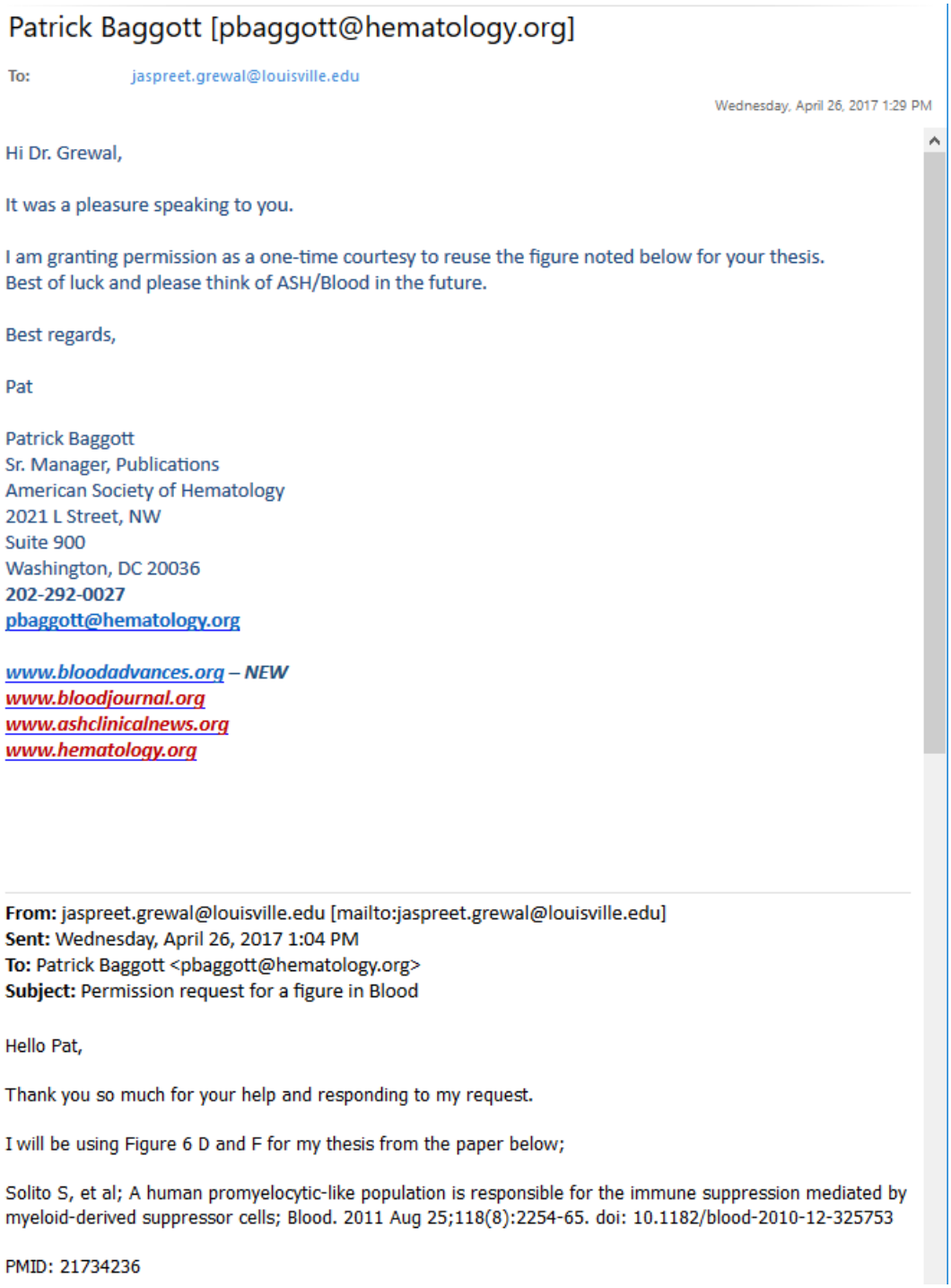

Patrick Baggott [pbaggott@hematology.org]

To: jaspreet.grewal@louisville.edu

Wednesday, April 26, 2017 1:29 PM

Hi Dr. Grewal,

It was a pleasure speaking to you.

I am granting permission as a one-time courtesy to reuse the figure noted below for your thesis.
Best of luck and please think of ASH/Blood in the future.

Best regards,

Pat

Patrick Baggott
Sr. Manager, Publications
American Society of Hematology
2021 L Street, NW
Suite 900
Washington, DC 20036
202-292-0027
pbaggott@hematology.org

www.bloodadvances.org – NEW
www.bloodjournal.org
www.ashclinicalnews.org
www.hematology.org

From: jaspreet.grewal@louisville.edu [mailto:jaspreet.grewal@louisville.edu]
Sent: Wednesday, April 26, 2017 1:04 PM
To: Patrick Baggott <pbaggott@hematology.org>
Subject: Permission request for a figure in Blood

Hello Pat,

Thank you so much for your help and responding to my request.

I will be using Figure 6 D and F for my thesis from the paper below;

Solito S, et al; A human promyelocytic-like population is responsible for the immune suppression mediated by myeloid-derived suppressor cells; Blood. 2011 Aug 25;118(8):2254-65. doi: 10.1182/blood-2010-12-325753

PMID: 21734236

8. Figure 7. Copyright permission granted. License number 4093741221695.

CURRICULUM VITAE

Jaspreet Singh Grewal, M.D., M.P.H., M.S.
Tel: (734)787-1510
Email: jsgrew01@louisville.edu

EDUCATION

08/2013 – 05-2017 **Doctor of Philosophy (Ph.D.)** – Pharmacology and Toxicology, University of Louisville, Louisville, Kentucky
Thesis project: TARGETING THE GLUCOSE METABOLISM OF MYELOID-DERVIED SUPPRESSOR CELLS (MDSCs) TO STIMULATE CANCER IMMUNITY
Mentor: Jason Chesney, M.D., Ph.D.

07/01/2012 - 06/30/2015 **Fellowship training in Hematology and Oncology**, University of Louisville, Louisville, Kentucky

09/2010 – 12/2014 **Master of Science (M.S.) in Clinical Laboratory Science**, Michigan State University (MSU), East Lansing, MI

01/2009 – 05/2012 **Master's in Public Health (M.P.H.) Professional Enhancement Program (PEP) in Health Policy Administration (HPA)**, University of Illinois at Chicago (UIC), Chicago, Illinois

05/2009 – 12/2011 **Certificate Non-Degree Program in Clinical Research Methods**, University of Illinois at Chicago (UIC), Chicago, Illinois

06/2011 **Certification in Immunodiagnostics and Clinical Flow Cytometry**, Michigan State University (MSU), East Lansing, MI

06/2011 **Certification in Molecular Laboratory Diagnostics**, Michigan State University (MSU), East Lansing, MI

07/01/2005 - 06/30/2008 **Residency training in Internal Medicine**, St. Joseph Mercy Hospital, Ann Arbor, Michigan

07/1996 - 01/2002 **Bachelor of Medicine and Bachelor of Surgery (M.B.B.S.)**, Christian Medical College, Ludhiana, India

ACADEMIC APPOINTMENTS

10/01/2015 – Present **Instructor,** Hematology/Oncology, University of Louisville, Kentucky

07/01/2015 – 09/30/2015 **Post-doctorate fellow**, University of Louisville, Kentucky

07/2014 – 06/2015 **Research Fellow** – Department of Microbiology and Immunology – Yan Lab, University of Louisville, Louisville, Kentucky

07/2012 – 06/2014 **Research Fellow** – Department of Biochemistry – Bates Lab, University of Louisville, Louisville, Kentucky

06/16/2009 – 12/2011 **Adjunct Assistant Professor for Internal Medicine** Central Michigan University (CMU), Mt. Pleasant, Michigan: Physician Assistant Program

03/2004 – 06/2005 **Clinical Research Associate**, Toronto General Hospital, University Health Network, Toronto, Ontario

CERTIFICATION AND LICENSURE

08/2008 American Board of Internal Medicine (ABIM) – Internal Medicine

10/2015 ABIM – subspecialty certification in Hematology – 2015

10/2015 ABIM – subspecialty certification in Medical Oncology – 2015

06/2012 Medical license – Kentucky

06/2004 Educational Commission for Medical Graduates (ECFMG)

06/2004 Medical Council of Canada (MCC)

PROFESSIONAL MEMBERSHIPS AND ACTIVITIES

06/2012 American Society of Clinical Oncology (ASCO)

06/2012 American Society of Hematology (ASH)

HONORS AND AWARDS

10/2014 First place: Poster presentation at the Annual Brown Cancer Center Retreat. University of Louisville

05/2007 First place: Poster presentation at the Annual Resident Research Forum: St. Joseph Mercy Hospital, Ann Arbor, Michigan

05/2008 First place: Poster presentation at the Annual Resident Research Forum: St. Joseph Mercy Hospital, Ann Arbor, Michigan

05/2008 Second place: Poster presentation at the Annual Resident Research Forum: St. Joseph Mercy Hospital, Ann Arbor, Michigan

05/2008 Second place: Oral presentation at the Michigan Chapter American College of Physicians Meeting

2008 Annual Resident Research Award: Academic Year of 2008

09/2008 Second place: Oral presentation at the Michigan Chapter American College of Physicians Meeting

COMMITTEE ASSIGNMENTS AND ADMINISTRATIVE SERVICES

2015 Member, Graduate Medical Education Committee, University of Louisville, Kentucky

2014 Member, House Staff Council, University of Louisville, Kentucky

2011 MidMichigan Health Clinical Transformation Project/Electronic Medical Record: Member, Physician Advisory Group

2010 Executive and Credentials Committee at MidMichigan Medical Center, Clare, Michigan

2010 Joint Conference Committee at MidMichigan Medical Center, Clare, Michigan

RESEARCH ACTIVITIES

01/2017 Flow cytometry based characterization of myeloid derived suppressor cell (MDSC) and regulatory T cell (Tregs) population following administration of exogenous granulocyte colony stimulating factors (G-CSFs) in peripheral blood samples of patients with late-stage malignancies

04/2016 – Ongoing	A Phase 1, Multicenter, Open-label Trial to Evaluate the Safety of Talimogene Laherparepvec Injected into Liver Tumors Amgen sponsored study Co-PI
2016 – Ongoing	Phase I/II Trial of the A-dmDT390-bisFv(UCHT1) Fusion Protein in Combination with Ionizing Radiation and Pembrolizumab for the Treatment of Stage IV Melanoma Co-investigator
12/2015	An Open-Label, Single Arm Phase II Study of Nivolumab in Combination with Ipilimumab as first line-therapy in stage IV Non-Small Cell Lung Cancer (NSCLC) BMS sponsored study Co-PI
12/2015 –	Phase II Trial (Investigator initiated trial): Open label phase II study evaluating the therapeutic efficacy of Idelalisib in patients with steroid-refractory graft-versus-host-disease (GvHD) following allogeneic hematopoietic stem cell transplantation (allo-HSCT) Protocol developed but study not approved by Gilead Sciences Co-PI
08/2015 – Ongoing	A Phase 1b/3 Multicenter, Randomized, Open-label Trial of Talimogene Laherparepvec in combination with Pembrolizumab for the Treatment of Subjects With Recurrent or Metastatic Squamous Cell Carcinoma of the Head and Neck Amgen sponsored study Co-PI
06/2015 –	Investigator initiated trial: Open label phase II study to evaluate the efficacy of Ongoing Dasatinib maintenance in adult Philadelphia chromosome-positive acute lymphoblastic leukemia (Ph+ ALL) following autologous hematopoietic stem cell transplantation (HCT) Co-investigator
2016	Open Label Phase II trial (Investigator initiated): Using Elotuzumab to Treat Steroid-refractory or -Dependent Chronic Graft versus Host Disease (GVHD) in Allogeneic Stem Cell Transplantation Draft protocol presented to BMS – After initial review and approval, BMS scientific team and medical director decided to not support the study

2013 Phase I/II Trial of the A-dmDT390-bisFv (UCHT1) Fusion Protein in Combination with Ionizing Radiation for the Treatment of Stage IV Melanoma
Co-investigator
Trial was terminated by FDA secondary to two unexpected deaths

06/2014 – 12/2014 Immunohistochemistry for Class I MHC Expression in Melanomas That Have Been Collected by the J.G. Brown Cancer Center Tissue Repository
Mentor: Jason Chesney, M.D., Ph.D.
Aim: To study if expression of MHC Class I in tumor cells and infiltration of tumor with T cells can predict response to immunotherapies targeting immune checkpoint such as PD-1 and CTLA-4.

07/2012 – 12/2014 Validation Studies Evaluating the Efficacy of a Novel Small Molecule Therapeutic Agent XB05 for Selective Inhibition of Malignant Cells in Acute Myeloid Leukemia (AML)
Mentor: Tariq Malik, Ph.D.

2007 – 2008 Adherence to Breast Cancer Treatment Guidelines in a Large Community Teaching Hospital
Co-investigators: Philip Stella, M.D.
Aims: Compliance and adherence of the physicians to NCCN guidelines in the treatment of breast cancer at the community cancer center
Data collection: NCCN breast cancer registry

CLINICAL ACTIVITIES

08/2015 – Onwards Bone Marrow Transplant Unit on-call coverage provider, University of Louisville Hospital, Louisville, Kentucky

05/2015 – Onwards Hospitalist Locums Tenens, Jewish and St. Mary's Hospitals, Louisville, Kentucky

11/2010 – 06/2012 Medical Director, Inpatient Services of Michigan, P.C., MidMichigan Medical Center in Clare, Michigan

11/2010 – 06/2012 Hospitalist, Inpatient Services of Michigan, P.C., MidMichigan Medical Center in Clare, Michigan

10/2008 – 11/2010 Medical Director, Hospitalist Physicians Medical Group, PC: MidMichigan Medical Center in Clare, Michigan

07/2008 – 11/2010 Hospitalist, Hospitalist Physicians Medical Group, PC: MidMichigan Medical Center in Clare, Michigan

11/2008 – 06/2009 Hospitalist, Hospitalist Physicians Medical Group, PC: Mercy Hospital in Grayling,Michigan

01/2001 – 01/2002 Medical Intern, Christian Medical College, Ludhiana, Punjab, India

ABSTRACTS AND PRESENTATIONS

ORAL PRESENTATIONS

1. **Grewal JS**, Shehab TM, Krasman ML, Whitehouse Jr WM. (2008, May). A Young Male Patient with Abdominal Pain and Weight Loss. A case of Median Arcuate Ligament Syndrome. Oral Presentation presented at: Michigan Chapter of the American College of Physicians Meeting; Sterling Heights, MI.
2. **Grewal JS**, Tworek JA, Chottiner EA, Sahijdak WM. (2008, September). Central Nervous System Involvement with Waldenström's Macroglobulinemia: Response to Cranial Radiation Treatment. Oral Presentation presented at: Michigan Chapter of the American College of Physicians Meeting; Dearborn, MI.
3. **Grewal JS**, Tworek JA, Chottiner EA, Sahijdak WM. (2008, May). Central Nervous System Involvement with Waldenström's Macroglobulinemia: Response to Cranial Radiation Treatment. Oral Presentation presented at: Michigan Chapter of the American College of Physicians meeting; Sterling Heights, MI.

POSTERS

1. **J. Grewal**, J. Ritchie, N. Al-Rayyan, P Schowe, C Falkner, S.Telang, K. Yaddanapudi, and J. Chesney. Targeting the Glucose Metabolism of Monocytic Myeloid-Derived Suppressor Cells to Stimulate Cancer Immunity. ASCO-SITC meeting in Orlando, FL, February 2017.
2. **J. Grewal**, J. Ritchie, N. Al-Rayyan, S.Telang, K. Yaddanapudi, and J. Chesney. Targeting the Glucose Metabolism of Monocytic Myeloid-Derived Suppressor Cells to Stimulate Cancer Immunity. Research Louisville 2016.
3. S Telang, K Yaddanapudi, **J Grewal**, G Tapolsky, R Redman and J Chesney. Targeting 6-Phosphofructo-2-Kinase (PFKFB3) as an Immunotherapeutic Strategy. ASCO 2016.
4. **J. Grewal**, J. Ritchie, N. Al-Rayyan, S.Telang, K. Yaddanapudi, and J. Chesney. 6-phosphofructo-2-kinase/fructose-2,6-biphosphatase 3

(PFKFB3) is Necessary for Human Melanoma MDSC Differentiation and Function. AAI Meeting in Seattle, WA 2016

5. **J. Grewal**, J. Ritchie, N. Al-Rayyan, S.Telang, K. Yaddanapudi, and J. Chesney. 6-phosphofructo-2-kinase/fructose-2,6-biphosphatase 3 (PFKFB3) is Necessary for Human Melanoma MDSC Differentiation and Function. Poster presented at Research! Louisville 2015; Louisville, KY.
6. Chuanlin Ding, Paul L. Dascani, **Jaspreet S. Grewal**, and Jun Yan. STAT3 Signaling in B cells is Essential for the Germinal Center Maintenance and Pathogenesis of Lupus. Poster presented at AAI meeting 2015; New Orleans, LA.
7. **Jaspreet Grewal**, Gina Bardi, Jugraj Dhanoa, Paula Bates, Tariq Malik. (2014). A Novel Small Molecule Therapeutic Agent for Selective Inhibition of Malignant Cells in Acute Myeloid Leukemia. Poster presented at: 13th Annual Brown Cancer Center Retreat at the University of Louisville; Louisville, KY.
8. **Jaspreet Grewal**, Gina Bardi, Jugraj Dhanoa, Paula Bates, Tariq Malik. (2014). A Novel Small Molecule Therapeutic Agent for Selective Inhibition of Malignant Cells in Acute Myeloid Leukemia. Poster presented at: Research! Louisville 2014; Louisville, KY.
9. Jugraj Dhanoa, Amaninderpal Ghotra, Wedersen Claudino, **Jaspreet Grewal**. (2014). Clostridium Septicum Sepsis - A Clue to Colon Cancer. Poster presented at: Research! Louisville 2014; Louisville, KY.
10. Jugraj Dhanoa, Amaninderpal Ghotra, Wedersen Claudino, **Jaspreet Grewal**. (2014). Clostridium Septicum Sepsis – A Clue to Colon Cancer. Poster presented at: 13th Annual Brown Cancer Center Retreat at the University of Louisville; Louisville, KY.
11. Jugraj Dhanoa, Amaninderpal Ghotra, Wederson Claudino and **Jaspreet Grewal**. (2014). Clostridium Septicum Sepsis - A Clue to Colon Cancer. Poster presented at: American College of Physicians - Kentucky Chapter; Louisville, KY.
12. Wedersen Claudino, Jugraj Dhanoa, **Jaspreet Grewal**, Amaninderpal Ghotra, Stephen Slone, Cesar Rodriguez. (2014). Myelodysplastic Syndrome with Myelofibrosis – Rare Disease with Challenging Diagnosis and Management. Poster presented at: Research! Louisville 2014; Louisville, KY.
13. Wedersen Claudino, Jugraj Dhanoa, **Jaspreet Grewal**, Amaninderpal Ghotra, Stephen Slone, Cesar Rodriguez. (2014). Myelodysplastic Syndrome with Myelofibrosis – Rare Disease with Challenging Diagnosis and Management. Poster presented at: 13th Annual Brown Cancer Center Retreat at the University of Louisville; Louisville, KY.
14. Wederson Claudino, Jugraj Dhanoa, Amaninderpal Ghotra, **Jaspreet Grewal**, Stephen Slone and Cesar Rodriguez. (2014). Myelodysplastic Syndrome with Myelofibrosis - Rare Disease with Challenging Diagnosis and Management. Poster presented at: American College of Physicians - Kentucky Chapter; Louisville, KY.

15. **Grewal J**, King B, Panchapakesan B and Kloecker G. Carbon Nanotube Devices for the Detection of Circulating Tumor Cells. Research Louisville! 2012.
16. **Grewal J**, King B, Panchapakesan B and Kloecker G. Carbon Nanotube Devices for the Detection of Circulating Tumor Cells. ESMO 2012, Vienna, Austria.
17. **Grewal J**, Smith LB, Winegarden III JD, Krauss JC, Tworek JA, Schnitzer B. (2006, September). Highly Aggressive ALK Positive Anaplastic Large Cell Lymphoma with a Leukemic Phase and Multi-organ Involvement: A Report of 3 Cases. Poster presented at: XXVI Congress of the International Academy of Pathology; Montreal, Quebec, Canada.
18. **Grewal JS**, Daniel AR, Carson E, Catanzaro AT, Shehab TM, Tworek JA. (2007, May). Metastatic Multicentric Epithelioid Angiosarcoma of the Small Bowel: A Case Report. Poster presented at: Annual Resident Research Forum at St. Joseph Mercy Hospital; Ann Arbor, MI.
19. **Grewal JS**, Daniel AR, Carson E, Catanzaro AT, Shehab TM, Tworek JA. (2007, September). Metastatic Multicentric Epithelioid Angiosarcoma of the Small Bowel: A Case Report. Poster presented at: Michigan Chapter of the American College of Physicians Meeting; Kalamazoo, MI.
20. **Grewal JS**, Gunaratnam NK, Krauss JC, Mais DD. (2008, May). A Case of Primary Burkitt's lymphoma of the Thyroid Gland with Secondary Pancreatic Involvement. Poster presented at: Michigan Chapter of the American College of Physicians Meeting; Sterling Heights, MI.
21. **Grewal JS**, Gunaratnam NT, Krauss JC, Mais DD. (2008, April). A Case of Primary Burkitt's lymphoma of the Thyroid Gland with Secondary Pancreatic Involvement. Poster presented at: Annual Resident Research Forum at St. Joseph Mercy Hospital; Ann Arbor, MI.
22. **Grewal JS**, Lall T, Hirsch SD, Winegarden III JD. (2008, May). Atypical Presentation of Acute Myelogenous Leukemia (Granulocytic Sarcoma) Involving the Female Genital Tract. Poster presented at: Michigan Chapter of the American College of Physicians Meeting; Sterling Heights, MI.
23. **Grewal JS**, Lall T, Hirsch SD, Winegarden JD. (2008, April). Atypical Presentation of Acute Myelogenous Leukemia (Granulocytic Sarcoma) Involving the Female Genital Tract. Poster presented at: Annual Resident Research Forum at St. Joseph Mercy Hospital; Ann Arbor, MI.
24. **Grewal JS**, Madala S, Salameh MA, Mais DD. (2008, April). Metastatic Ewing's Sarcoma Presenting as an Intra-cardiac Mass. Poster presented at: Annual Resident Research Forum at St. Joseph Mercy Hospital; Ann Arbor, MI.
25. **Grewal JS**, Madala S, Salameh MA, Mais DD. (2008, May). Metastatic Ewing's Sarcoma Presenting as an Intra-cardiac Mass. Poster presented at: Michigan Chapter of the American College of Physicians Meeting; Sterling Heights, MI.
26. **Grewal JS**, Reed MJ, Kimball BC, Schaldenbrand JD. (2008, April). A case of colon adenocarcinoma metastasis to the thyroid gland. Poster

presented at: Annual Resident Research Forum at St. Joseph Mercy Hospital; Ann Arbor, MI.

27. **Grewal JS**, Reed MJ, Kimball BC, Schaldenbrand JD. (2008, May). A case of colon adenocarcinoma metastasis to the thyroid gland. Poster presented at: Michigan Chapter of the American College of Physicians Meeting; Sterling Heights, MI.
28. **Grewal JS**, Salameh MA, Alpern AG, Patton WF. (2008, April). Microscopic Pulmonary Tumor Emboli: A Rare Cause of Dyspnea. Poster presented at: Annual Resident Research Forum at St. Joseph Mercy Hospital; Ann Arbor, MI.
29. **Grewal JS**, Salameh MA, Alpern AG, Patton WF. (2008, May). Microscopic Pulmonary Tumor Emboli: A Rare Cause of Dyspnea. Poster presented at: Michigan Chapter of the American College of Physicians Meeting; Sterling Heights, MI.
30. **Grewal JS**, Salameh MA, Alpern AG, Patton WF. (2007, October). Microscopic Pulmonary Tumor Emboli: Often Reviewed and Clinically Forgotten. Poster presented at: International Conference on Thrombosis and Hemostasis Issues in Cancer (ICTHIC); Bergamo, Italy.
31. **Grewal JS**, Salameh MA, Alpern AG, Patton WF. (2008, April). Microscopic Pulmonary Tumor Emboli: A Rare Cause of Dyspnea. Poster presented at: Society of Hospital Medicine Meeting; San Diego, CA.
32. **Grewal JS**, Shehab TM, Krasman ML, Whitehouse Jr WM. (2008, April). A Young Male Patient with Abdominal Pain and Weight Loss: A Case of Median Arcuate Ligament Syndrome. Poster presented at: Annual Resident Research Forum at St. Joseph Mercy Hospital; Ann Arbor, MI.
33. **Grewal JS**, Sidhu NS, Daniel AR, Swarup R, Shehab TM. (2008, April). Cardiac Compromise In A Young Patient With Bipolar Disease. Poster presented at: Annual Resident Research Forum at St. Joseph Mercy Hospital; Ann Arbor, MI.
34. **Grewal JS**, Sidhu NS, Daniel AR, Swarup R, Shehab TM. (2008, April). Cardiac Compromise In A Young Patient With Bipolar Disease. Poster presented at: Society of Hospital Medicine Meeting; San Diego, CA.
35. **Grewal JS**, Sidhu NS, Daniel AR, Swarup R, Shehab TM. (2008, May). Cardiac Compromise In A Young Patient With Bipolar Disease. Poster presented at: Michigan Chapter of the American College of Physicians Meeting; Sterling Heights, MI.
36. **Grewal JS**, Smith LB, Winegarden III JD, Krauss JC, Tworek JA, Schnitzer B. (2007, May). Highly Aggressive ALK Positive Anaplastic Large Cell Lymphoma with a Leukemic Phase and Multi-organ Involvement: A Report of 3 Cases. Poster presented at: Annual Resident Research Forum at St. Joseph Mercy Hospital; Ann Arbor, MI.
37. **Grewal JS**, Tworek JA, Chottiner EG, Sahijdak WM. (2008, April). Central Nervous System Involvement with Waldenström's Macroglobulinemia: Favorable Response to Cranial Radiation Treatment. Poster presented at: Annual Resident Research Forum at St. Joseph Mercy Hospital; Ann Arbor, MI.

38. **Grewal JS**, Wei I, Daniel RA. (2007, May). A Young Patient with Fever, Rash and Lymphadenopathy: A Diagnostic Dilemma (A case of Dilantin Hypersensitivity Syndrome). Poster presented at: Annual Resident Research Forum at St. Joseph Mercy Hospital; Ann Arbor, MI.
39. **Grewal JS**, Wei I, Daniel RA. (2007, May). A Young Patient with Fever, Rash and Lymphadenopathy: A Diagnostic Dilemma (A case of Dilantin Hypersensitivity Syndrome). Poster presented at: Michigan Chapter of the American College of Physicians Meeting; East Lansing, MI.
40. **Grewal JS**, Winegarden III JD, Catanzaro A, Tworek JA. (2007, May). Goblet Cell Carcinoid (Adenocarcinoid) of the Right Colon: A Rare Presentation of a Rare Malignancy. Poster presented at: Michigan Chapter of the American College of Physicians Meeting; East Lansing, MI.
41. **Grewal JS**, Winegarden III JD, Catanzaro A, Tworek JA. (2007, May). Goblet Cell Carcinoid (Adenocarcinoid) of the Right Colon: A Rare Presentation of a Rare Malignancy. Poster presented at: Annual Resident Research Forum at St. Joseph Mercy Hospital; Ann Arbor, MI.
42. **Grewal JS**, Winegarden III JD, Mais DD., Schaldenbrand JD. (2008, April). Highly Aggressive Philadelphia Chromosome Positive Acute Myeloid Leukemia: Effective Clinical Response to Treatment with Imatinib. Poster presented at: Annual Resident Research Forum at St. Joseph Mercy Hospital; Ann Arbor, MI.
43. **Grewal JS**, Winegarden III JD, Mais MD, Schaldenbrand JD. (2008, May). Highly Aggressive Philadelphia Chromosome Positive Acute Myeloid Leukemia: Effective Clinical Response to Treatment with Imatinib. Poster presented at: Michigan Chapter of the American College of Physicians Meeting; Sterling Heights, MI.
44. **Grewal JS**, Winegarden III JD, Tworek JA. (2007, September). Primary Diffuse Large B-Cell Lymphoma of the Uterus: A case report. Poster presented at: Michigan Chapter of the American College of Physicians Meeting; Kalamazoo, MI.
45. **Grewal JS**, Winegarden III JD, Tworek JA. (2008, April). Primary Diffuse Large B-Cell Lymphoma of the Uterus: A case report. Poster presented at: Annual Resident Research Forum at St. Joseph Mercy Hospital; Ann Arbor, MI.

PUBLICATIONS

Articles Published in Peer-Reviewed Journals:

1. Claudino WM, Gibson B, Tse W, Krem M, **Grewal J**. Methotrexate-associated Primary Cutaneous CD30-positive Cutaneous T-cell Lymphoproliferative Disorder: A Case Illustration and a Brief Review. American Journal of Blood Research. 2016 May 18;6(1):1-5
2. **Grewal JS,** Gunaratnam NT, Krauss JC, Smith LB. Unusual Case of Burkitt Lymphoma with Thyroid Gland and Abdominal Involvement. The American Journal of Case Reports. 2010 Jan; 11: 16-19.

3. **Grewal JS,** Chottiner EG, Brar PK, Sahijdak WM, Tworek JA. Bing-Neel Syndrome: A Case Report and a Systematic Review of Clinical Manifestations, Diagnosis and Treatment Options. Clinical Lymphoma and Myeloma. 2009 Dec; 9(6): 462-466. Cited in PubMed; PMID: 19951888.
4. **Grewal JS,** Daniel AR, Carson EJ, Catanzaro AT, Shehab TM, Tworek JA. Rapidly progressive metastatic multicentric epithelioid angiosarcoma of the small bowel: a case report and a review of literature. International Journal of Colorectal Disease. 2008 Aug; 23(8): 745-756. Cited in PubMed; PMID: 18080128.
5. **Grewal JS,** Smith LB, Winegarden JD 3rd, Krauss JC, Tworek JA, Schnitzer B. Highly aggressive ALK-positive anaplastic large cell lymphoma with a leukemic phase and multi-organ involvement: a report of three cases and a review of the literature. Annals of Hematology. 2007 Mar; 86(7): 499-508. Cited in PubMed; PMID: 17396261.
6. Perkins BA, Orszag A, **Grewal J,** Ng E, Ngo M, Bril V. Multi-site testing with a point-of-care nerve conduction device can be used in an algorithm to diagnose diabetic sensorimotor polyneuropathy. Diabetes Care. 2008 Mar; 31(3): 522-524. Cited in PubMed; PMID: 18070992.
7. Perkins BA, **Grewal J,** Ng E, Ngo M, Bril V. Validation of a novel point-of-care nerve conduction device for the detection of diabetic sensorimotor polyneuropathy. Diabetes Care. 2006 Sep; 29(9): 2023-2027. Cited in PubMed; PMID: 16936147.
8. **Grewal J,** Bril V, Lewis GF, Perkins BA. Objective evidence for the reversibility of nerve injury in diabetic neuropathic cachexia. Diabetes Care. 2006 Feb; 29(2): 473. Cited in PubMed; PMID: 16443922.